Space Programs Summary No. 37-29, Volume VI

for the period July 1, 1964 to August 31, 1964

Space Exploration Programs and Space Sciences

jpl

JET PROPULSION LABORATORY
CALIFORNIA INSTITUTE OF TECHNOLOGY
PASADENA, CALIFORNIA

September 30, 1964

Space Programs Summary No. 37-29, Volume VI

for the period July 1, 1964 to August 31, 1964

Space Exploration Programs and Space Sciences

JET PROPULSION LABORATORY
CALIFORNIA INSTITUTE OF TECHNOLOGY
PASADENA, CALIFORNIA

September 30, 1964

Preface

The *Space Programs Summary* is a six volume, bimonthly publication designed to report on JPL space exploration programs, and related supporting research and advanced development projects. The subtitles of all volumes of the *Space Programs Summary* are:

Vol. I. The Lunar Program (Confidential)

Vol. II. The Planetary–Interplanetary Program (Confidential)

Vol. III. The Deep Space Network (Unclassified)

Vol. IV. Supporting Research and Advanced Development (Unclassified)

Vol. V. Supporting Research and Advanced Development (Confidential)

Vol. VI. Space Exploration Programs and Space Sciences (Unclassified)

The *Space Programs Summary*, Volume VI consists of an unclassified digest of appropriate material from Volumes I, II, and III and a reprint of the space science instrumentation studies of Volumes I and II. This instrumentation work is conducted by the JPL Space Sciences Division and also by individuals of various colleges, universities, and other organizations. All such projects are supported by the Laboratory and are concerned with the development of instruments for use in the NASA space flight programs.

W. H. Pickering, *Director*
Jet Propulsion Laboratory

Space Programs Summary No. 37-29, Volume VI

Contents

LUNAR PROGRAM

THE PLANETARY-INTERPLANETARY PROGRAM

THE DEEP SPACE NETWORK

SPACE SCIENCES

BLANK PAGE

LUNAR PROGRAM

I. *Ranger* Project

A. Introduction

The *Ranger* Project was established to develop a space flight technology for transporting engineering and scientific instruments to the Moon and planets. Nine *Ranger* launchings, using *Atlas D–Agena B* vehicles, are now planned; seven of these flights have been made.

Rangers 1 and 2 (Block I) were not lunar-oriented, but were engineering evaluation flights to test the basic systems to be employed in later lunar and planetary missions. Several scientific experiments were carried on a noninterference basis. Indications are that both spacecraft performed satisfactorily within the constraints of the obtained satellite orbit. *Rangers 3, 4,* and *5* (Block II) carried a gamma-ray instrument, a TV camera, and a rough-landing seismometer capsule; all three of these flights experienced failures.

The objective of the *Ranger* Block III (*Rangers 6* through 9) flights is to obtain TV pictures of the lunar surface which will be of benefit to both the scientific program and the U.S. manned lunar flight program. The *Ranger 6* spacecraft, which was launched from Cape Kennedy, Florida, on January 30, 1964, and impacted the Moon on target on February 2, 1964, did not accomplish the primary flight objective due to a failure of the TV subsystem to transmit pictures. An extensive failure analysis was conducted. A document was prepared which covered the findings of the analysis as well as the recommendations for the *Ranger 7* through 9 configuration.

Reassembly of the *Ranger 7* TV subsystem from new and reworked units was completed, and the subsystem was returned to JPL from RCA. Extensive testing of the TV subsystem as a subsystem and as part of the *Ranger 7* spacecraft was carried out at JPL, after which the *Ranger 7* spacecraft was shipped to Cape Kennedy on June 17, 1964. Testing of the proof test model continued at JPL.

All preflight tests carried out at the Air Force Eastern Test Range were accomplished on schedule. The first launch attempt (July 27, 1964) was scrubbed because of a launch vehicle problem. The second launch attempt on July 28, 1964, concluded in the successful launching of *Ranger 7* with liftoff occurring at 16:50:08 GMT. The outstanding events of the mission were the precision of the midcourse maneuver and the transmission of 4316 video pictures of the lunar surface.

Ranger Block IV, planned as a series of three flights, and Ranger Block V, planned as a six-flight series, were cancelled due to budgetary reasons by the Office of Space Sciences, NASA, in July and December, 1963, respectively.

B. Ranger 7 Operations

1. Preflight Operations

a. Space Flight Operations (SFO) System. The SFO System preparations for mission readiness were conducted in accordance with the SFO Test Plan. This plan provides for the following preflight tests: (1) spacecraft–DSIF/SFO Facility compatibility, (2) operational training, (3) operational command procedures, (4) DSIF training, (5) SFO Facility/DSIF integration, and (6) operational readiness.

b. Spacecraft checkout at ETR. The spacecraft, TV subsystem, and associated equipment arrived at the Air Force Eastern Test Range on June 21, 1964.

The spare TV subsystem was tested to verify proper functioning of the operational support equipment. The midcourse motor was tested in the explosive safe area for high-pressure leak. A leak was detected at one of the valve seals at a pressure of 3300 psi; this seal was replaced. A backup functions system test showed normal operation for all backup command functions. A system test indicated normal spacecraft operation. The only problems detected during these tests were found to originate in the operational support equipment. These problems were corrected.

A review of the computer/teletype data reduction showed that the outputs for the TV subsystem and the spacecraft low-rate telemetry measurements did not represent actual spacecraft performance. These data-handling problems were solved by cognizant personnel.

An RF link test was performed utilizing spacecraft batteries. All spacecraft direct-access connectors were removed in order to simulate flight operations. Commands furnished by space flight operations personnel were used for both the midcourse and terminal maneuvers. Spacecraft performance throughout the sequence was normal.

Results of testing the spacecraft in the explosive safe area were normal. A precountdown test run showed a TV RFI problem and the Deep Space Instrumentation Facility at Woomera, Australia, reported discrepancies with the space loss measurements and varying signal strength. An RFI test was performed with all agencies participating. The results indicated that RFI would not be a problem during the launch countdown, and normal spacecraft performance was noted. No event correlation was detected regarding the discrepancies reported at Woomera.

A countdown test to approximately $T-100$ was run to verify that all equipment was ready for the joint flight acceptance composite test (J-FACT). Normal spacecraft operations were indicated. A record evaluation period confirmed that all testing at Complex 12 was normal. The J-FACT testing started at $T-215$ and ran through umbilical connector removal, which occurred at approximately $T+28$. Spacecraft Monitoring reported a power failure and transferred to the auxiliary generator at approximately $T-44$. Spacecraft performance was normal.

TV subsystem calibrations were completed without any adjustment being required. Final flight assembly was completed and documented photographically. Spacecraft power was turned on for an attitude-control Sun-sensor test and a pyrotechnic midcourse-motor verification test. Results of the tests showed normal spacecraft operation.

The preflight system test indicated that the spacecraft was ready for flight. Then each solar panel was excited with the solar simulator, and proper operation was checked for all individual solar panel sections.

The autopilot, midcourse-motor transducer, and TV high-power tests were performed. An evaluation of the test results showed nominal spacecraft operation. Spacecraft weight and center-of-gravity measurements indicated that approximately 3 lb of weight would be required to properly locate the center of gravity through the midcourse-motor, thrust axis. The final flight weight was 809.57 lb.

The spacecraft was transferred to the Agena adapter for final flight mating. The pyrotechnics were installed, verified, and connected. The attitude-control gas system was charged to a flight pressure of 3600 psi. Spacecraft functions were verified with the Agena shroud installed.

The spacecraft participated in a combined simulated launch. The test was run to $T-18$ sec and then recycled

to $T-7$ min. It was concluded that spacecraft operation was normal.

The first countdown started at 06:47 EST on July 27. Some correlation between Spacecraft Monitoring space loss changes and *Agena* tanking start and stop was noted. All other operations were normal. At $T-51$, the *Atlas* personnel called a 30-min hold to replace a telemetry battery. The hold was extended an additional 40 min in order to complete the battery installation. Time was recycled to $T-55$, and the countdown was resumed. Another 30-min hold was called at $T-22$ due to an *Atlas* ground guidance problem. The hold was extended on an indefinite basis until 12:35 EST, when it was decided to delay the launch.

The second countdown started at 07:04 EST on July 28. Test sequences were performed as scheduled throughout the countdown. The spacecraft was launched at 11:50 EST, 8 sec into the first window opportunity.

2. Space Flight Operations

The major events of the mission are given in Table 1 in chronological order.

a. Space Flight Operations System. The Space Flight Operations (SFO) System performs those functions during flight that are required to achieve the mission objectives. These functions include determining the trajectory of the spacecraft, defining and performing corrections to the trajectory, obtaining and evaluating telemetry from the spacecraft, transmitting required command functions to the spacecraft, and receiving and recording the video signals from the spacecraft. To fulfill the required functions, the SFO System makes use of the operational groups required to direct the mission, the tracking nets required to obtain tracking and telemetry data from the spacecraft and to transmit commands to the spacecraft, the Earth-based communications between all of the groups, the data processing and computing facilities required to support the operation, and the computer programs. The SFO System which supported the *Ranger 7* mission consisted of the Air Force Eastern Test Range (ETR), the Deep Space Instrumentation Facility (DSIF), and the SFO Facility at JPL.

b. SFO System performance. The Spacecraft Data Analysis Team continuously and satisfactorily monitored and analyzed the operation of the spacecraft. The Space Science Analysis and Command Group selected aiming points to the target and determined the TV picture quality to be expected.

The Flight Path Analysis and Command Group determined the trajectory of the spacecraft and the required spacecraft midcourse and terminal maneuvers. The schedule for the earliest orbit determination was not maintained primarily due to a lack of early tracking data. This problem was not considered critical because of the nominal appearance of the tracking data, which indicated a very good spacecraft injection. An input to the maneuver program caused a time error of 80 sec in the midcourse maneuver. This problem was not felt to be sufficiently significant to necessitate repeating the calculations.

Trajectory information based on premidcourse orbit data indicated that *Ranger 7* was on a grazing, backside impact trajectory with the Moon at -12-deg latitude and 204-deg longitude. The midcourse maneuver to correct the trajectory was initiated at approximately liftoff plus 17 hr. Data received during the midcourse maneuver indicated that the spacecraft performed the commanded maneuver.

Trajectory information based on the third postmidcourse orbit computation indicated that *Ranger 7* impacted the Moon at selenographic 10.7-deg south latitude and 20.7-deg west longitude. (The midcourse maneuver aiming point was 11-deg south latitude and 21-deg west longitude.) The Moon-referenced impact velocity was approximately 5850 mph, and the altitude from Earth was 243,655 mi. More complete trajectory information is given in Table 2.

Communications operations within the SFO Facility were very satisfactory. The data processing and computing facilities all functioned well within the allowed failure rates. No problems were encountered in the computer programs, except for engineering data evaluation, which required much more time than expected.

The DSIF provided the prime tracking operations for *Ranger 7*. The ETR tracked the spacecraft downrange and provided look angles to the DSIF. Although the look angles were somewhat delayed, most of the required data were received.

Communications for the mission were generally satisfactory, with the exception of the circuits to Johannesburg, South Africa, where excessive outages were experienced. Significant improvement was noted over the circuit into Johannesburg via Australia. Communications into Australia were very good. Complete spacecraft analog telemetry data were received during much of the mission by

Table 1. Major events of the *Ranger 7* mission

Prelaunch holds, 7-28-64			
T − time, min	Start, GMT	End, GMT	Reason
T − 60	14:40	15:50	Schedule hold
T − 07	16:33	16:43	Schedule hold

Spacecraft events and postlaunch events		
Event (sec after liftoff, nominal/actual)	Time, GMT	Date
Launch Plan 28F (Plan F, dated 7-28-64)	—	
Launch azimuth, 96.5 deg	—	
Transmission of two RTC-2's (real time commands)	13:34:00	7-28-64
Spacecraft to internal power central computer and sequencer (CC&S)	16:45:00	
CC&S inhibit released	16:48:00	
CC&S clear relays (B-2-1 event)	16:49:00	
Liftoff	16:50:08	
Mark 1, booster cutoff	(nominal time)	
Mark 2, booster jettison	(nominal time)	
Mark 3, sustainer cutoff	(nominal time)	
Mark 4, vernier cutoff	(nominal time)	
Mark 5, shroud ejection (307.4/305.0)	(nominal time)	
Mark 6, Atlas–Agena separation (310.4/308.1)	(nominal time)	
Mark 7, first Agena ignition (358.9/349.7)	(nominal time)	
Mark 8, first Agena cutoff (511.7/506.4)	(nominal time)	
Command spacecraft power up	17:13:00	
Mark 9, second Agena ignition (1704/1704.1)	(nominal time)	
Mark 10, second Agena cutoff (1792.2/1793.0)	(nominal time)	
Mark 11, firing of payload interface connectors (1984/1943.3)	17:22:31.1	
Mark 12, Spacecraft separation from Agena (1947.3/1948.1)	17:22:36.1	
Mark 13, Agena retro ignition (2332.7/2332.3)	17:29:06.3	
Command solar panel extension by CC&S	17:50:00	
Solar panels extended	17:50:00	
Begin Sun acquisition	17:53:00	
Complete Sun acquisition	18:05:00	
Begin Earth acquisition	20:21:00	
Complete Earth acquisition	20:44:00	
First RTC-0 initiated	21:15:00	
First RTC-0 verified	21:15:38	
Second RTC-0 initiated	21:17:00	
Second RTC-0 verified	21:17:38	
RTC-3 initiated, switch to high-gain antenna	21:19:00	
RTC-3 verified, switch to high-gain antenna	21:19:38	
TV subsystem backup clock 8-hr pulse	01:22:36	7-29-64
Midcourse phase by DSIF-12 (Echo Site) begun	08:50:00	
First RTC-0 initiated	08:50:00	
First RTC-0 verified	08:50:39	
Second RTC-0 initiated	08:52:00	
Second RTC-0 verified	08:52:39	
SC-1, roll turn initiated (24 sec nominal)	08:54:00	
SC-1, roll turn complete (24-sec positive roll)	08:54:39	
SC-2, pitch turn initiated (392 sec nominal)	08:56:00	
SC-2, pitch turn complete (392-sec negative pitch)	08:56:39	
SC-3, motor burn initiated (49-sec burn)	08:58:00	
SC-3, verified	08:58:00	
TV subsystem backup clock 16-hr pulse	09:22:40	
First RTC-0 initiated	09:36:00	
First RTC-0 verified	09:36:39	

Spacecraft events and postlaunch events (cont'd)		
Event (sec after liftoff, nominal/actual)	Time, GMT	Date
Second RTC-0 initiated	09:38:00	7 29-64
Second RTC-0 verified	09:38:39	
RTC-3 initiated, switch to low-gain antenna	09:40:00	
RTC-3 verified, switch to low-gain antenna	09:40:39	
RTC-4 initiated, initiate midcourse maneuver sequence	10:00:00	
RTC-4 verified	10:00:39	
CC&S command SC-1, roll maneuver start	10:00:44	
CC&S command SC-1, stop	10:01:08	
CC&S command SC-2, pitch maneuver start	10:10:09	
CC&S command SC-2, stop	10:16:41	
CC&S command motor burn	10:27:09	
CC&S command motor off (49-sec burn)	10:27:58	
Begin Sun reacquisition	10:30:39	
Complete Sun reacquisition	10:36:00	
Begin Earth reacquisition	10:58:39	
Complete Earth reacquisition	10:58:39	
First RTC-0 initiated	11:21:00	
First RTC-0 verified	11:21:39	
Second RTC-0 initiated	11:23:00	
Second RTC-0 verified	11:23:39	
RTC-3 initiated, switch to high-gain antenna	11:25:00	
RTC-3 verified	11:25:39	
Antenna switch-over complete	11:25:43	
TV subsystem backup clock		
24-hr pulse	17:22:40	
32-hr pulse	09:22:37	7-31-64
48-hr pulse	17:22:31	
64-hr pulse	01:22:23	
DSIF-12 transmitted terminal stored commands	11:15:00	
First RTC-0 initiated	11:15:30	
First RTC-0 verified	11:16:10	
Second RTC-0 initiated	11:17:30	
Second RTC-0 verified	11:18:10	
SC-4 initiated (1-sec positive pitch)	11:19:30	
SC-4 verified	11:20:10	
SC-5 initiated (1-sec positive yaw)	11:21:30	
SC-5 verified	11:22:09	
SC-6 initiated (1-sec positive pitch)	11:23:30	
SC-6 verified	11:24:09	
First RTC-0 initiated	11:51:00	
First RTC-0 verified	11:51:38	
Second RTC-0 initiated	11:53:00	
Second RTC-0 verified	11:53:39	
RTC-8 initiated, disconnect CC&S from attitude control	11:55:00	
RTC-8 verified	11:55:39	
RTC-6 initiated, start terminal maneuver sequence	12:25:08	
RTC-6 verified	12:25:47	
F-channel warmup commanded by TV subsystem clock	13:07:15	
F-channel on full power	13:08:35	
P-channel warmup commanded by CC&S	13:10:49	
P-channel on full power	13:12:09	
CC&S commanded TV on full power (backup)	13:13:49	
Impact	13:25:49	

Table 2. Flight path analysis parameters for pre-midcourse and postmidcourse orbit computations and the midcourse maneuver

Premidcourse maneuver trajectory	
Target conditions (selenographic)	
Latitude at impact	−12.35 deg
Longitude at impact	203.94 deg
Epoch at impact	12:43:29 GMT
	±5.2 sec, 7-31-64
Velocity at impact	2.630 km/sec
Path angle	−17.02 deg
Azimuth angle	267.63 deg
Orbit conditions	
Semimajor axis	269,582 km
Eccentricity	0.97565
Inclination (from equator)	28.958 deg
Right ascension of ascending node	17.046 deg
Argument of perigee	204.264 deg
Earth-fixed spherical coordinates at injection	
Epoch	17:19:56 GMT,
	7-28-64
Range	6567.6 km
Latitude	−12.676 deg
Longitude	14.648 deg
Velocity	10.533 km/sec
Path angle	1.380 deg
Azimuth angle	117.38 deg

Midcourse maneuver information	
Commanded spacecraft maneuver	
Spacecraft roll turn	5.56 deg
Spacecraft pitch turn	−86.80 deg
Maneuver velocity magnitude	29.89 m/sec
Nominal maneuver aiming information	
Impact time	13:25:30.43 GMT,
	7-31-64

Midcourse maneuver information (cont'd)	
Impact selenographic latitude	−11.0 deg
Impact selenographic longitude	−21.0 deg
Commanded midcourse maneuver velocity vectors	
with probe-Earth vector	13.03 deg
with probe-Sun vector	86.80 deg

Postmidcourse maneuver trajectory	
Actual target conditions (selenographic)	
Latitude at impact	−10.68 deg
Longitude at impact	−20.68 deg
Epoch of impact	13:25:48.455 GMT,
	±1.0 sec, 7-31-64
Velocity at impact	2.616 km/sec
Path angle	−64.20 deg
Azimuth angle	114.87 deg
Orbit conditions (based on fifth postmidcourse orbit computation on 7-31-64)	
Semimajor axis	244,087 km
Eccentricity	0.97402
Inclination (from equator)	28.707 deg
Right ascension of ascending node	16.907 deg
Argument of perigee	203.783 deg
Earth-fixed spherical coordinates at midcourse maneuver	
Epoch	10:27:58.0 GMT,
	7-29-64
Range	169,075 km
Latitude	2.739 deg
Longitude	277.825 deg
Velocity	12.071 km/sec
Path angle	8.121 deg
Azimuth angle	270.959 deg

use of voice-quality lines. Microwave transmission to the Goldstone Tracking Station worked very well during the mission.

C. Ranger 7 TV Subsystem Description and Flight Performance

The *Ranger* Block III TV subsystem is designed to obtain video pictures of the lunar surface that are at least an order-of-magnitude better in resolution than any available Earth-based lunar photographs. The TV sub-

system is electrically complete and is essentially independent of the spacecraft, except for receipt of commands from either the spacecraft receiver or the central computer and sequencer (CC&S) and utilization of the directional antenna

1. Major Assemblies

a. *Cameras.* The camera system is comprised of two full-(F-)scan (400 optical line pairs) cameras, F_a and F_b, and four partial-(P-)scan (100 optical line pairs) cameras, P1 through P4. The F-cameras operate alternately over communications Channel F, and the P-cameras operate alternately over communications Channel P. The nominal fields of view for the cameras are given in Fig. 1. Each camera consists of a camera head assembly and its individual camera electronics assembly. Synchronization and
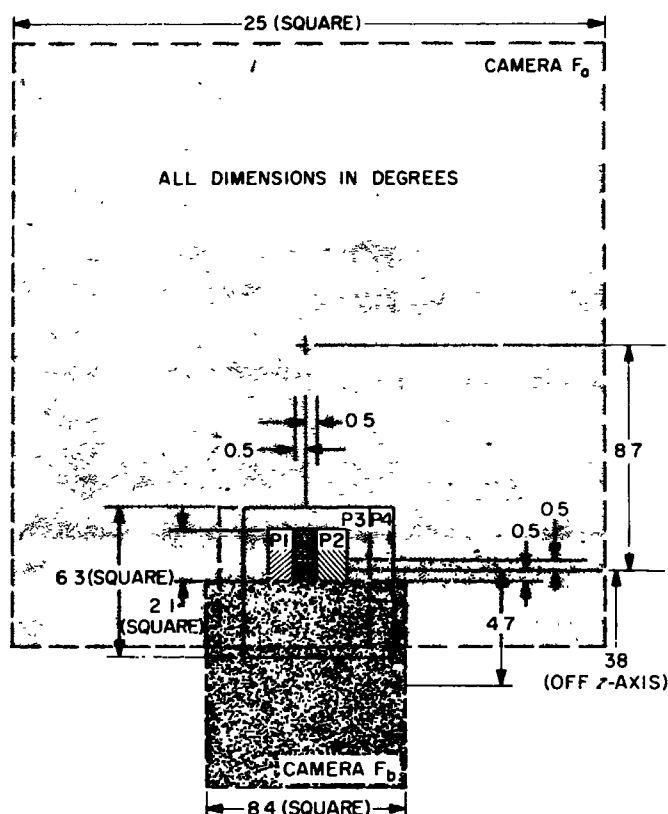
Fig. 1. Camera fields of view, showing overlap pattern

control signals for the F- and P-cameras are provided by their respective camera sequencers, and the amplified video outputs from the cameras are fed to their respective video combiners for transmission. The F- and P-camera outputs modulate the Channel F and P transmitters, respectively.

The dynamic ranges of the cameras are set such that the range of lunar luminance from 20 to 2700 ft-L is covered. Cameras F_a, P3, and P4 are set to cover 20 to 650 ft-L, while Cameras F_b, P1, and P2 are set to cover 80 to 2700 ft-L. The F- and P-cameras have shutter exposure times of 5 and 2 msec, respectively. Cameras F_a, P3, and P4 have 25-mm focal-length lenses, and Cameras F_b, P1, and P2 have 75-mm focal-length lenses.

b Camera and control sequencer. The sequencer consists of two separate links: Channel F and Channel P. Each link contains a video combiner, control programmer, camera sequencer, and sequencer power supply. The group generates synchronizing signals for the individual cameras, controls camera exposure and readout, combines the video from the individual cameras with sync and tone code signals (Camera F_b video only is identified by a 144-kc tone burst), applies the composite video signal to

the respective RF transmitter channel modulator, and generates the internal full-power command for the transmitter 80 sec after the warmup command is received by the TV subsystem.

c. Telecommunications. The communications equipment is made up of two transmitting channels and an RF combining section. Each channel contains an L-band frequency-modulated transmitter (with a modulator, two frequency multipliers, and an intermediate power amplifier), a 60-w power amplifier, a telemetry processor, and a transmitter power supply. Each transmitter operates within a bandwidth of approximately 900 kc, with the outputs of the Channel F and P transmitters centered at 959.52 and 960.58 Mc, respectively. A 160-kc band between the transmitter output frequencies is reserved for the spacecraft transponder transmitter. A four-port hybrid ring in the RF section is used to mix the outputs of the two transmitting channels, the combined output being fed to the spacecraft RF coupler. A dummy load is included in the RF equipment to dissipate the combining loss.

A 15-point sampling switch operating at a rate of 1 point/sec is used to sample the critical temperatures and voltages. During the cruise mode, the output of the 15-point switch drives a Channel 8 Inter-Range Instrumentation Group subcarrier 3-kc voltage-controlled oscillator (VCO). An AC amplifier and transformer connect the oscillator output across the spacecraft interface, where it is mixed with other telemetry signals for transmission by the spacecraft telemetry system.

During the terminal mode, a 90-point sampling switch operating at a rate of 3 points/sec samples subsystem parameters to provide detailed diagnostic telemetry data. The 90-point data contain engineering measurements of the operating parameters during the TV warmup and video transmission periods (full power). The commutated output drives two redundant chains for transmission of these data. Upon full-power initiation, these telemetry data are transmitted over Channel P and Channel 8.

d. Electrical power. The TV power assembly consists of batteries and voltage regulators, with Channels F and P each having an individual battery and high-current voltage regulator for supplying unregulated and regulated power to the operating assemblies. Each battery is comprised of 22 series-connected silver–zinc oxide cells

and has a capacity of 40 amp-hr. The high-current voltage regulators supply -27.5 ± 0.5 v dc and the unregulated battery voltage between -30.5 and -36 v dc. Each has a silicon-controlled rectifier (SCR) turn-on device that is used to switch on prime power to the system. A low-current voltage regulator supplies power from the Channel P battery to the cruise-mode telemetry.

e. Command and control. Control circuits are included in this unit to:

(1) Turn off Channels F and P by means of Real-Time Command 5 (RTC-5).

(2) Transfer the clock-start command to the distribution control unit.

(3) Inhibit clock turn-on of Channel F before separation plus 32 hr.

(4) Inhibit clock turn-off by RTC-5 before separation plus 32 hr.

(5) Turn on cruise-mode telemetry either prior to launch or at separation plus 30 min.

(6) Control and allow (using isolation diodes) redundant powering of the telemetry assembly by either the Channel F or P regulated voltage outputs.

f. TV backup clock. This clock, a solid-state timer with an over-all accuracy of ± 5 min, is used as a backup for Channel F turn-on in case of a failure in both the CC&S and the RTC-7 links. It is activated at Agena separation and can be disabled by an RTC-5 after separation plus 32 hr. (The *Ranger* 7 clock was set to activate Channel F at 67¾ hr after *Agena*–spacecraft separation.)

g. Structure and thermal control. The external structure is that of the frustum of a right circular cone topped by a cylindrical section. Its primary strength is provided by an external box span consisting of stiffened panel sections supported by eight longerons. The electric assemblies mount on structural decks supported by the longerons. The cameras are mounted on a solid machined camera bracket housing within the top cylindrical section, with a view area provided in the external thermal shroud.

The thermal control of the TV subsystem is entirely passive, with a thermal shield (mounted external to the structure body) and fins used to control the radiative ex-

change of energy between the TV subsystem and other sources (or links) of thermal energy. The thermal mass of the structure is the primary heat sink during the terminal mode of operation.

2. Modes of Operation

The *Ranger* TV subsystem is required to operate in the following two basic modes during the *Ranger* Block III missions:

a. Cruise mode. Cruise-mode TV subsystem operation furnishes (for subsequent transmission to the Earth-based data recovery stations) commutated 15-point TV subsystem telemetry data from the telemetry assembly 3-kc VCO to the spacecraft bus data-encoder Channel 8 carrier. The telemetry is initiated prior to launch and remains on throughout the mission, with the exception of spacecraft Mode II operation during the midcourse maneuver.

Also operating during the cruise mode is the TV backup clock, which is initiated at *Agena*–spacecraft separation. The clock is pre-set to initiate the Channel F terminal-phase video operation at a predetermined turn-on interval before the nominal predicted impact time. The TV backup clock output and turn-off by RTC-5 are inhibited until separation plus 32 hr.

b. Terminal mode. At the initiation of TV warmup during the terminal video phase, the 15-point data are switched from Channel 8 to the TV subsystem Channel F carrier, and 90-point data are transmitted over the Channel 8 carrier; the 90-point data are also transmitted over the Channel P carrier. Terminal-mode TV operation furnishes a dual-channel (Channels F and P) frequency-modulated signal in the 960-Mc band for transmission of video and telemetry to the Earth-based data recovery stations. Channel F, centered at 959.52 Mc, contains composite video signals (0- to 177-kc video base band) from the two F-cameras and 225-kc telemetry data (15 points). Channel P, centered at 960.58-Mc, contains composite video signals (0- to 144-kc video base band) from the four P-cameras and 225-kc telemetry data (90 points). The bit capacities of the F- and P-cameras are 2.6×10^5 and 2×10^5 bits/sec, respectively, for each camera. The capacity of the RF link for each channel is 11.7×10^5 bits/sec.

The terminal mode is normally initiated 15 min before lunar impact by the CC&S warmup command (TV-2).

The CC&S is backed up by an RTC-7 turn-on command at 12 min before impact. The battery outputs are applied to the respective high-current voltage regulators by means of the warmup signal. The −27.5-v dc output from the high-current voltage regulator is applied to the camera and sequencer electronics and transmitter modulator, and the unregulated battery output is applied to the telemetry, shutters, and communications equipment. Each channel, after an 80-sec warmup cycle, is switched to the full-power mode by a command from the sequencer unit. The full-power command causes the relays in the respective transmitter power supplies to apply high voltage to the intermediate and final power amplifiers in the communications chains. A backup for the full-power mode is provided by a CC&S full-power command (TV-3), which is given 5 min after the initial CC&S warmup command; this command will switch the transmitter power supply relays if the full-power command from the internal sequencer fails. The TV backup clock will initiate Channel F operation at a predetermined time before impact, independent of the spacecraft commands (nominally 30 min before impact).

3. Ranger 7 TV Subsystem Flight Performance

The performance of the *Ranger* 7 TV subsystem from its prelaunch checkout to its operation in the terminal phase of the mission was normal. All operating parameters were within design specification during the 68 hr, 35 min, 43 sec of the mission. There was a slow drift of 1 or 2 cps of the Channel 8 VCO for the entire mission, which is within the over-all tolerance of ±2 cps for this unit. The communications signal level was normal. The F- and P-cameras took 4316 photographs of the lunar surface with good contrast and exceptionally noise-clean signals. The lunar lighting conditions, although higher than predicted, were such that all six cameras rendered high-quality pictures whose resolution was many times greater than that of existing lunar photographs.

It was anticipated, and subsequently noted, that Telemetry Points 15-3 and 15-10, Channels P and F, battery current measurements would be difficult to interpret throughout the cruise-mode portion of the mission. The only engineering information obtained from these readings was that the system current fell between ½ and 0 amp. (The nominal cruise-mode current is 150 ma on Channel P and 50 ma on Channel F.) Cruise-mode resolution was sacrificed to obtain high resolution for the terminal phase.

During the mission it was determined that the attitude of the Sun-oriented spacecraft would be such as to give an acceptable figure of merit for good-quality TV pictures. Therefore, it was decided to turn on Channel P 15 min prior to impact by initiating the CC&S counter with a terminal RTC-8/-6. Since the backup clock would command Channel F warmup at 18 min, 30 sec before impact, this clock would not be inhibited by an RTC-5. From these considerations it was decided that the RTC-7 would be held in readiness to be given at impact minus 12 min if the CC&S turn-on of Channel P failed to occur.
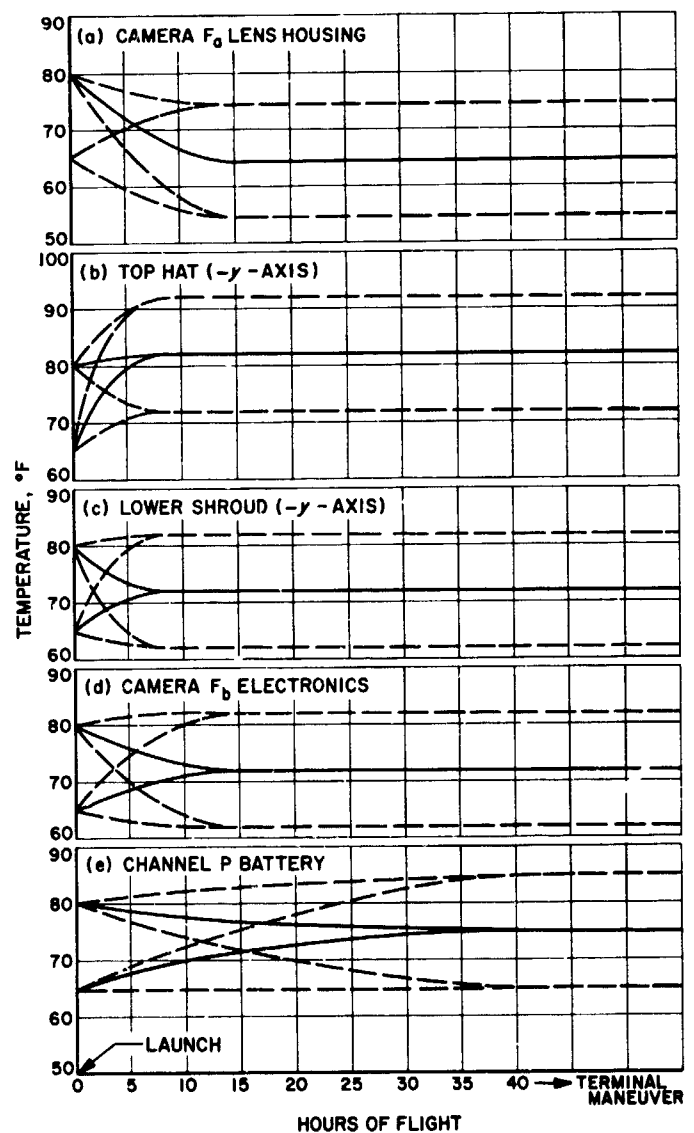

Fig. 2. Nominal cruise-mode temperatures plotted prior to the Ranger 7 flight

Fig. 2 shows the nominal temperature curves for the TV subsystem that were plotted before the *Ranger 7* mission. It should be noted that all of the cruise temperatures during the actual flight came within 4°F of the nominal temperatures (solid lines), which were well within the flight limitations (dashed lines). Fig. 3 provides actual temperatures for the TV subsystem (lens
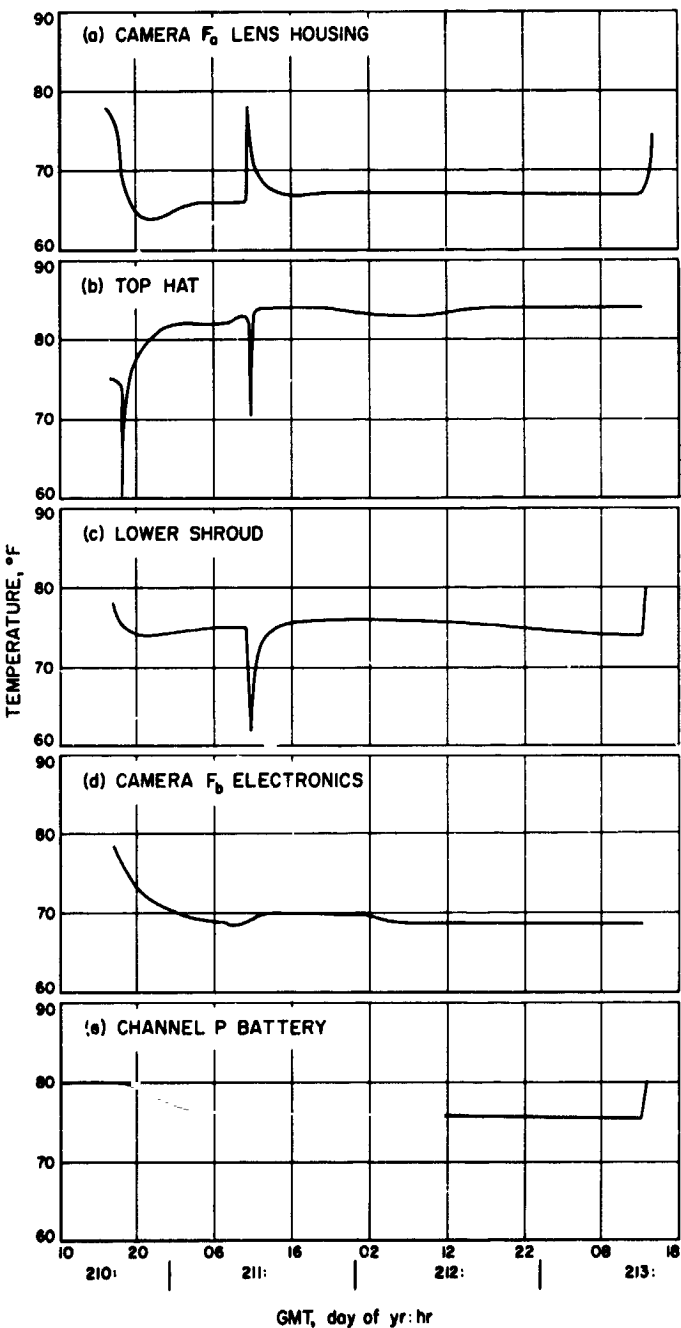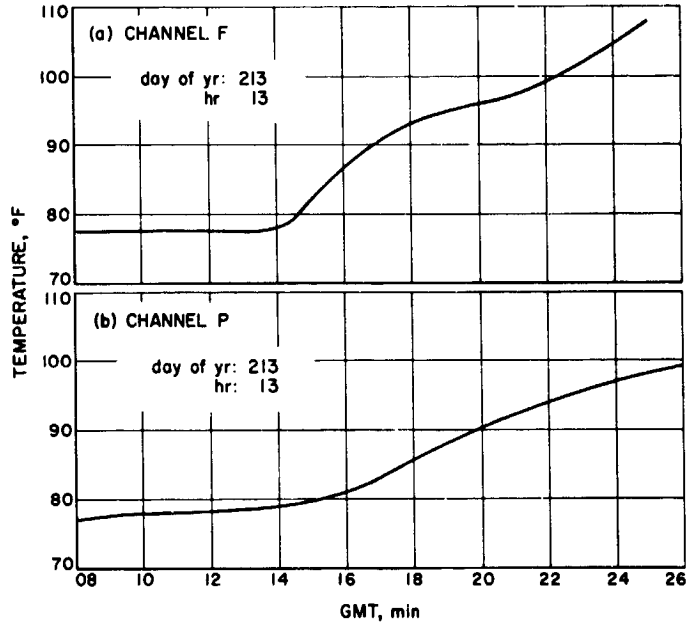

Fig. 4. Channel F and P battery voltages during the cruise mode and terminal operation of *Ranger 7*

housing, top hat, lower shroud, Camera F_b electronics, Channel P battery) obtained during the cruise mode and the terminal operation. Fig. 4 gives temperatures of the Channel F and P heat sinks during the terminal operation.

During the cruise mode, the temperature of the lens housing held steady at approximately 67°F (Fig. 3a); the nominal temperature was 64.5°F. The first group of high temperatures was caused by: (1) the lens temperature on Earth before launch was 78°F, and (2) the spacecraft was tumbling and the lens may have absorbed reflected light from the Earth during this period (until the spacecraft was attitude-stabilized). The second group of high temperatures occurred during the midcourse maneuver, during which the lenses were pointed directly into the Sun, thereby causing their temperatures to rise. When the spacecraft was brought back to its proper attitude, the temperatures returned to normal. The third group of high readings, which occurred during the terminal phase, was caused by light energy reflected from the lunar surface.

The top hat temperature stabilized at 84°F (Fig. 3b); the nominal temperature was 82°F. The first sharp drop in temperature took place when the spacecraft was in the Earth's shadow and no light emanating from the Sun warmed the top hat. The second drop occurred during the midcourse maneuver, when the spacecraft was again

Fig. 3. Actual temperatures obtained during the cruise mode and terminal operation of *Ranger 7*

so oriented that little of the Sun's light warmed the top hat. The fast thermal response of the top hat accounts for the sharpness of the changes.

The lower shroud temperature was normally between 74 and 76°F (Fig. 3c); the nominal temperature was 72°F. The drop in temperature during the midcourse maneuver took place since the spacecraft was so oriented that little light from the Sun warmed the lower shroud. The sharp rise in temperature during the terminal phase was caused by internal heating from the TV subsystem in full-power operation. The sharp changes in temperature were due to the fast thermal response of the lower shroud.

The Camera F_b electronics temperature was normally between 69 and 70°F (Fig. 3d); the nominal temperature was 72°F

During the cruise mode, the Channel P battery temperature was about 76°F (Fig. 3e); the nominal temperature was 75°F. The sharp rise in temperature at the end of the mission was caused by the high current demands (16 amp) imposed on the battery at that time. The slow drop in temperature at the beginning of the mission was caused by the battery's high thermal mass.

The Channel P battery plateaued at -34.3 v, while the Channel F battery plateaued at -34.6 v. The reasons for the Channel F battery taking so long to reach its plateau are as follows: (1) during testing the Channel F battery was subjected to less drain than the Channel P battery: 14 amp, as compared to 16 amp; and (2) during cruise its drain was only 0.05 amp, as compared to 0.15 amp for Channel P. The sudden drop in battery voltage during the terminal phase was caused by the high current demands at that stage of the mission. Yet, the high voltage levels of -32.4 v on Channel F and -31.9 v on Channel P indicated that the batteries had at least another 30 min of life in them at the end of the mission.

The normal rise in temperature for the Channel F and P transmitter heat sinks is shown in Fig. 4. The high reading of the Channel F transmitter heat sink of 106°F was well below the maximum safe level of 140°F, and the high reading of the Channel P transmitter heat sink of 98°F was well below the maximum safe level of 132°F. This indicates that the temperatures were low enough to permit operation of the TV subsystem for at least another 22 min.

D. Combined Space Sciences and Systems Analyses

1. Ranger 7 Camera Calibration and Mission Analysis[1]

a. Introduction. The fundamental objective in calibration and analysis of a space photographic system is to maximize the value of the system as a scientific instrument. Information may also be obtained which can be used for improving design and for providing definitive specifications for future procurements; however, this discussion will be primarily concerned with those factors which can increase the usefulness of an existing design. There are two important areas to be considered: (1) the selection of the optimum areas on the lunar surface and the determination of the proper lighting conditions, and (2) the determination of camera operating characteristics such as sensitivity and resolution. There is some overlap between these areas; however, it is convenient to discuss them separately.

The selection of the optimum impact area requires an essentially mathematical analysis since the object is not available for testing. A study of the photometric characteristics of the object—in this case, the lunar surface— and a mathematical description of the camera system are required. Once this has been accomplished, one can predict the performance of the camera and, in fact, determine the size of the smallest known object which may be detected in the data for various areas. The complete mathematical description of a real optical system is extremely complicated. With a TV subsystem, one must consider the scanning operations and the image sensor, which further complicate the analysis. It quickly becomes apparent that a complete characterization is impractical and that some approximations are required for mathematical simplicity. For the impact area selection, it is obvious that a complete description of the camera is not required. One may carry through the entire analysis for a single point on the optical axis. The results can then be applied with fairly minor errors over the entire field of view. Further, the effects of the scan lines may be ignored since their contribution will be the same for any area considered. With these simplifications, a mathematical model of the camera has been constructed along with a photometric model. This mathematical model is discussed in Part b that follows.

The determination of the camera parameters serves: (1) to provide the camera characteristics required for the mathematical model, including sine-wave response, light transfer characteristic, system noise, and film granularity; and (2) to obtain information for surface luminance measurements. This parameter determination and the lunar impact area selection process, trajectory, mission sequence, and terminal mode analysis for the *Ranger 7* flight are discussed in detail later in this article.

b. Mathematical model development. The selection of optimum lunar aiming areas for the *Ranger* spacecraft requires consideration of lunar topography and photometry, camera characteristics, and spacecraft viewing geometry and trajectories. In addition, possible non-standard flights after selection of a desired impact area offer an infinite number of situations from which the optimum terminal mode of operation must be selected. A quantitative method for quickly arriving at such decisions prior to and during flight is thus a necessity. For this purpose, a mathematical model utilizing a camera system description, a generalized lunar photometric function, a human observer model, and a trajectory–spacecraft description has been developed and programmed into a digital computer (Refs. 1 and 2). Because of simplifying mathematical assumptions and lack of experimental verification prior to the *Ranger 7* flight, the output of the computer program was considered only a relative indicator of system performance. This performance indicator, denoted as the figure of merit, is an estimate of the smallest surface feature that can be detected by an observer viewing the output 35-mm film positive from the camera system. More explicitly, the figure of merit is defined as the size of the smallest square element on the lunar surface with representative contrast with the background (contrast defined here as the magnitude of the difference in luminance between the object and the background) which can be detected by an observer viewing the 35-mm film.

Detection of something in a film implies that the particular detail of interest has contrast with the background (as reproduced on the film display) such that it is lifted sufficiently out of the background noise (i.e., film granularity, TV scan pattern, electronic noise, etc.). That is, for a given detail to be detectable, it must have a signal to root-mean-square (rms) noise ratio (S/N) greater than some predictable value. Of course, S/N for threshold detection varies from observer to observer and from day to day for a particular observer. Therefore, when specifying detection, one should actually state a probability of detection. No extensive investigation of detec-

tion probability versus S/N has been made by the authors of Ref. 1; however, Schade (Ref. 3), among others, has shown that an educated observer can detect, with a "good" probability, features that produce $S/N = 3$ for the observer. Note that (1) $S/N = 3$ for the observer implies that the observer has been allowed optimum viewing and filtering of S and N, and (2) detection does not require shape and size interpretability.

To specify the contrast of the square surface element and the general surface luminance distribution, one must have knowledge of the lunar photometric properties. In deriving a generalized photometric function, mare observations were selected from the work of Sytinskaya and Sharonov (Ref. 4). (This work was chosen because of its completeness and convenient data form.) The mare data were combined and averaged to obtain a generalized lunar reflectivity model as a function of phase angle and luminance longitude (Ref. 5). The phase angle is the angle formed by the line of incidence from the Sun and the line of emission to the observer from the observed point; the luminance longitude is the projection of the emission angle (the angle formed by the local normal and the line of emission to the observer) into the plane containing the phase angle. A sign convention is applied to the luminance longitude depending upon whether the longitude is toward the Sun ($-$) or away from the Sun ($+$) (see Fig. 5). The data averaging process was performed by plotting mare reflectance values versus luminance longitude for a constant phase angle and then constructing an average line through these points. This plotting and averaging was done for approximately ten phase values. Using these curves, plots of the photometric function versus phase angle were made for constant luminance longitude. Slight modifications were made in the data points to give smooth curves, thereby ensuring internal consistency. The resulting function is plotted in Fig. 6.

Upon combining this lunar reflectivity function with the solar illumination constant (taken here to be 12,900 ft-c), a predicted lunar luminance in ft-L can be calculated for any viewing geometry. Note that surface homogeneity is assumed so that luminance variations arise solely from changes in surface orientation. The appropriate element contrast with the background to be used for calculating the figure of merit would then be that obtained in an average over the most probable surface orientations of lunar relief. For mathematical simplicity a right circular cone, whose base angle is a computer input parameter, has been chosen as a representative surface feature. Interpretation of radar reflection data
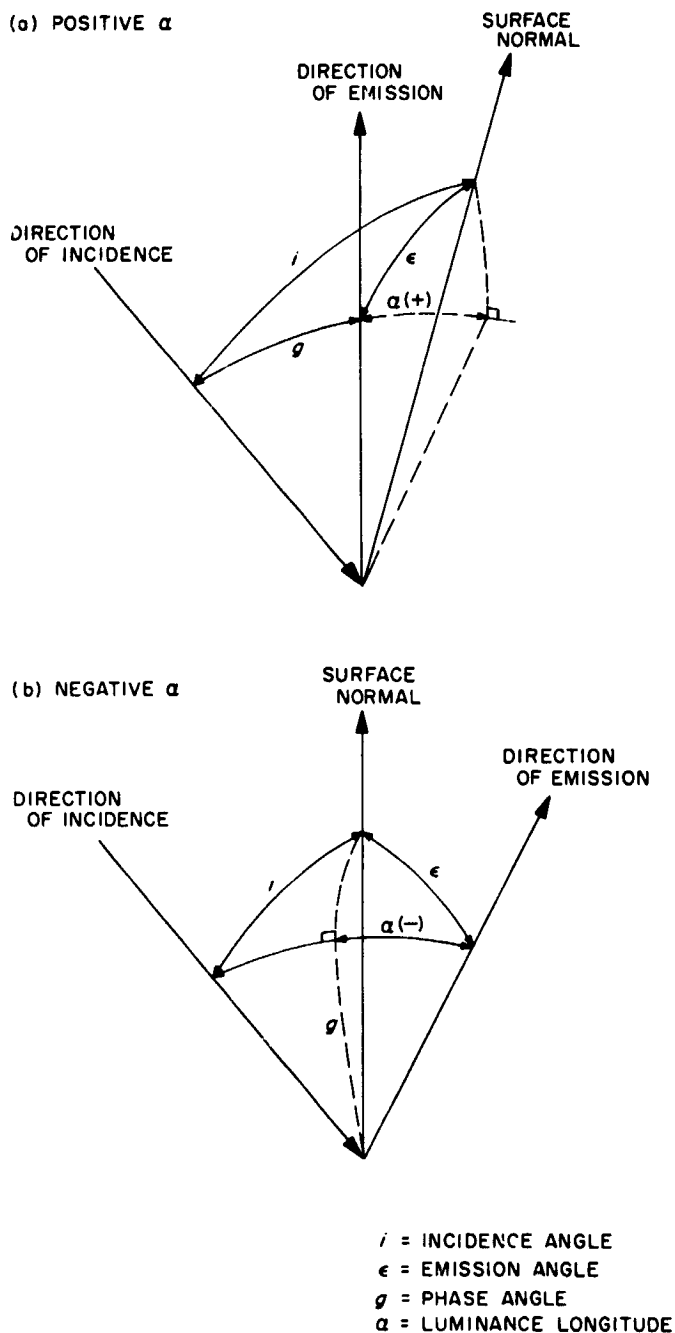
(a) POSITIVE α

SURFACE NORMAL

DIRECTION OF EMISSION

DIRECTION OF INCIDENCE

i

ε

α(+)

g

(b) NEGATIVE α

SURFACE NORMAL

DIRECTION OF EMISSION

DIRECTION OF INCIDENCE

i

ε

α(−)

g

i = INCIDENCE ANGLE
ε = EMISSION ANGLE
g = PHASE ANGLE
α = LUMINANCE LONGITUDE

Fig. 5. Viewing geometry and definition of phase and luminance longitude

off the lunar surface has shown a mean surface orientation of 15 deg with the local horizontal. Because relief detail is of interest, a larger angle should be assumed, since the sloping portions of the surface must offset the flat areas in producing the over-all average of 15 deg. Furthermore, the angle of repose of vacuum-deposited dust is approximately 30 deg. For these reasons, a representative cone base angle of 30 deg has been chosen.

The contrast with respect to the background is calculated at several points on the cone, and an average value is selected for the square surface element. This averaging includes any shadows the cone might produce since shadow area contributes to feature detection. The figure of merit is then calculated by determining the size of the smallest surface element with this contrast which, when projected through the TV subsystem, produces $S/N = 3$ for the observer. It should be noted that the viewing geometry is dependent upon the position of the lunar impact area with respect to the terminator, the trajectory characteristics, and the terminal mode orientation of the spacecraft; hence, the average contrast determined above (and consequently the figure of merit) is strongly dependent upon the position of the observed point and, thus, the impact point on the lunar surface.

With appropriate restrictions of system linearity, photosensitive surface uniformity, and vertical and horizontal scan independence, and with the neglect of scan line structure (not a serious assumption here because of the large number of scan lines involved), the image of the square surface element through the TV subsystem to the 35-mm film output is calculated with the following equation derived from Fourier analysis:

$$T(\xi,\eta) = T_0 + \frac{A}{(2\pi)^2} \int_{-\infty}^{+\infty} du$$

$$\times \int_{-\infty}^{+\infty} dv\, B(x-u, y-v)\, f_x(u)\, f_y(v),$$

where

$B(x,y)$ = the input luminance distribution

T_0, A = the coefficients in the system light transfer function, assumed at least piecewise linear

$f_x(u), f_y(v)$ = the Fourier transforms of the independent horizontal (parallel to the line scan) and vertical (perpendicular to the line scan) sine-wave response functions

$T(\xi,\eta)$ = the film transmission distribution in the image of $B(x,y)$

Further mathematical simplification has been made by neglecting phase shifts in the sine-wave response functions and assuming that the amplitude of the response functions can be approximated by a gaussian curve. Thus, the sine-wave response functions can each be specified by one term: the gaussian width parameter.
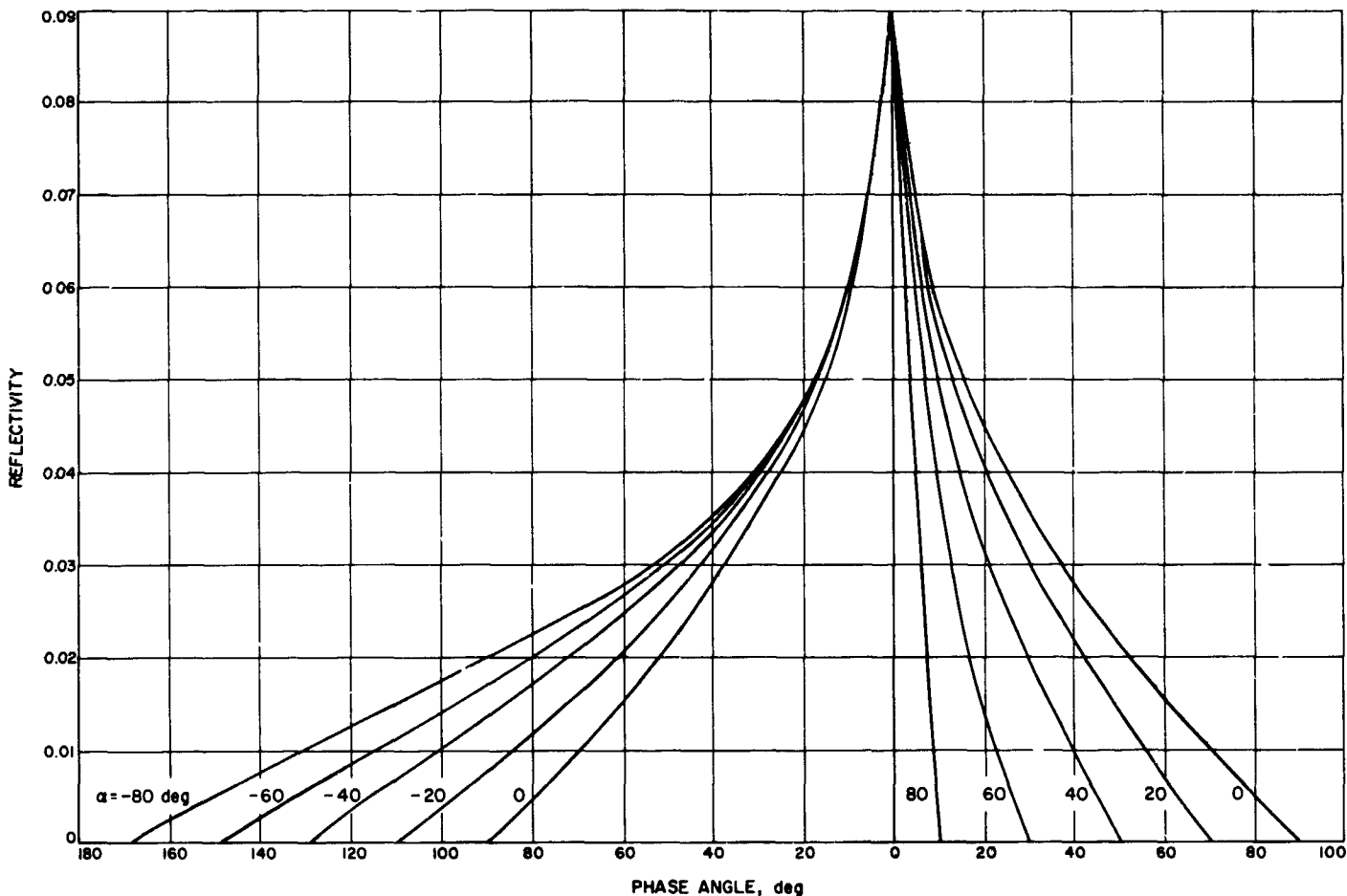
Fig. 6. Generalized lunar photometric function

The calibration data necessary for deriving the light transfer coefficients and the gaussian width parameters will be discussed later in this article.

With the specification of the camera transfer characteristics and the viewing geometry, the output signal on the 35-mm film can be computed solely as a function of the square surface element dimension.

The next step is for the human observer to view and interpret the resultant film image. It has been assumed that the observer optimizes viewing conditions such that the image stands out from the background noise as much as possible. In the mathematical treatment, the observer is represented as a low pass optimizing filter, $H(k_x,k_y)$. Thus, the signal presented to the observer by the square surface element after optimization of viewing conditions is:

$$g(\xi,\eta) = \iint_{-\infty}^{+\infty} dk_x \, dk_y \, H(k_x,k_y) \, T(k_x,k_y),$$

where $T(k_x,k_y)$ is the frequency transform of $T(\xi,\eta)$, with the constant term T_0 neglected.

The observer will, of course, see a certain amount of film noise contributed primarily by system electronics and film granularity. With the further assumption of gaussian white noise (justification for this assumption will not be presented here), the amplitude of the noise as seen by the observer can be determined as follows. Again from Fourier analysis, the rms noise is:

$$\langle N^2 \rangle = (2\pi)^2 K_r \iint_{-\infty}^{+\infty} dk_x \, dk_y \, |H(k_x,k_y)|^2 \,,$$

where K_r is a film proportionality factor which is a function of the mean film transmission. The constant K_r can be measured by scanning the film with a microphotometer. For a square scanning aperture of width a, it can be shown that

$$K_r = \frac{a^2 \langle N_0^2 \rangle}{(2\pi)^4},$$

where $<N_0^2>$ is the rms fluctuation in the micropho-
tometer output. Therefore, from a microphotometer trace
of film strip, reproductions with various mean trans-
missions, K_r can be determined as a function of mean
transmission. Hence, through the light transfer function,
K_r is known as a function of input scene luminance and,
further, the rms noise after viewing optimization by the
observer is known.

No specification has yet been made of the filter form
of the observer, $H(k_x, k_y)$. As has been shown, the filter
affects both S and N, so one would suspect that an opti-
mum filter form does exist. By proper positioning of
frequency cutoff points, many filter forms can approxi-
mate the optimum filter results. Since it is, therefore, not
an unreasonable approach to do so, we have assumed that
the human observer can also approximate the results
of the optimum filter device. It can be shown by use of
the Schwarz inequality that this optimum filter form is
completely specified by the input signal $T(k_x, k_y)$, so that
the resultant S/N is again solely a function of the square
surface element. Hence, the S/N presented to the ob-
server after viewing optimization can be shown to be:

$$S/N = \frac{1}{(2\pi)^2 K_r} \iint_{-\infty}^{+\infty} d\xi\, d\eta \left| \frac{A}{(2\pi)^2} \int_{-\infty}^{+\infty} du \right.$$

$$\times \left. \int_{-\infty}^{+\infty} dv\, B(x-u, y-v)f_x(u)f_y(v) \right|^2.$$

The element dimension is contained within the expression
$B(x,y)$, so the element dimension or figure of merit for
which $S/N = 3$ can be determined.

The figure of merit, as defined above, provides a very
useful indicator of a spacecraft TV subsystem's perform-
ance capabilities in terms of resolution. It incorporates
the effects of the environment in which the subsystem
must operate, the nature of the scene being viewed, the
subsystem's inherent parameters, and the human observer
capabilities into a measure of the smallest objects de-
tectable in the scene.

c. Parameter measurement

Light transfer characteristic. In order to obtain abso-
lute photometric information about the lunar surface,
camera sensitivity is measured as a function of incident
illumination at the camera. Because the camera lenses
are focused for an object at infinity, it is necessary to
illuminate the cameras with collimators. The illumination
is adjusted with neutral-density filters through the entire
useful range of the camera in 12 steps. At each step, a

series of photographs is taken. The film density at each
light level is then measured with a scanning micro-
photometer, and a brightness–density plot is made. A
typical plot is shown in Fig. 7.

The main problem in making the light transfer meas-
urements is to account for the differences in the emission
spectra of the collimators and the reflected solar radi-
ation from the Moon. It is usually not practical to dupli-
cate the solar spectral characteristics with calibration
collimators; however, by measuring the spectral charac-
teristics of the collimators, vidicons, and photometers,
sufficient data can be obtained to calculate a correction
factor. This correction factor is used to adjust the colli-
mator brightness so that the camera illumination directly
corresponds to the equivalent solar radiation. The proce-
dure used to obtain the spectral correction factor is
described in Ref. 6.

There are many other practical problems involved in
making these measurements (such as variations in shut-
ter exposure times and variations in vidicon sensitivity
across the target surface) which reduce the accuracy of
the measurement. With all factors considered, a measure-
ment accuracy of ±20% is expected. The use of all six
cameras should improve the ±20% figure somewhat
because the measurement from each camera can be used
to check the other cameras and, if good agreement is
found between the cameras, the confidence in the meas-
urement is greatly increased. The preliminary Ranger 7
results have not shown good agreement between all
cameras; however, three of the six cameras agree within
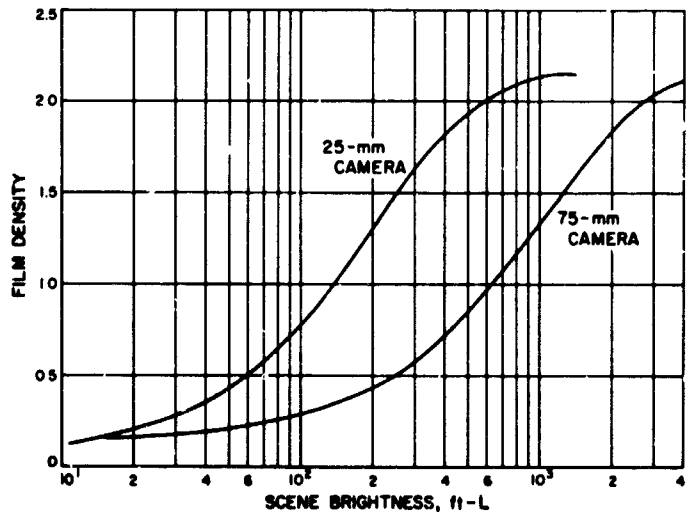10%. The data reduction is still in progress and the

Fig. 7. Typical light transfer characteristic

final results are expected to give an absolute luminance measurement of the impact area with an accuracy of 10 to 15%.

Modulation transfer function. The Fourier transform techniques used in the mathematical description of the cameras require a knowledge of the spatial frequency response of the system. The most straightforward way of obtaining the frequency response of the system is to photograph an object which has a sinusoidal variation in brightness. The resulting film is then analyzed to determine the reduction in modulation caused by the transfer through the camera system. Repeating this process for spatial frequencies from zero to the limiting resolution of the system provides the necessary information to plot the loss in modulation as a function of spatial frequency.

The above procedure provides only one part of the modulation transfer function: the amplitude response. The other portion of the transfer function which must generally be considered is the phase shift in the signal caused by the system. Since phase shift is considerably more difficult to measure in a TV subsystem, it is pertinent to determine whether phase response is important in this particular case. For systems with a symmetrical point spread function, it can easily be shown that the phase shift is zero at all spatial frequencies. One would expect, however, that a vidicon camera would not have a symmetrical point spread function because of the nature of the scanning process, which involves charging the vidicon target with the electron beam. In order to establish whether phase was important, a special slide was prepared with a very narrow bar across it. The slide was placed in a collimator which was photographed with the camera system. The image of the slide on the 35-mm film was then analyzed and found to be nearly symmetric. The width of the bar was reduced so that it was barely discernible in the system noise, and the symmetry was maintained. On the basis of these measurements, the phase response was assumed to be constant within the frequency range of interest, and the expected phase shift from the charging of the vidicon target was therefore assumed to occur beyond the passband of the system.

It is implicit, of course, that the system is considered linear when one applies Fourier techniques. A TV subsystem is not linear for large amplitude signals, so the linearity assumption requires a careful consideration of signal amplitude when making spatial frequency measurements. The usual technique for analysis of physical systems is to use small signals such that the system may

be considered linear over the amplitude range of the signal. Since the purpose of the mathematical model of the system is to determine minimum detectable object dimensions under various conditions, it is apparent that small signals will be the basis of the analysis and that no generality is lost in the linearity assumption.

For measurement convenience, it is desirable to use the highest modulation in the test slides which is commensurate with the linearity assumptions. The criterion used to establish the maximum modulation in the sine-wave slides was a maximum peak-to-peak error in the output signal of 7%. Using the measured light transfer characteristic, a series expansion is made for a sinusoidal input signal, and the modulation is calculated based on the distortion criterion. The maximum modulation was found to be 25%; this value was used to obtain the typical response curve in Fig. 8.

The actual measurement of the transfer function is made using slides with sinusoidal variations in transmission on one axis and with constant transmission along the orthogonal direction. The slides are placed in collimators which illuminate the cameras and are photographed. A series of these slides, each with a different spatial frequency, is used. The horizontal response is determined by positioning the slides so that the direction of constant transmission is perpendicular to the scan lines. The vertical response is obtained by rotating the collimators 90 deg.
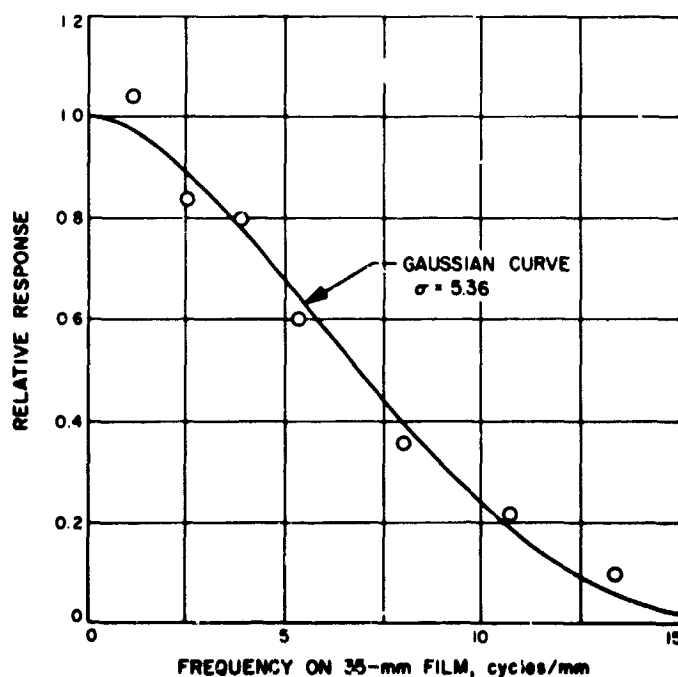

Fig. 8. Typical sine-wave response

The peak transmission of the slides was 50%, and the minimum transmission was 30%.

System noise. System noise is made up of the electrical noise generated in the camera and the receiver, as well as the granularity in the 35-mm film. Since all three sources of noise have roughly the same character, it is convenient to group them together as the total system noise. The measurement of system noise is made by scanning the film with a microphotometer. The resulting record is analyzed graphically to determine the rms value of the fluctuations as a function of film density. This value is used in the mathematical description of the cameras to determine S/N. Camera noise and communication noise are also indicative of system performance, and measurements are made during testing by other means.

It is worth noting that, due to the very high S/N values in both the camera and communication system (30 to 40 db), the film granularity is significant. The film recording process must, therefore, be optimized so as to reduce the effects of the film grain as much as possible. The optimization involves selection of the film density range, development gamma, cathode ray tube brightness, and the choice of the film itself. A density range of 1.5 and a film gamma of 1.4 are currently being used; the film is Eastman Kodak Type 5374 TV recording film.

d. Ranger 7 mission analysis. During a preflight operational mode, necessary system parameters and encounter geometry are known. With the assumption of a time before impact at which the last picture is taken, and with the specification of the spacecraft terminal mode orientation, the figure of merit can be calculated as a function of impact latitude and longitude. In addition, the rms image motion over the camera field of view is calculated for each impact point, and contours are drawn using only the larger of the two values (figure of merit or image motion). Where image motion is the larger, the contours are dashed. In practice, two terminal orientations are examined prior to launch: (1) the nominal orientation of the central reference camera axis along the trajectory or velocity vector, thus minimizing image motion; and (2) the no-terminal-maneuver orientation.

Representative contours used in the *Ranger 7* operational analysis are shown in Fig. 9. One will note that the optimum impact areas for Camera F_b—i.e., the contour which indicates the smallest figure-of-merit value—occur approximately 25 deg from the terminator, while for Camera F_a the optimum is about 10 deg from the

terminator. Note also the computer program input parameters utilized in deriving these particular contours. The contours were further superimposed with lunar topographic characteristics (mare impact areas were desired) and predicted spacecraft aiming accuracies to obtain a primary target area of 11-deg south latitude and 21-deg west longitude for a July 28, 1964, launch. Primary aiming points were also selected for all other possible launch dates.

The *Ranger 7* spacecraft was launched at 16:50:08 GMT on July 28, 1964, from the Air Force Eastern Test Range at Cape Kennedy, Florida, using an *Atlas D-Agena B* boost vehicle. The inertial direction of flight relative to the launch site was 96.6 deg east of north. The initial boost phase was terminated 506 sec from launch when the *Agena*-spacecraft was placed in a 187-km-altitude circular parking orbit at a geocentric latitude and longitude of 25.0 and 298.3 deg, respectively. The *Agena*-spacecraft coasted in the parking orbit in a southeasterly direction over the Atlantic Ocean for 19.97 min to a geocentric latitude and longitude of -9.7 and 9.1 deg, respectively, where the second *Agena* boost phase was initiated. This boost phase continued for 1.5 min, during which time the *vis viva* energy of the spacecraft was increased from -60.7 to -1.47 km²/sec². The termination of this boost phase (injection) concluded the boost portion of flight.

The spacecraft was injected into an Earth–Moon transfer orbit 29.9 min from launch at a geocentric latitude and longitude of -12.9 and 15.1 deg, respectively. Injection occurred at a true anomaly of 3.16 deg in the transfer orbit. This transfer orbit, inclined 28.9 deg to the Earth's equatorial plane, exhibited a semimajor axis of 269,700 km and an eccentricity of 0.3757.

Within 1 hr after injection, the spacecraft was receding from the Earth in an almost radial direction with decreasing speed. This reduced the geocentric angular rate of the spacecraft (in inertial coordinates) until, at 1.4 hr after injection, the angular rate of the Earth exceeded that of the spacecraft. This caused the Earth track of the spacecraft to reverse its direction from increasing to decreasing Earth longitude (Fig. 10).

Tracking data gathered and reduced prior to the midcourse maneuver indicated that the spacecraft would impact the Moon at a selenographic latitude and longitude of -12.4 and 203.5 deg, respectively. The lunar transit time from injection was then 67.4 hr.
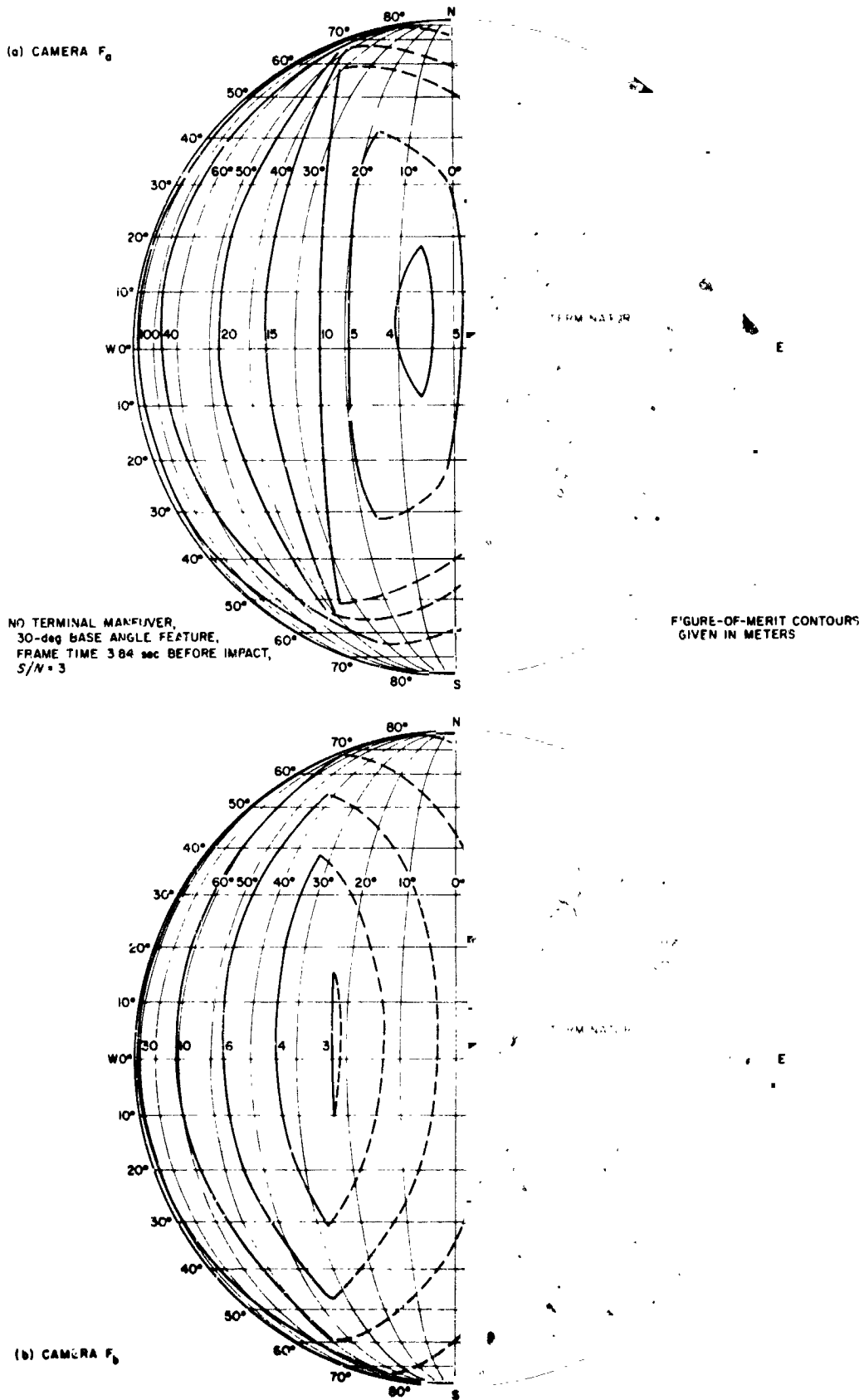
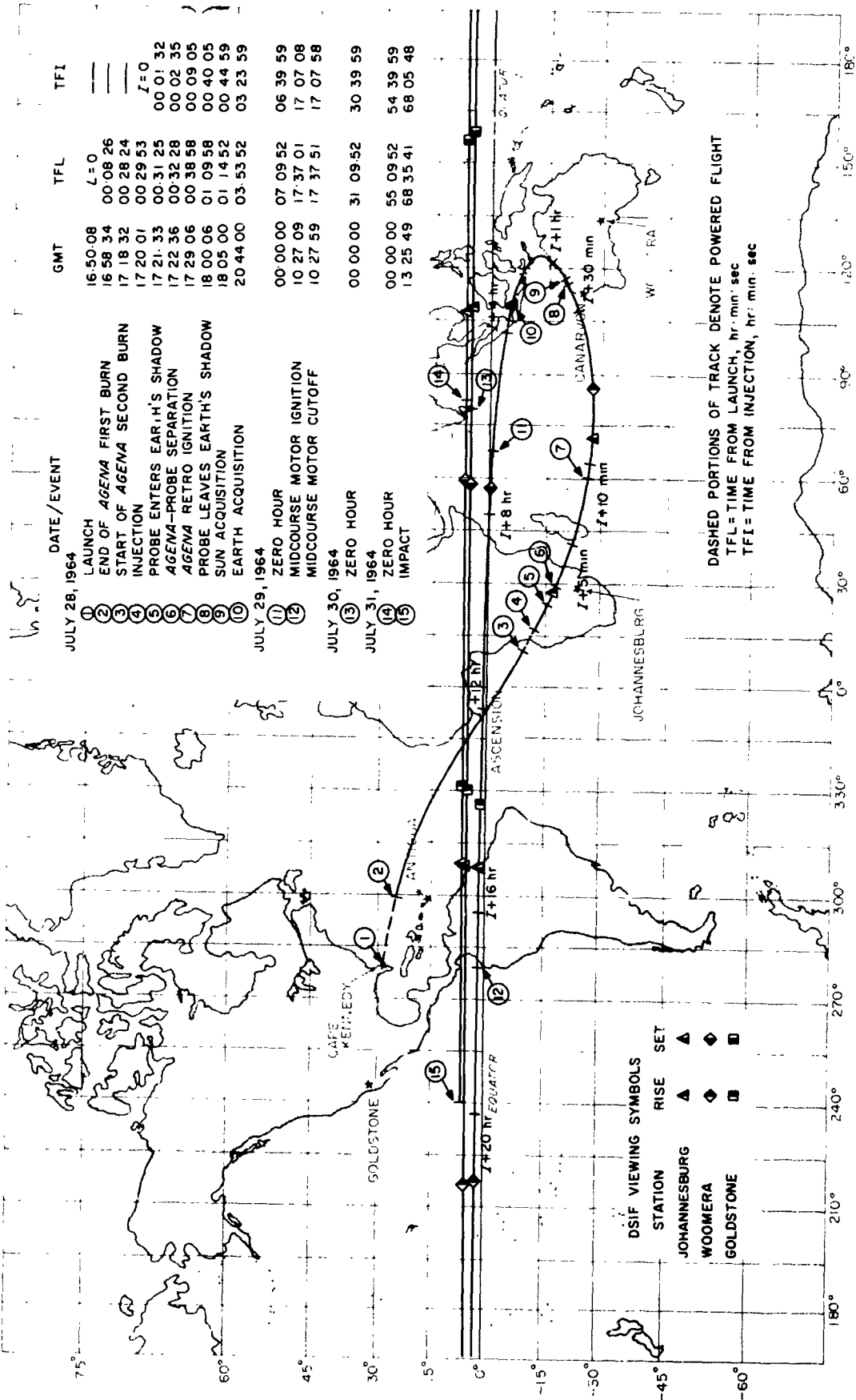Fig. 9. *Ranger 7 preflight analysis, Camera F_a and F_b figure-of-merit contours*

Fig. 10. Earth track of Ranger 7 trajectory

The midcourse maneuver was calculated to adjust the trajectory to impact at the primary target area of 11.0-deg south selenographic latitude and 21.0-deg west selenographic longitude. In addition, the midcourse maneuver was selected to adjust the flight time from injection to impact to be 68.1 hr in order to allow the TV camera backup turn-on clock to be utilized as designed. This maneuver required a 24.89-m/sec change in velocity. To properly align the thrust direction of the midcourse motor for the maneuver, a 5.6-deg roll turn and −86.8-deg pitch turn were required. The midcourse motor was ignited at 10:27:09 GMT on July 29, 1964. At the end of the 50-sec burn duration of the midcourse motor, the geocentric distance was 169,075 km and the inertial speed relative to the Earth was 1.755 km/sec. Analog telemetry data received at the Goldstone Tracking Station and relayed to the Space Flight Operations Facility at JPL gave every indication that the midcourse maneuver was executed exactly as commanded. This was further verified by the observed doppler tracking data being essentially the same as that predicted for the maneuver.

Following the midcourse maneuver the spacecraft reacquired the Sun and Earth, thus returning to the cruise mode on its way to lunar impact. Early postmidcourse tracking data were reduced and indicated that the spacecraft would impact the Moon at a selenocentric south latitude of 10.7 deg and selenocentric west longitude of 20.7 deg. The flight time from injection was resolved to be 68.1 hr.

Following this impact area verification, the detailed terminal mode study was begun. In all, seven terminal orientations were examined. The small amount of image motion (0.7 m in the last P-camera frame), the very desirable surface trace in the no-terminal-maneuver case, and the relative insensitivity of the figure of merit to orientation changes within those considered made the no-terminal-maneuver orientation nearly optimum.

At about 63 hr from injection the spacecraft experienced a minimum inertial velocity of 0.850 km/sec relative to Earth. This gave evidence that the spacecraft was being accelerated towards the Moon by the lunar gravity.

The spacecraft encountered the Moon in direct motion along a hyperbolic trajectory, with an incoming asymptote direction at an angle of −5.57 deg from the lunar equator. The orbit plane was inclined 26.84 deg to the lunar equator. Thus, the lunar trace of the spacecraft was initially above the lunar equator by approximately 5 deg

and proceeded in a south-easterly direction, crossing the equator 46 min prior to impact at a selenocentric west longitude of 42.2 deg in a direction 28.6 deg south of east.

The first F-channel pictures were taken 17.22 min prior to impact at an altitude of 2126 km. At this time, the spacecraft selenocentric south latitude and west longitude were 3.3 and 35.9 deg, respectively. At impact, the velocity vector was 25.8 deg from the local vertical in a direction, projected into the local horizon, 114.9 deg east of north.

The encounter geometry illustrated in Fig. 11 relates the trajectory and lunar trace to the lunar area viewed by the F_a- and F_b-cameras. In addition, Fig. 11 gives the trace on the lunar surface viewed by the optical axis of the F_a- and F_b-cameras prior to lunar impact.

During the cruise mode and terminal portion of flight, the Ranger 7 spacecraft was stabilized by a cold gas jet attitude-control system. This system derived its reference from the Sun and Earth. The Sun sensors allowed the spacecraft roll axis to be aligned with the −z-axis toward the Sun. The Earth sensor was used to orient the high-gain antenna toward Earth, which consequently kept the Earth in the -y, z plane of the spacecraft. (The x, y, and z orthogonal coordinate system associated with the spacecraft is defined in Fig. 12.)

The reference direction for the camera alignment was 38 deg from the z (or roll) spacecraft axis. The optical centers of all the cameras were within 0.5 deg of the spacecraft y, z plane. The relative camera alignment with reference to the spacecraft coordinates is shown in Fig. 13.

At lunar encounter, the Moon was very near its third quarter, with the projection of the Sun at a selenographic north latitude and west longitude of 0.9 and 87.6 deg, respectively. The lunar libration was such that the projection of the Earth was at a lunar north latitude and west longitude of 5.8 and 5.2 deg, respectively. Thus, with the Sun and Earth as reference, the y, z spacecraft plane was then inclined to the lunar equator by approximately 5 deg. Because the camera axes are nearly contained in the y, z spacecraft plane, the cameras were, in general, pointing south of the lunar equatorial plane by approximately 5 deg. This explains the southerly position from the trajectory trace of the area viewed by the optical centers, as illustrated in Fig. 11.
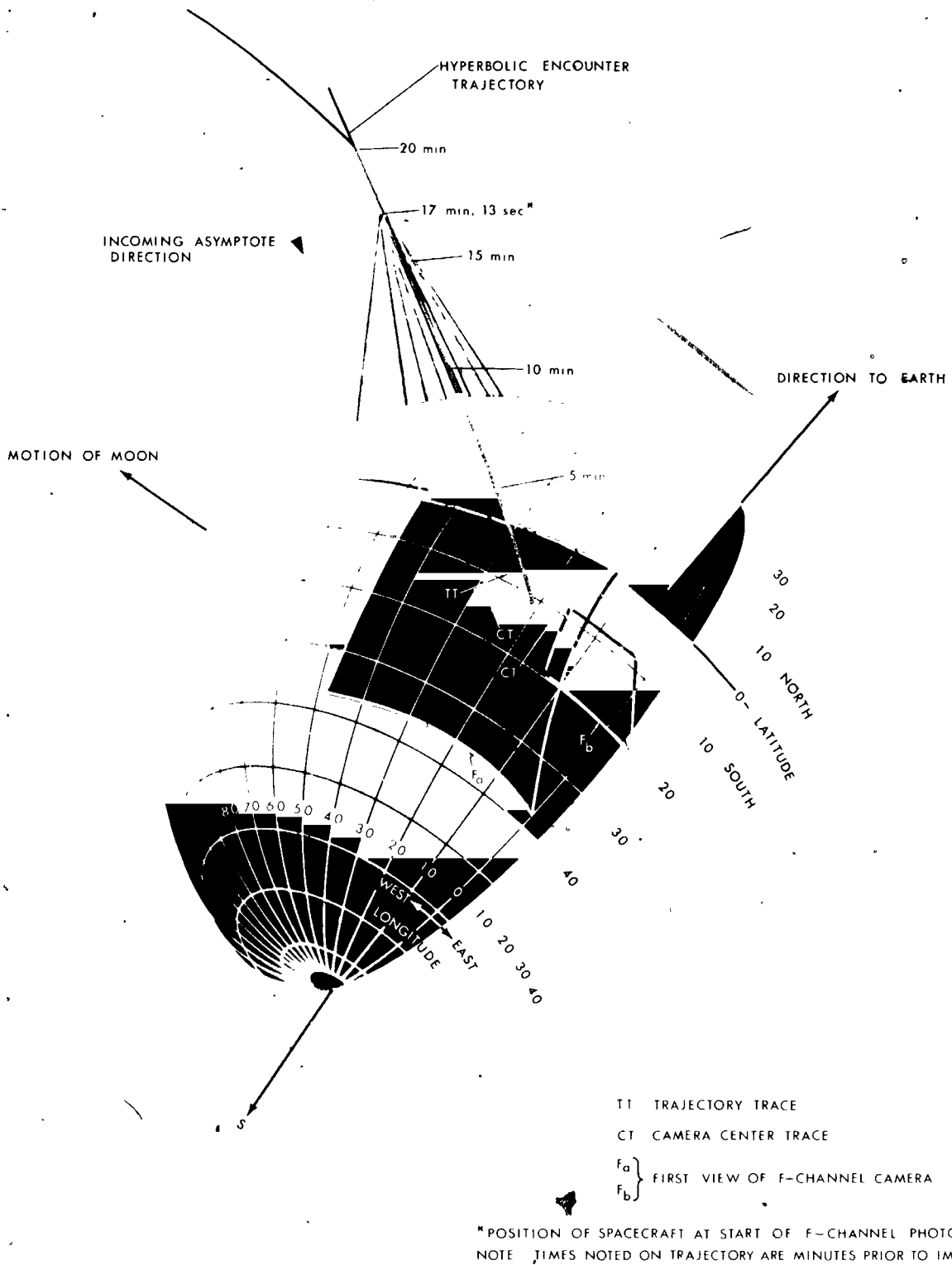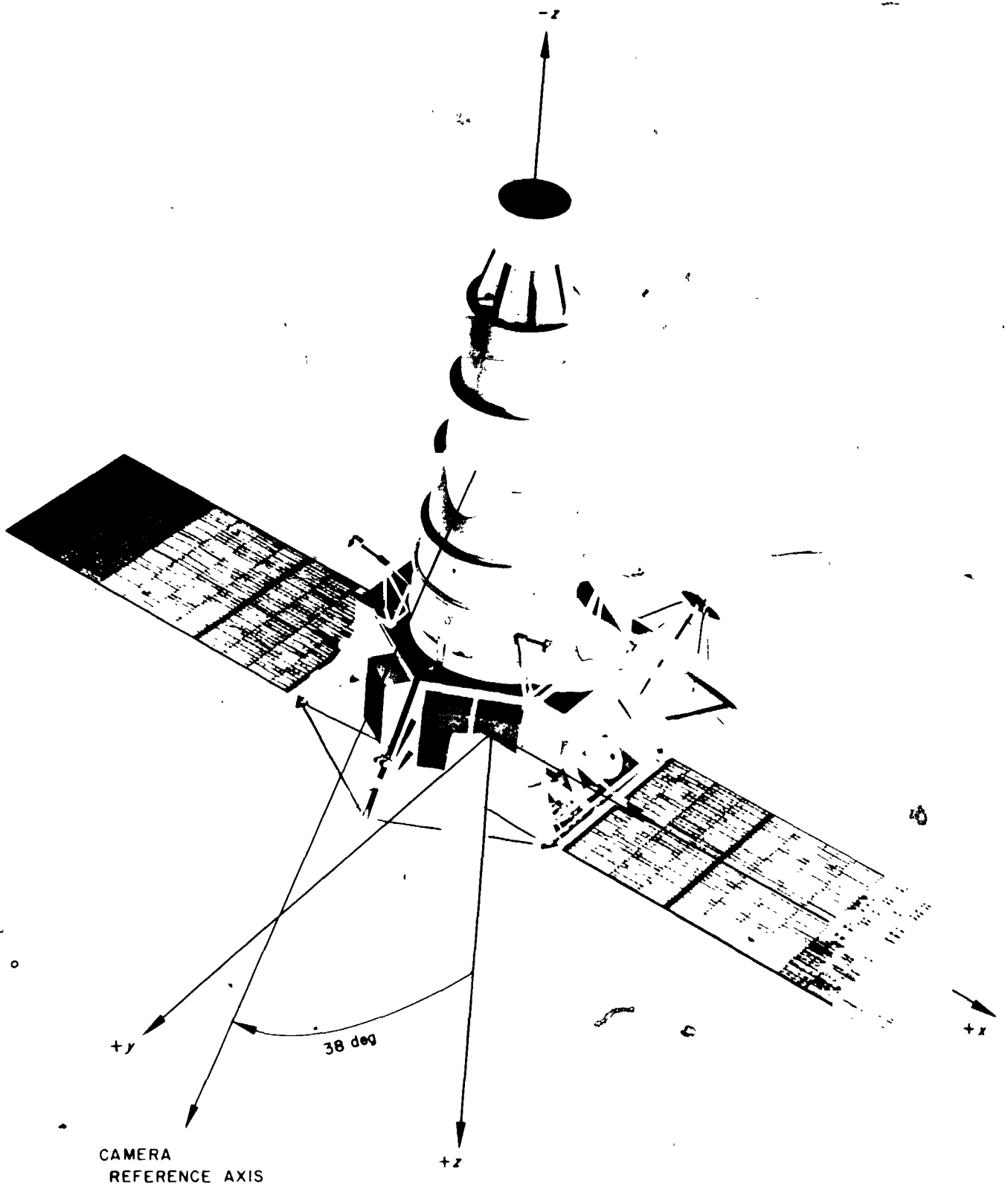
HYPERBOLIC ENCOUNTER
TRAJECTORY

20 min

17 min, 13 sec*

INCOMING ASYMPTOTE
DIRECTION

15 min

10 min

DIRECTION TO EARTH

MOTION OF MOON

5 min

TT

CT

CT

30

20

10 NORTH

0 LATITUDE

10 SOUTH

20

30

40

Fb

Fa

80 70 60 50 40 30 20 10 0

WEST

LONGITUDE

EAST

10 20 30 40

S

TT   TRAJECTORY TRACE

CT   CAMERA CENTER TRACE

Fa
Fb } FIRST VIEW OF F-CHANNEL CAMERA

*POSITION OF SPACECRAFT AT START OF F-CHANNEL PHOTOGRAPHS
NOTE   TIMES NOTED ON TRAJECTORY ARE MINUTES PRIOR TO IMPACT

Fig. 11. Lunar encounter geometry

Fig. 12. Spacecraft coordinate system
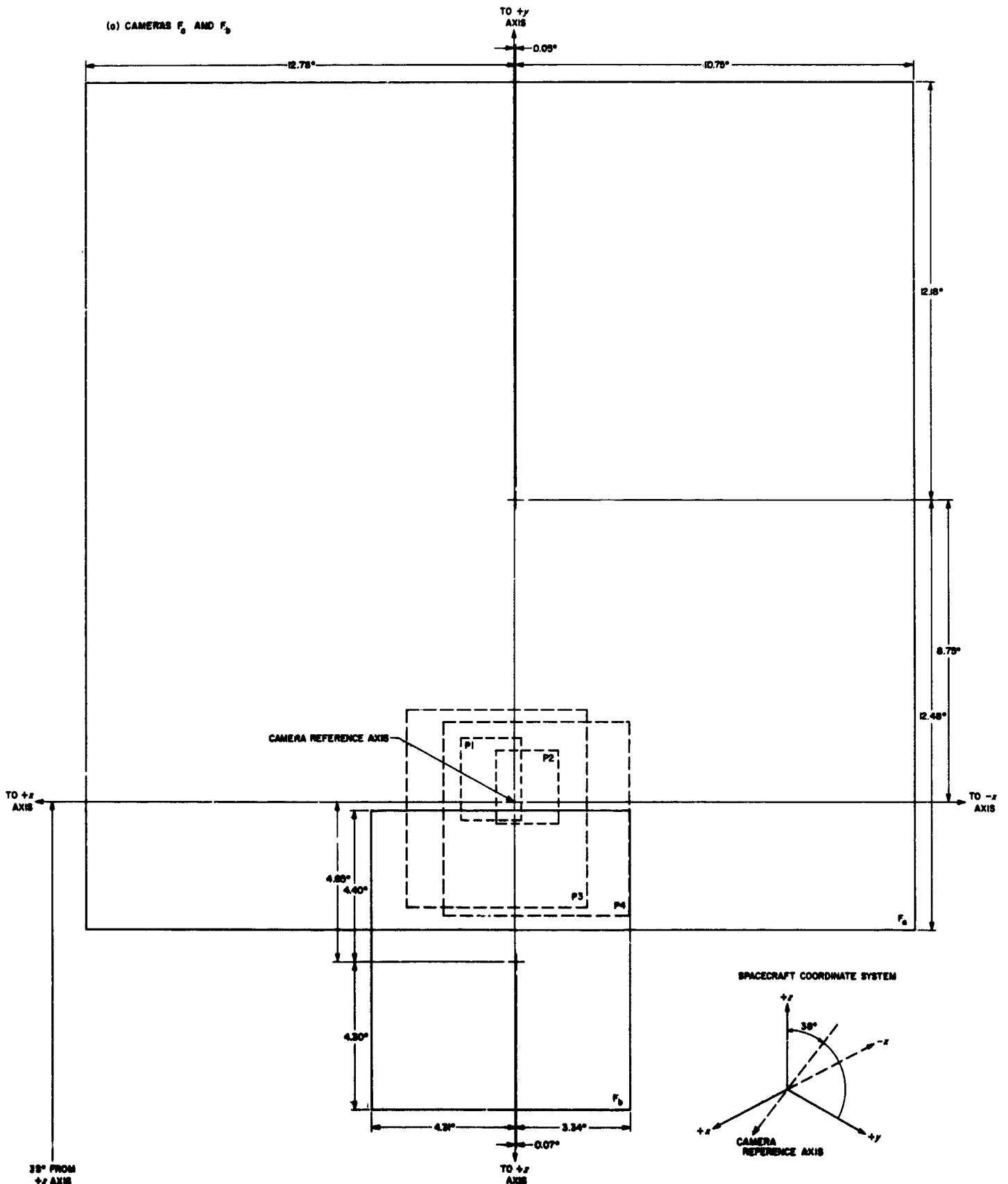
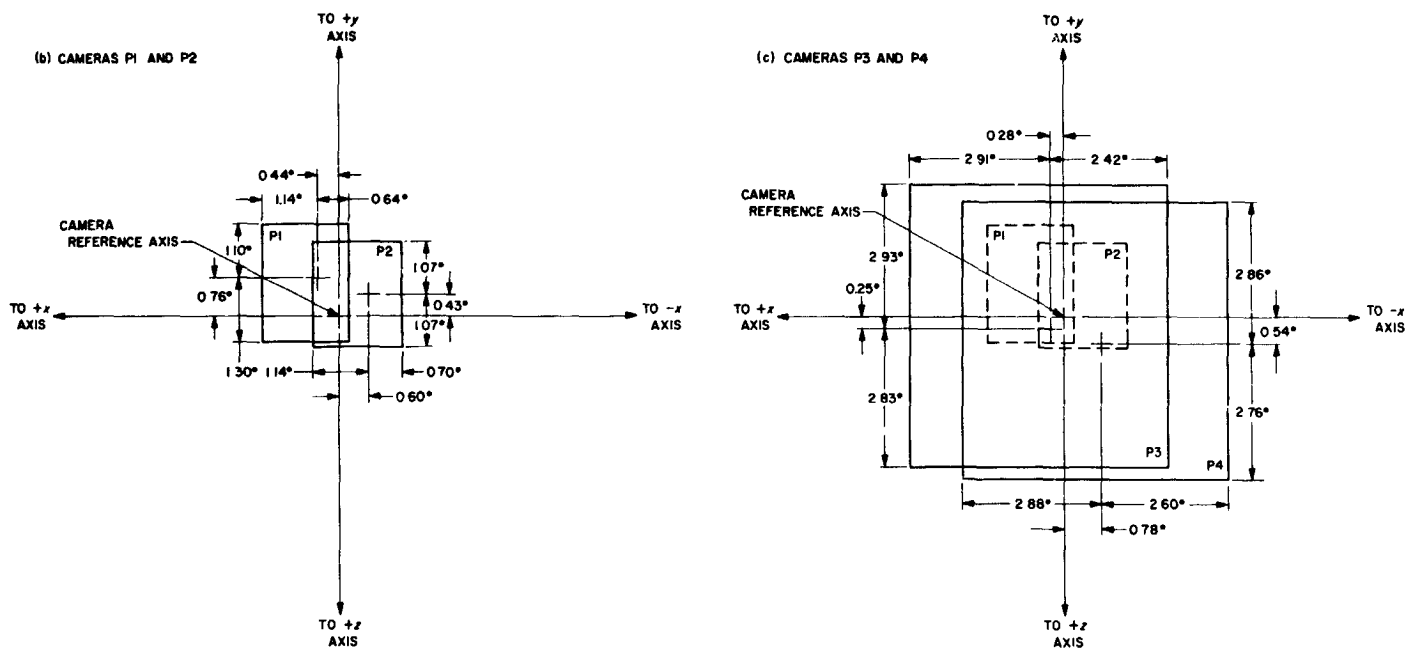**Fig. 13.** *Ranger 7 camera fields of view*

Fig. 13. *Ranger 7 camera fields of view (cont'd)*

E. *Ranger 7* Power Subsystem

1. Solar Panels

Testing. The flight solar panels were handled according to the standard preflight test sequence, which includes an inspection, an electrical performance test in sunlight, an insulation leakage check, a zener regulator check, and cleaning and surface touchup as required. All tests were completed on schedule with satisfactory results.

Flight performance. The solar panels on the *Ranger 7* spacecraft operated within expected limits during the entire flight. During and immediately following the first Sun acquisition, the $-x$ panel supplied more current to the spacecraft load than did the $+x$ panel. This was a direct result of the $-x$ panel being illuminated first, thereby allowing it to supply current and warm up faster than the $+x$ panel. As the temperatures stabilized on both panels, the current sharing became equal and the panel voltages increased. When thermal equilibrium was achieved, the voltages stabilized at equal values.

During the spacecraft cruise mode, the solar panels supplied 123 ±3 w of raw power to the power switch

and logic module (Fig. 14). The solar cell temperatures were stabilized at 47 and 45°C for the $+x$ and $-x$ panels, respectively. The back temperature transducer on the $+x$ panel indicated a temperature of 44 to 45°C, which indicated that sufficient power was being dissipated in the middle shunt regulator of the $+x$ panel to raise the back transducer temperature to nearly equal the solar cell temperature.

At the start of the midcourse maneuver at 10:00 GMT on July 30, 1964, the solar panel raw power load increased to approximately 150 w. The spacecraft started its pitch turn at 10:10:07 GMT. Fig. 14 illustrates the solar panel performance for several pitch angle (θ_p) values. At a pitch angle of 47.4 to 49.6 deg (between 10:13:41 and 10:13:51 GMT), the solar panels were not able to supply the 150-w raw power load, causing a switch to the solar panel–battery sharing mode. After the midcourse motor burn, the spacecraft reacquired the Sun. About 10:32:55 GMT, the panels were again able to supply the complete power load.

At approximately 68 min prior to impact, the solar panel temperatures began to increase due to intercepted radiant energy from the Moon. The last reading before impact showed that the front temperatures had increased 13°F and the back temperatures had increased 16°F over the cruise temperatures.
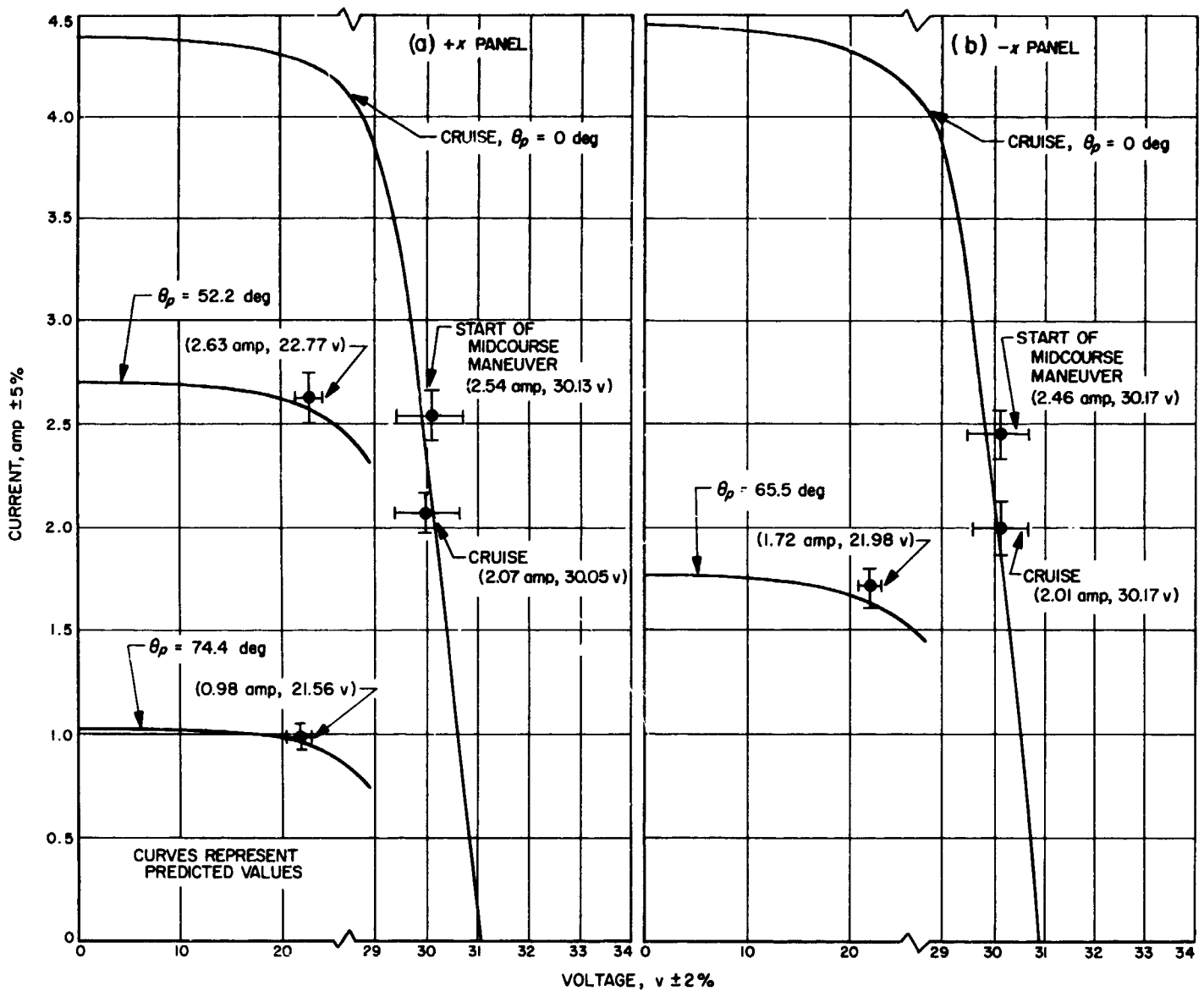
Fig. 14. Solar panel performance during the *Ranger 7* mission

The solar panels were supplying a nominal 123 ±3 w to the power switch and logic module when impact occurred at 13:25:50 GMT on July 31, 1964.

2. Batteries

Testing. Electrical bench checks were performed on the flight batteries. The units were coated to give added protection to the circuit-board terminals and component leads. Between checks, the units were stored in a controlled environment at the specified 50°F temperature. The flight batteries were not installed on the spacecraft until 2 days prior to the final system test. Operating use prior to launch was approximately 7 amp-hr, which was greater than that for *Ranger 6*.

Flight performance. Battery launch use, 8 amp-hr, was greater than that for *Ranger 6* due to a difference in Earth shadow conditions. The 2 amp-hr used in the midcourse maneuver brought the total usage to 17 amp-hr; this is less than 20% of the minimum capacity available from the two batteries.

The temperatures were generally lower for *Ranger 7* than for *Ranger 6*. The Case 5 battery was held between 76 and 88°F, and the Case 6 battery was held between 80 and 92°F; these values are well within the battery operating temperature range of 50 to 130°F.

The voltages under load were as predicted and agreed with the *Ranger 6* values. The open-circuit voltages were

as predicted, but were lower than those of *Ranger 6* due to differences in preflight environments as well as differences in use.

F. Guidance and Control Sub-systems and Components, *Ranger 7*

1. Sun and Earth Sensors

The Sun sensors and Earth sensor used for angular attitude reference during the *Ranger 7* mission performed

in a highly satisfactory manner. The Sun sensor set, which contains two pairs of primary Sun sensors and two secondary Sun sensors, has a 4π-steradian field of view; the Earth sensor has a field of view of 20 deg in hinge and 10 deg in roll (Fig. 15). Sun sensors are energized 1 hr after launch to provide two-axis (pitch and yaw, Fig. 15) error signals to the attitude-control switching logic and gas jets, which then act to null the Sun sensor error signals. The third axis (roll) position of the *Ranger* is controlled by error signals from the Earth sensor, which is energized about 4 hr after launch. The directional radio antenna is then pointed toward Earth by a combination of spacecraft-roll and antenna-hinge-axis positioning.

Flight performance. The *Ranger 7* spacecraft was within the shadow of the Earth when the Sun sensors
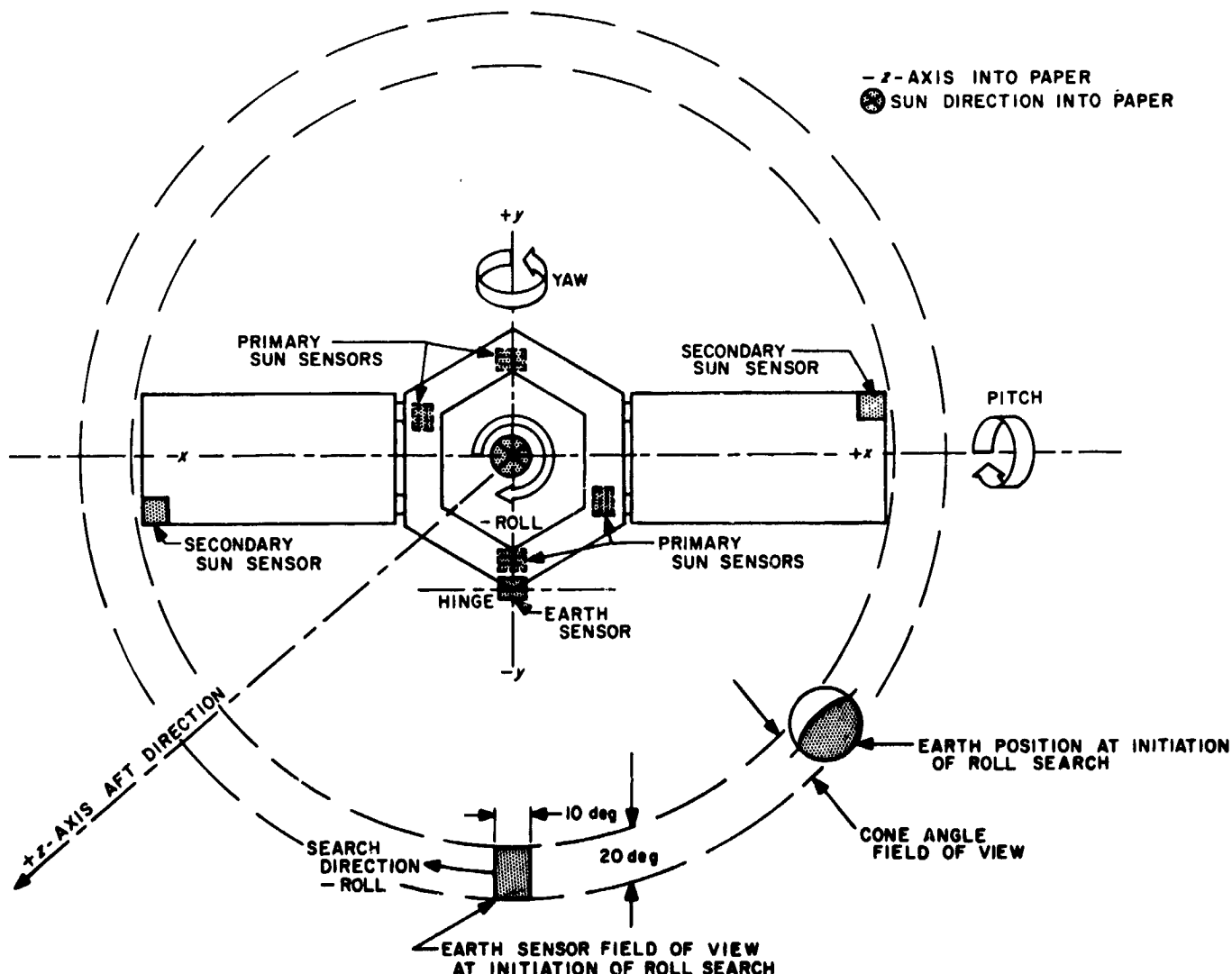

Fig. 15. *Ranger 7* relative configuration when Earth reacquisition command was given

were first energized and remained there until about 7 min after the Sun acquisition command was given. During this time, no position error signals were available from the Sun sensors. When the spacecraft emerged into the sunlight, it rotated toward null about 110 deg in yaw and 26 deg in pitch. Sun acquisition was completed 6.5 min after the spacecraft emerged into the sunlight.

The Earth-probe-Sun angle was 55 deg when the Earth acquisition command was given. The Earth sensor had to search 310 deg about the roll axis before it "found" the Earth (Fig. 15). Earth acquisition was completed 23 min after the command was given.

The midcourse maneuver consisted of a 5.56-deg roll turn, a −86.8-deg pitch turn, and a 29.89-m/sec motor burn. The Sun sensors reacquired the Sun 5 min, 40 sec after the reacquisition command was given. Because of the residual roll rate after motor burn, the Earth was only −2 deg from the Earth sensor null when the Earth reacquisition command was given. Therefore, the Earth sensor immediately acquired the Earth when its power was turned on.

Fig. 16 shows a preliminary comparison of Earth light-intensity data telemetered from the *Ranger* 7 Earth sensor and various theoretical predictions. All the predictions considered the Earth to be a perfectly diffuse reflector. For the first 2 hr of flight after the Earth sensor was first energized, the angular diameter of the Earth was larger than the field of view of the Earth sensor. The Earth light-intensity calibration curve for the Earth sensor includes a 1.9 correction factor to compensate for the difference in spectral characteristics of the light reflected from the Earth as seen by the Earth sensor and the Earth simulator which was used to calibrate the Earth sensor.

The temperatures of the primary Sun sensors and the Earth sensor during the *Ranger* 7 flight were improved over those during previous *Ranger* flights. A thermal shield was installed on the *Ranger* 7 antenna yoke to lower the temperature of the Earth sensor. The Earth sensor temperature during most of the flight was 62°F, compared to 86°F for the *Ranger* 6 flight. The maximum allowable Earth sensor temperature is 95°F. There was only a 2°F temperature difference in the two pitch primary Sun sensors for the *Ranger* 7 flight, compared to about a 10°F difference for the *Ranger* 6 flight.
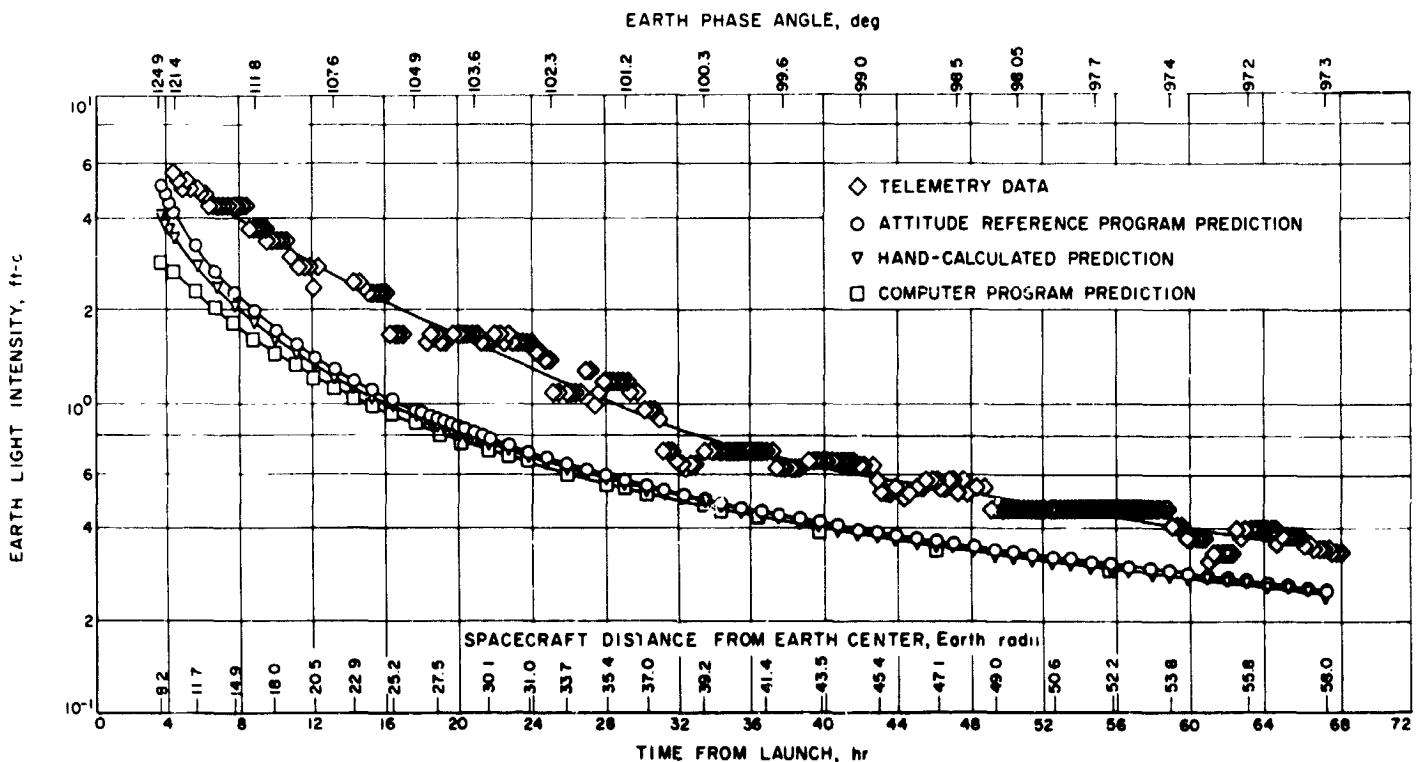

Fig. 16. Comparison of *Ranger* 7 Earth sensor light-intensity telemetry data and predicted values

2. Antenna Actuator

The function of the antenna actuato: on the *Ranger* spacecraft is to support and position the high-gain antenna. In certain operating modes (such as at launch, at the midcourse maneuver, and prior to Earth acquisition), the antenna is moved to and held in a predetermine·l fired position (Fig. 17). At Earth acquisition, the antenna position is continuously corrected to maintain orientation toward Earth.

Functionally, the actuator loop operates as a relay servo; the characteristics of the servo are such that, when the antenna position error exceeds 2 deg, the antenna is driven 1 deg to reduce the error to 1 deg.

The power required to operate the actuator is less than 4 w. No power is required to hold a position; once the commanded position is reached, the circuit remains *off* until a correction is to be applied.

Physically, the antenna actuator consists of a gear train assembly, a housing, an output gear assembly, a yoke assembly, and a dual potentiometer, with a total weight of 8.5 lb. One element of the potentiometer is used in a feedback loop for positioning the antenna at a pre-determined angle prior to Earth acquisition. (This angle is determined and set just before launch.) The other element furnishes a position signal to the telemetry.

Fig. 17. Ranger antenna actuator with yoke in stowed position

Flight performance. On the *Ranger* 7 mission, the antenna actuator held the antenna in a stowed position from launch until roll search prior to Earth acquisition, at which time it was extended to a predetermined angle of approximately 135 deg. At Earth acquisition and throughout the cruise phases of the flight, it positioned the antenna toward Earth on commands from the Earth sensor circuit. During the midcourse maneuver, the actuator, on command, moved the antenna to an extended position to clear the exhaust path of the midcourse motor. At the completion of Sun reacquisition, the Earth was in the field of view of the Earth sensor; therefore, the reacquisition of Earth took only a few seconds instead of the allotted ¹⁄₂ hr.

3. Jet Vane Actuators

Three-axis control of the *Ranger* spacecraft during the midcourse maneuver is provided by four vanes located in the exhaust stream ·f th· midcourse motor. Each of the vanes is attached to an actuator, independently controllable to rotate the vane ± 25 deg from the trail position to deflect the exhaust stream for thrust vector control. The assembly of four actuators and vanes and a mounting ring weighs 3.5 lb.

The actuator consists of a DC torquer and a dual potentiometer, whose center-tap corresponds to the null or trail position of the vane. Functioning as continuous control servos in a linear position control loop, the actuators comprise the output stage of the midcourse autopilot. During the midcourse maneuver, attitude error signals from the gyros are processed by the autopilot electronics and are applied to the torquers as DC voltages essentially proportional to the vane deflection force required.

Pitch and yaw signals are applied to the respective pair of actuators, and roll control signals are superimposed on those to all four actuators. In each actuator, one element of the potentiometer furnishes a feedback signal to the control system, and the other provides a position signal for telemetry readout.

The actuator's DC torque motor provides constant torque at constant voltage independent of position. Current drain is 60 ma at the rated torque, which is 2 oz-in.

To isolate the potentiometers from the space environment, the actuator is sealed with an internal atmosphere of 90% nitrogen and 10% helium. The allowable leak rate of 5×10^{-2} standard cm³/hr provides an ample margin over the normal duration of lunar missions.

Flight performance. During the *Ranger 7* mission, the jet vane actuators maintained the spacecraft in the attitude to which it was turned for the duration of the midcourse motor firing.

4. Attitude-Control Gas Subsystem

The *Ranger* spacecraft is stabilized after injection, positioned for various maneuvers, and held within limits during cruise, by reaction thrusts from cold-gas jets. The attitude-control gas subsystem provides the supply of gas and generates the thrusts required by the control subsystem.

As part of the redundancy concept, this subsystem consists of two identical halves mounted on opposite sides of the spacecraft. In each half-system, an equipment plate (which also serves as a shear plate in the spacecraft structure) supports a pressure vessel, a pressure regulator, a shutoff valve, a two-jet-valve manifold assembly, and a main electrical connection. Also mounted on this plate are a pressure transducer and a fill manifold with a protective filter and bleed check valve arrangement, as well as a separate test temperature transducer connection and the necessary thermal shielding. The four additional jet valves completing the half-system are mounted on legs of the spacecraft and are piped to the pressure regulator outlet.

In operation, gaseous nitrogen is initially supplied to the pressure regulator from the 231-in.^{3} pressure vessel at a pressure of 3650 psi (it may eventually reduce to 200 psi with usage) and is delivered to the various valves at 15 psi above ambient by the pressure regulator. The solenoid-operated valves expel the gas through jet nozzles in response to control demands as determined by the attitude-control subsystem. The jet valves fire in pairs, which are so located as to produce approximate couples about the yaw and roll axes. Pitch torques are not generated as couples.

Each half-system is capable of both positive and negative torques about all three axes, giving complete redundancy, in case one half-system is lost for any reason. The pressure vessel is sized to supply the worst-case conditions (as well as counteracting the thrust from a valve stuck in the open position at launch) and to provide a small reserve.

In addition to providing torques to the spacecraft for positioning, the gas subsystem is instrumented with a pressure transducer and a temperature transducer, which provide data on the high-pressure subsystem for telemetry transmission to Earth so that a gas usage analysis can be made.

Flight performance. During the *Ranger 7* flight, the gas subsystem provided torques to stabilize the spacecraft after injection, to turn it for Sun and Earth acquisition, to maintain cruise attitude within the allowable limits, and to orient the spacecraft for the midcourse correction. Gas usage was somewhat lower than nominal; no malfunctions occurred to cause excess usage provided for, and some maneuvers occurred at optimum timing.

A large quantity of data on temperatures and pressures in the two gas storage vessels was received; very stable temperatures were indicated, giving evidence of good thermal control.

References

1. Rindfleisch, T. C., and Willingham, D. E., *Figure of Merit as a Measure of Picture Resolution*, Technical Report No. 32-666, Jet Propulsion Laboratory, Pasadena, California (To be published).

2. Kirhofer, W. E., *Television Constraints and Digital Computer Program*, Technical Report No. 32-667, Jet Propulsion Laboratory, Pasadena, California (To be published).

References (Cont'd)

3. Schade, Otto, H., Sr., *An Evaluation of Photographic Image Quality*, EM-7752, pp. 24–38, Electron Tube Division, Radio Corporation of America, December 14, 1962.

4. Sytinskaya, N. N., and Sharonov, V. V., "Study of the Reflecting Power of the Moon's Surface," *Uchenye Zapiski Lgu*, No. 153, p. 114, 1952 (translated by Space Technology Laboratories, Inc., Los Angeles, California, as STL-TR-61-5110-23, May 1961).

5. Willingham, D. E., *The Lunar Reflectivity Model for Ranger Block III Analysis*, Technical Report No. 32-664, Jet Propulsion Laboratory, Pasadena, California (To be published).

6. Smith, G. M., and Willingham, D. E., *Ranger Photometric Calibration*, Technical Report No. 32-665, Jet Propulsion Laboratory, Pasadena, California (To be published).

II. *Surveyor* Project

A. Introduction

The *Surveyor* Project will take the next step in developing lunar technology by attempting soft landings on the Moon with a group of test missions whose objective is to demonstrate successful soft landing by post-landing spacecraft operation. An engineering payload including elements of redundancy, increased diagnostic telemetry, touchdown instrumentation, and survey TV will be used.

Following the test missions, the general objective is to conduct lunar exploration to extend our knowledge of the nature of the Moon and to discover and verify the suitability of sites for *Apollo* spacecraft landings. These flights will carry a scientific payload selected from the following experiments: two-camera TV, micrometeorite ejecta, single-axis seismometer, alpha-particle scattering, soil properties (surface sampler), and touchdown dynamics.

Through 1966 spacecraft will be injected into the lunar trajectory by direct ascent, using single-burn *Atlas–Centaur* vehicles. For launches prior to 1966 a 50-m/sec midcourse correction capability will exist. Launches performed in 1966 will require a 30-m/sec midcourse correction capability.

Hughes Aircraft Company is under contract to develop and manufacture the first seven spacecraft.

B. Spacecraft System Development

The following material relating to the *Surveyor* spacecraft system development was prepared by the Hughes Aircraft Company. The principal model designations and vehicles discussed are defined in Table 1.

Table 1. Model and vehicle designations

Designation	Description
SC-1—4	Flight spacecraft with engineering payload
SC-5—7	Flight spacecraft with scientific payload
A-21	Model designation for spacecraft with engineering payload (SC-1—4)
A-21A	Model designation for spacecraft with scientific payload (SC-5—7)
T-21.	Model A-21 prototype system 1st spacecraft
T-21A	Model A-21A prototype system ·st spacecraft
T-2	Simplified spacecraft for evaluation of terminal descent propulsion and flight control
S-2	Test spaceframe for vibration, shock, and static structural tests
S-6, -7	Test spaceframe for vernier propulsion system tests
S-8	Test spacecraft for flight control buzz tests

System engineering. Only slight changes in the A-21 and A-21A spacecraft configurations were made during this period. A detailed evaluation of the use of the 79 silicon controlled rectifiers on the A-21 spacecraft was made. The conditions under which their operation is marginal were defined, and circuit studies are under way to eliminate any marginal conditions.

Scientific payload. Possible incorporation of a touch-down dynamics experiment is being investigated. The auxiliaries for the seismometer, alpha scattering, and micrometeorite ejecta detection experiments were designed and activities leading to type-approval testing are approaching completion. A developmental model of the alpha scattering deployment device is being built; it incorporates a new knob for redeployment of the sensor head by the surface sampler. A change in the soil mechanics/surface sampler to enable it to reach one of the spacecraft footpads for calibration purposes is being studied. The TV approach camera is ready for assembly on SC-1, and the survey camera is receiving flight acceptance tests. Type approval testing of the survey camera is under way. Modifications have been incorporated in the variable focal length lens to correct difficulties encountered in type-approval testing. The TV mirror unit with externally detented stepping motors is expected to meet all positioning accuracy requirements after one further modification.

System analysis. The analyses reported include: (1) a study of time-of-flight uncertainty, (2) a determination of the effect of error in midcourse correction time on landing accuracy, (3) an examination of conditions under which moonlight might cause loss of lock in the Canopus

sensor, (4) development of a statistical method for determining position and thrust of the roll control nozzle for spacecraft stabilization in the presence of random disturbance torques, (5) an analysis of thermal control constraints on lunar day operation of the A-21A spacecraft, (6) design of the mission sequence evaluation program, and (7) development of a computer program for linearity analysis of TV pictures.

Flight control. The attitude control system functioned satisfactorily in firing of the vernier engines on T-2 while tethered from a balloon. A more refined calculation of nitrogen gas consumption for attitude control indicates that the gas supply margin is greater than previously estimated. Chassis core material in the flight control electronics unit was changed from a foam to a honeycomb to overcome separation of components from the circuit boards under vibration.

Electronics. A procedure for custom tuning of the planar array antennas was developed to overcome excessive VSWR encountered with some antennas in thermal-vacuum tests. A new thermal control scheme was determined to keep the temperature of the altitude marking radar within permissible bounds; two test versions of the marking radar with performance improvements are being evaluated. The first flight-type radar altimeter and doppler velocity sensor (RADVS) was delivered from Ryan, and the S/N-1 model is nearing completion of type-approval tests.

Electrical power supply. Acceptance testing of the second flight-type solar panel was completed. Of 10,000 solar cell modules received to date from Heliotek, 99% have been acceptable for flight. The space calibrated solar cell — solar panel correlation program was completed. Four prototype main batteries with the new cell design passed type-approval vibration tests; performance in preliminary thermal-vacuum tests was satisfactory.

Thermal control. A study of the Compartment B wiring harness indicates that harness heat losses are less than expected, which improves the compartment performance estimate. Thermal control requirements for the vernier engine were defined for Reaction Motors Division (RMD); the change from aluminum to titanium for the propellant tanks will require use of tank insulation blankets. A portion of the solar-thermal-vacuum tests conducted previously at JPL on the MT-1 Sector I thermal test spacecraft was repeated in the Hughes space simulator; the results confirmed that the environments of the two facilities are similar.

Engineering mechanics. Burst testing of the fourth type-approval shock absorber indicated adequate strength. New thermal control coatings and variation of preload with temperature were evaluated on a shock absorber in the MT-1 landing gear. The mathematical model for modal vibration of the S-2A vehicle is being modified to suit the upgraded vehicle. Type-approval vibration testing of the S-2A vehicle has started; a motor housing fracture in the antenna/solar panel positioner during lateral vibration is being investigated.

Spacecraft vehicle and mechanisms for basic bus. Test vehicle assembly included upgrading of the structural test vehicle (S-2A) and the current upgrading of the T-21 system test spacecraft prior to resumption of system functional tests in mid-September. A new backup vehicle for the T-2 descent tests is being built, and the first flight-type spacecraft, SC-1, is being assembled for system tests to start in early September. In the mechanisms area, the two omnidirectional antenna mechanisms for the SC-1 spacecraft completed flight-acceptance tests. A developmental antenna/solar panel positioner with modifications to meet higher loads has been built for test on the S-2A vehicle. The detent mechanisms for TV mirror stepping performed satisfactorily in life tests.

Reliability, quality assurance, and system test. Reliability analysis and vendor surveillance continued during the period. The reliability test program was started, and improvements in both the Canopus sensor and the auxiliary battery will result from the tests. An active quality assurance effort, including technical problem investiga-

tion, subcontractor audit, field operation surveillance, and type-approval test review was carried on during this period.

The former spare vehicle for the descent system tests, T-2S, was upgraded to replace the destroyed T-2 vehicle and was successfully drop-tested in a partially complete configuration from a balloon at Air Force Missile Development Center (AFMDC) to verify the improved recovery system. The complete T-2S system, including vernier engines, was then operated while tethered from the balloon. Descent tests are planned to start in September. Testing of the RADVS and associated equipment in the T-2H helicopter installation was successfully concluded. System functional testing of the T-21 spacecraft disclosed problems to be corrected in the current upgrading of T-21; RFI and static discharge tests were completed and preparations are being made for the vibration and thermal–vacuum–solar test phases.

Mission operations. From initial tests of command and data handling console compatibility with the Goldstone Deep Space Station, no basic equipment problems are expected in the formal tests to follow. Assembly of the safety console that will accompany the spacecraft from the explosive safe area to the launch pad is approaching completion; detailed procedures for conducting this transport were formulated. A system was worked out for supplying Air Force Eastern Test Range (AFETR) with omnidirectional antenna patterns to aid in tracking and data validation. Two of the three operations consoles to perform power and safety functions during the prelaunch period have been built.

THE PLANETARY—INTERPLANETARY PROGRAM

III. *Mariner* Project

A. Introduction

The early objective of the Planetary-Interplanetary Program is the initial probing of the planets Mars and Venus by unmanned spacecraft. The initial probing of Venus was successfully accomplished by *Mariner 2*. The next step toward this objective is the initial probing of Mars by two *Mariner C* spacecraft planned for the 1964-1965 opportunity.

The primary objective of the *Mariner C* mission (*Mariner* Mars 1964 Project) is to conduct closeup (flyby) scientific observations of the planet Mars during the 1964-1965 opportunity and to transmit the results of these observations back to Earth. The planetary observations should, to the greatest practical extent, provide maximum information about Mars. TV, cosmic dust, and a reasonable complement of fields and particles experiments will be carried. In addition, Earth occultation experiment equipment will be carried on at least one of the spacecraft to obtain data relating to the scale height and pressure in the atmosphere of Mars. The occultation experiment may be waived on the second mission if such action maximizes its probability of success.

A secondary objective is to provide experience and knowledge about the performance of the basic engineering equipment of an attitude-stabilized flyby spacecraft during a long duration flight in space farther away from the Sun than the Earth. An additional secondary objective is to perform certain field and/or particle measurements in interplanetary space during the trip and in the vicinity of Mars.

Plans have been made for two launchings of the *Mariner C* design spacecraft from two separate pads. All activities will be planned to exploit the limited launch period to the maximum extent. To accomplish this, spacecraft and launch vehicles will be processed in parallel, so that following the launch of the first spacecraft, the second may be launched without delay, no earlier than two days after the first.

Both *Atlas D* vehicles have arrived at the Air Force Eastern Test Range (AFETR). The first *Atlas* was erected on Launch Complex 13 in preparation for the combined system test. The first *Agena D* is also at AFETR and the second is scheduled for shipment early in September.

The first of the flight spacecraft (Mariner C-2) successfully completed system tests and was shipped to the AFETR for the launch preparation. The second flight spacecraft (Mariner C-3) will be subjected to the same test sequence in about 2 wk. Mariner C-4 (spare) spacecraft testing will follow in approximately another 2 wk. No problem areas have been found in any of the systems which would preclude launching on schedule.

B. Spacecraft Systems Testing

1. First Flight Spacecraft (Mariner C-2)

The first Agena matchmate test, which consisted of mating the spacecraft with the Agena flight adapter and shroud, was performed successfully. The formal precountdown and the simulated countdown were completed. Operational support equipment problems experienced during precountdown would have delayed the launch, and operational support equipment would have again caused a hold on the launch day; however, the countdown was very successful. The procedures and personnel were checked out satisfactorily, and the actual countdown procedure was finalized.

A matchmate test with the spare adapter and shroud was performed. There was an unacceptable amount of RF leakage in the shroud, and several items needed to be sealed to permit spacecraft purging. The inflight disconnect was 180 deg out-of-phase, the spacecraft V-band safety straps came in contact with the louvers, the separation-initiated timer bracket was found to be too close to the spacecraft thermal shield, and the transporter hardware boxes interfered with the shroud guide-rail system. These problems will be corrected prior to flight.

System Test 2 consisted of engineering exercises, cruise science and radio checks, a normal encounter, playback of one picture, a two-lines scan of all other pictures, and a cruise-science statistical data quiet test. The spacecraft was in a flight configuration except for a nonflight Canopus tracker, a Mariner C-1 radio subsystem, and a nonflight nonreal-time automation system. The over-all system test results were satisfactory.

The spacecraft was suspended in the 25-ft Space Simulator and all direct-access cables were installed. A system verification test was performed. The chamber doors were closed and spacecraft power was turned on. Spacecraft operation was satisfactory until it was discovered that the Canopus tracker was not operating properly. Atmospheric conditions were restored, and a test indicated that the high-voltage circuitry had failed. The type-approval tracker was installed and tested satisfactorily. The chamber doors were then closed again, a vacuum established, and RF power turned up.

The test sequence was resumed with the post-injection propulsion system maneuver and continued satisfactorily for 250 hr of uninterrupted time followed by 90 hr in a minimum-operational-support-equipment-test-cables configuration. During the early part of the test sequence the magnetometer z-axis came out of saturation several times. The question is whether the magnitude of the Earth's field, as seen by the magnetometer z-axis sensor, went to a low value or whether the instrument partially failed during these periods. This problem is under investigation.

2. Second Flight Spacecraft (Mariner C-3)

System Test 1 was conducted to obtain a brief survey of the over-all spacecraft; difficulties with the science operational support equipment were corrected. A formal matchmate test was performed with the spare adapter and shroud; results were satisfactory. The spacecraft was mated with the flight adapter and shroud, and a formal precountdown test was accomplished. Several difficulties experienced during this test (e.g., the cosmic dust detector did not reset, and TV picture noise spots were produced) are being investigated.

The simulated countdown was successfully performed. The test team went through the complete normal exercise (including some typical holds from the booster and range areas), and in a real countdown the spacecraft would have been launched.

System Test 2 was performed with all flight hardware installed on the spacecraft except for the Canopus tracker, radio system (dual-cavity amplifiers), prototype magnetometer, prototype science cover, and prototype cosmic-dust detector. Problems during the test were: (1) the radio had a low power output; (2) the magnetometer experienced a z-axis dropout of null during quiet periods, and did not have the capability of the 60-gamma nulling steps incorporated in the operational support equipment; and (3) the TV could not be put into fast shutter with the cover lights, and five words were lost at the

end of each picture line, in addition to two lines lost at the end of each picture. These problems are not considered serious.

3. Proof Test Model (Mariner C-1)

A compatibility test between the Space Flight Operations Facility and the spacecraft was conducted. Launch plus the Sun and Canopus acquisition modes were performed twice; no spacecraft failures occurred. Two midcourse maneuvers were performed. The first maneuver was aborted due to difficulty in updating output data. During the second maneuver, an inadvertent encounter science command was issued to the spacecraft. Testing proceeded with this nonstandard operation, and full recovery was obtained within 1 hr. The spacecraft was then exercised through two encounter modes and one playback mode. All spacecraft functions were normal.

The spacecraft was vibrated in the x-y plane and the z-axis; no visual damage was observed. Special noise investigations revealed that: (1) data encoder susceptibility to half-phase resets and loss of sync in the lower decks occurred when the power system was put into and out of boost mode; (2) the hybrid radio system switched power amplifiers every time the spacecraft boost-mode on, off commands were issued, and (3) effects of high-voltage breakdown in the spacecraft circuitry could be eliminated by appropriate filtering on all lines going to the ultraviolet experiment or by isolating the ultraviolet photometer cabling.

The on-board spacecraft logic concerned with monitoring, switching, and inhibiting functions was examined; satisfactory results were obtained. In order to obtain a basis for a comparison of free-mode and cable-mode testing, the free-mode test procedure was performed while the spacecraft was connected to the system test complex with all direct-access cables.

A free-mode test established the compatibility of the solar panels and spacecraft, the ability of the spacecraft to give valid data even though connected to direct-access cables, and the adequacy of the on-board circuitry to operate in a sharing mode with the battery and on full solar power. The test was considered very successful and demonstrated that the transients that affected radio power amplifier and exciter switching, data encoder half-phase resets, and data encoder deck skipping were also present when there were no connections to the operational support equipment.

The transfer of radio power amplifiers and exciters, the data encoder half-phase resets, and the deck skipping phenomena which occurred with power transients were investigated. The skip deck phenomena could not be isolated to a single circuit and were probably the result of cumulative pickup in cable harnessing in general; they are not considered a serious problem. Radio switching originated in the command isolation pulse switch; the half-phase reset originated in the spacecraft harness. Design changes were made to eliminate these power transients.

The free-mode configuration was again established so that magnetometer personnel could see the current-field changes in this configuration. A special Helmholtz coil was used to take the magnetometer sensor out of saturation; the initial results indicated that the current field was insignificant.

A parameter variation test was run to establish if margins of operation had increased as a result of changes incorporated in the power subsystem. The spacecraft was operated through five modes of parameter variation, and in all cases normal spacecraft functions were observed up to the encounter phase. During encounter the video storage data automation system and TV would not operate properly. The Canopus tracker operated normally in all the tests, as well as on the backup 38.4-kc isolator in the power subsystem and on the free running mode of the power subsystem.

Video storage and encounter science systems were run through a special test at ±2% frequency variations. Performance of all systems was normal. Video storage also worked well when recording at +2% and playing back at −2%.

4. Data Simulation

The preflight mission simulation capability of the Mariner Mars 1964 project has progressed steadily. This capability is being used to test the Space Flight Operations System [the Space Flight Operations Facility at JPL, the Deep Space Instrumentation Facility (DSIF), and the Air Force Eastern Test Range (AFETR) launch site] under simulated flight conditions, to develop hardware, to check out computer programs, and to train personnel.

A prime requirement is to simulate the data to be sent from the Mariner spacecraft during the actual mission. This will consist of tracking data (antenna angles and

received doppler frequency count); and telemetry data (engineering and science experiment measurements transmitted by the spacecraft radio system). Preflight tracking data must, of necessity, be computer generated; telemetry data may be derived directly from the spacecraft itself, although this source is of limited usefulness due to the many constraints imposed by the ground environment. Computer programs are being developed for the generation of both tracking and telemetry data.

Computer programs for the simulation of tracking data are currently based upon the actual programs used in the reduction of tracking data during the mission. In order to render the reduction of this data nontrivial and realistic, discrete known perturbations are added during the simulation process. The end product of the tracking data simulation is a package of data for each test, in the DSIF or AFETR formats. A realistic trajectory is plotted which upon reduction may require a midcourse maneuver or other correction action. These data are transmitted to the SFO complex during the test, with the insertion point being either local or at a remote site, depending largely upon the over-all test objectives. Personnel and facilities in the operations complex process these data as they would during the actual flight.

At this time, tracking data are generated with the JPL orbit determination program (ODP) by a data tape containing prediction information computed by the ODP. This data tape is then read by one of two computer programs (one for AFETR data punching, the other for DSIF data punching) and punched into standard format cards on teletype tape. This method is somewhat undesirable for the following reasons: (1) The ODP computers transmit only center-count doppler, while the DSIF stations normally transmit end-count doppler; (2) ODP input restrictions are not compatible with simulation requirements; (3) there is no adequate way to check out the calculation of the data types in the ODP (other than hand calculation), and therefore an error in these calculations might not be caught until a mission is flown; (4) because the ODP must be capable of fitting real data in a reasonable time; and (5) it is generally undesirable and often extremely difficult to add improved models in a flight program such as the ODP.

A more comprehensive tracking data simulator computer program is currently being developed to meet the increasing requirements for providing more realistic tracking data for mission simulation. Some of the capabilities of the program are: (1) simulation of acquisition characteristics such as switching from the acquisition aid to the main antenna, acquisition in one-way, two-way, or three-way, and generation of search patterns; and (2) simulation of powered flight portions of the trajectory such as booster burns, retros, midcourse and terminal burns.

Computer programs used for the generation of telemetry are not true spacecraft simulators in that they do not calculate the various telemetry measurements from a mathematical model of the spacecraft. Rather, they plan functions and formats which process data tables of the normal time-versus-function value relationships supplied by engineers familiar with each spacecraft subsystem. The computer simulates the commutation function of the spacecraft data encoder, sampling the various measurements in the proper sequence; and, with appropriate scaling conversion factors, provides as output a digital magnetic tape having a bit configuration equivalent to the spacecraft bit stream. These resulting data are used to modulate appropriate data and synchronization subcarrier signals in real-time during the SFO tests. For tests involving remote DSIF playback of data, analog recordings of the composite signal are supplied to the DSIF sites, where the signal is relayed through the station's data-handling system (the DSIF to Pasadena communications link) and hence into the control and operation facility at JPL. There the data are processed by a control and data-handling system and analyzed in real-time by spacecraft performance analysts. When these data are received concurrently with tracking data, a realistic mission is simulated.

5. Spacecraft Simulator

The function of the spacecraft simulator is to test the launch complex facility, including the operational support equipment (OSE) launch pad, the blockhouse installation areas, and the umbilical connector interface on the spacecraft. It is, as its nomenclature implies, the electrical counterpart simplified to make it a portable piece of test equipment. It may be carried and operated by one man. The panel layout and chassis view is given in Fig. 1.

The waterproof case is 18 in. wide, 17½ in. high, and 11 in. deep. Cables are stored in a compartment located in the lid, bringing the total weight of the unit to 25 lb.

Power voltage sources are independently variable. This capability is nonexistent in either the spacecraft or other test equipment.

Fig. 1. Panel-chassis assembly

A form of the air-half umbilical receptable (Fig. 2) is mounted in the simulator. This is accessible under a hinged door in the case. To facilitate mounting, the funnel housing has been removed, since it is not needed. Power connectors and test points are provided under a door on the opposite side of the simulator.

The catenary umbilical launch complex cable can be connected to the simulator, and all OSE functions and operations can be performed as if a spacecraft were being tested. The simulator checks the operation of the cabling and its wire conductivity, the umbilical tower junction box and amplifier, and the signal condition and operation of each of the OSE subsystems. Cali-

bration adjustments on equipment can be made from signal sources within the simulator.

C. Design and Development

1. Flight Command Subsystem

Command subsystem operation. Mariner C flight command subsystem design is similar to that of the Mariner R. The command subsystem (Fig. 3) consists of two major functional units: the command detector and the
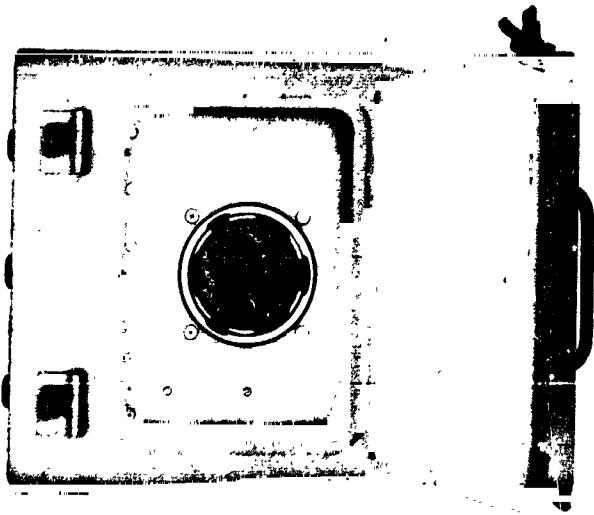
Fig. 2. Spacecraft umbilical receptacle
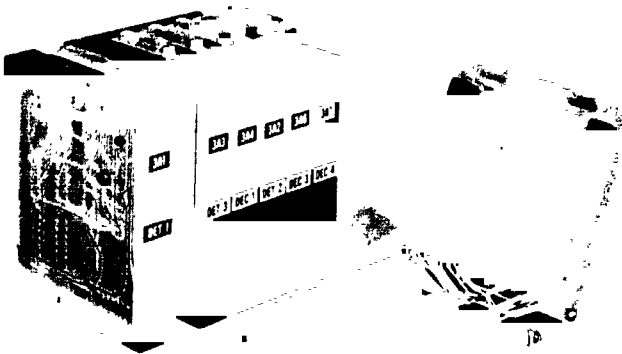
Fig. 3. Command subassembly

command decoder. Also included is a transformer rectifier unit which converts the spacecraft 2.4-kc voltage into the AC and DC voltages required by the subsystem.

A simplified block diagram of the detector is given in Fig. 4. The detector receives the composite command signal subcarrier from the radio system. The subcarrier contains the command word information (a sequence of binary digits) in the form of a biphase modulated sinusoidal signal added to a synchronization (sync) signal.

A simplified block diagram of the command decoder is given in Fig. 5. Upon recognition of the decoder start

bits, the decoder sequences a binary counter with the detector bit sync pulses. At the correct bit sync pulse, the decoder matrix is interrogated. Depending on the address bits stored in the decoder address storage flip-flops, one of the *nand* gates is gated to close an output isolation switch (or switches) in the case of a direct command (DC). For a quantitative command (QC), the interrogation permits the QC command bits to be directed to the spacecraft central computer and sequencer (CC&S) subsystem along with QC bit sync pulses. When no QC bits are transmitted to CC&S, alert pulses are directed, one per second, to the subsystem to clear the QC command storage registers.

If an out-of-lock indication occurs during decoder function, the decoder generates an inhibit signal which immediately stops the decoder command word processing and allows no further decoder functioning until 26 consecutive command zero bits are directed to the decoder after the lock signal indicates in lock once again.

Command subsystem telemetry. Three command subsystem signals are directed to the spacecraft telemetry subsystem to be telemetered to Earth. The signals time-share the telemetry transmission channel and are sampled at a rate determined by the telemetry mode.

Detector bit sync pulses are sent to the telemetry subsystem to be conditioned into information concerning the detector VCO frequency. Between telemetry data sample times, reference pulses at the spacecraft 2.4-kc frequency are counted in the interval between two consecutive bit sync pulses. The number counted is indirectly proportional to the VCO frequency. Thus, an average of the VCO frequency (over an approximate 1-sec interval) is telemetered each telemetry-data sample time. The VCO frequency data are required to determine the proper ground command signal frequency that will minimize command lock acquisition time.

The detector lock signal is directed to the telemetry subsystem to be converted into one bit of information regarding the detector lock condition. If the lock signal indicates out-of-lock for at least 1 sec in the interval between telemetry sampling times, the detector lock telemetry data will be at the binary state, indicating out-of-lock at the next sampling time. If no out-of-lock indications occur, the binary state indicating in lock will result. The detector lock data indicate when the command subsystem is capable of detecting and processing the command signal.
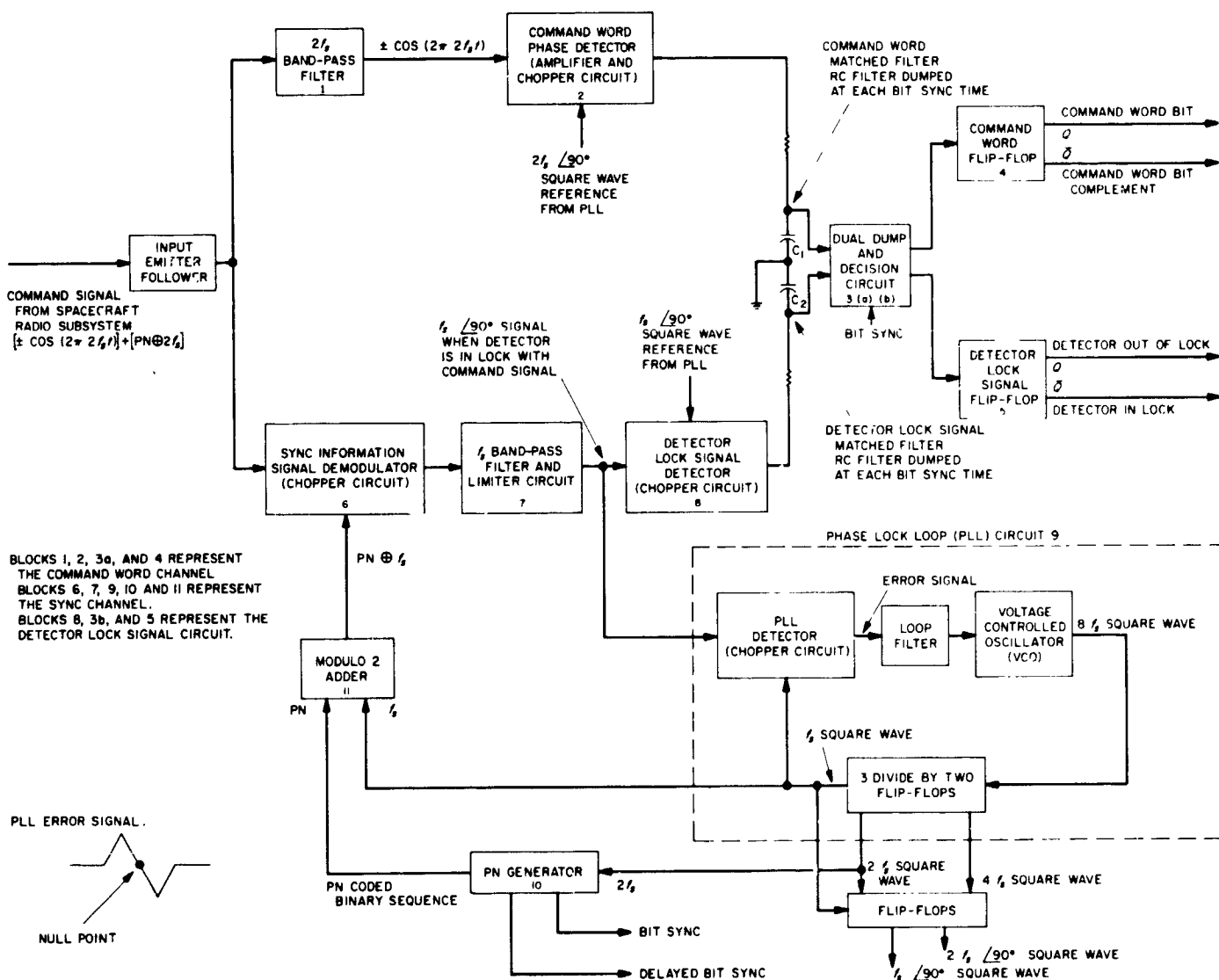
Fig. 4. Command detector simplified block diagram

Command event pulses are telemetered approximately 10 sec after the command decoder has recognized the decoder start bits of a command word. The event pulse indicates normal decoding timing function upon reception of the start bits. It is also normally coincident with a command address recognition and a DC command execution by the decoder. In the case of a QC command, a second event pulse will be telemetered, immediately after the last QC bit is directed to the CC&S subsystem.

2. Telemetry System

The Mariner C telemetry system is very similar to the Mariner R system used successfully in 1962. The main difference is the allocation of more power to synchronization for Mariner C, and the use of a square-wave subcarrier where a sine wave was used for Mariner R.

Basically, both telemetry modulation systems are PCM/PSK/PM—that is, continuous information is quantized (pulse coded) into binary bits, which control the phase (phase shift key) of a subcarrier, which phase modulates the main RF carrier. Furthermore, both systems are coherent, with power being allocated to a separate synchronizing subcarrier which is used to produce bit and word timing pulses in the ground demodulator. This synchronizing information is continuously transmitted down the channel, in parallel with the data subcarrier. Both systems are uncoded in the sense that no error
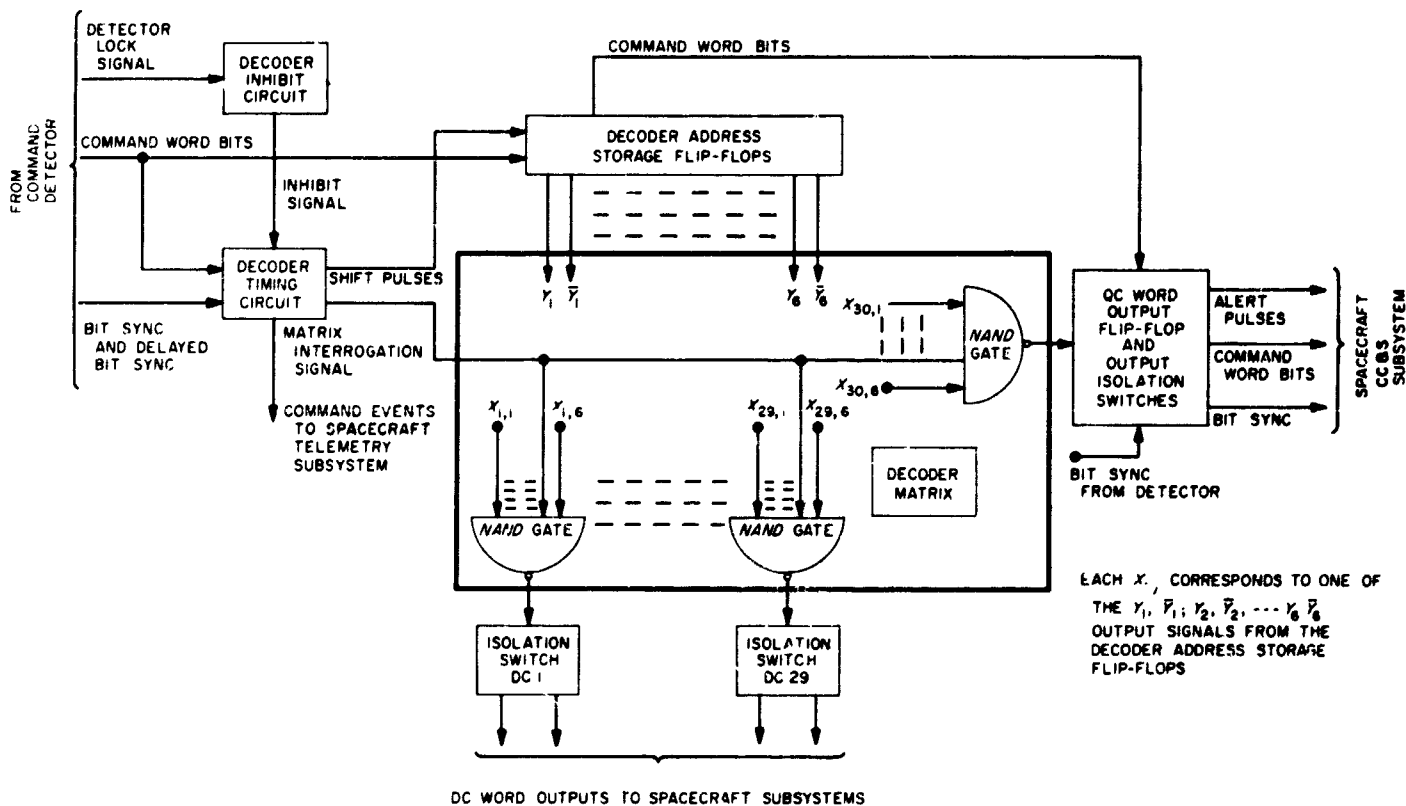
Fig. 5. Command decoder simplified block diagram

detection capability is inherent in the encoding into channel words. A pseudonoise (PN) code is used as a "pilot tone" for synchronization.

Fig. 6 is a partial diagram of the Mariner C S-band telemetry ground receiver. The telemetry output is derived in the receiver by multiplication of the modulated carrier at an IF by a reference derived from the carrier-tracking loop. The multiplier (carrier demodulator) input is taken from the receiver IF after the limiter which
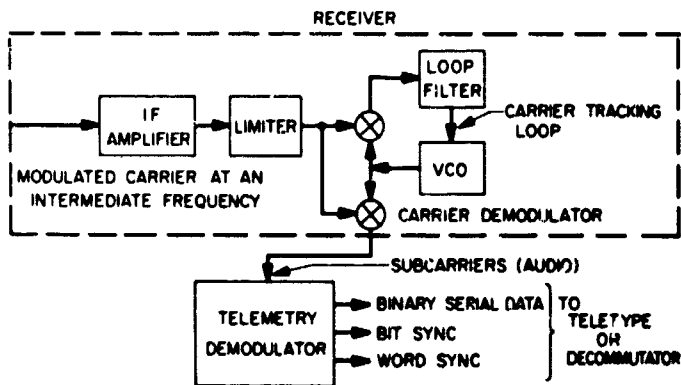
Fig. 6. Receiver-demodulator interface

precedes the loop. Consequently, there are no large voltage excursions at the telemetry output.

The pertinent parameters of the Mariner C telemetry receiver are: IF bandwidth, 4.5 kc; two-sided loop bandwidth at threshold, 12 cps; limiter suppression factor at threshold, 0.075.

Fig. 7 is a block diagram of the telemetry demodulator, which is the almost fully automated ground equipment that reconstructs telemetered binary data from the noisy audio output of the S-band ground receiver and sends outputs to a teletype encoder, decommutator, or computer. The demodulator has three major functional elements: the data recovery channel, the code acquisition channel, and the clock reconstructor.

3. Canopus Tracker

The Canopus tracker design is frozen and has been environmentally qualified (Fig. 8). The structural fraction of the weight is 38.4%, which includes the chassis and the dust covers and all aluminum parts. Low weight has been achieved for a chassis resonance of 350 cps. Low power consumption can be attributed to: (1) the
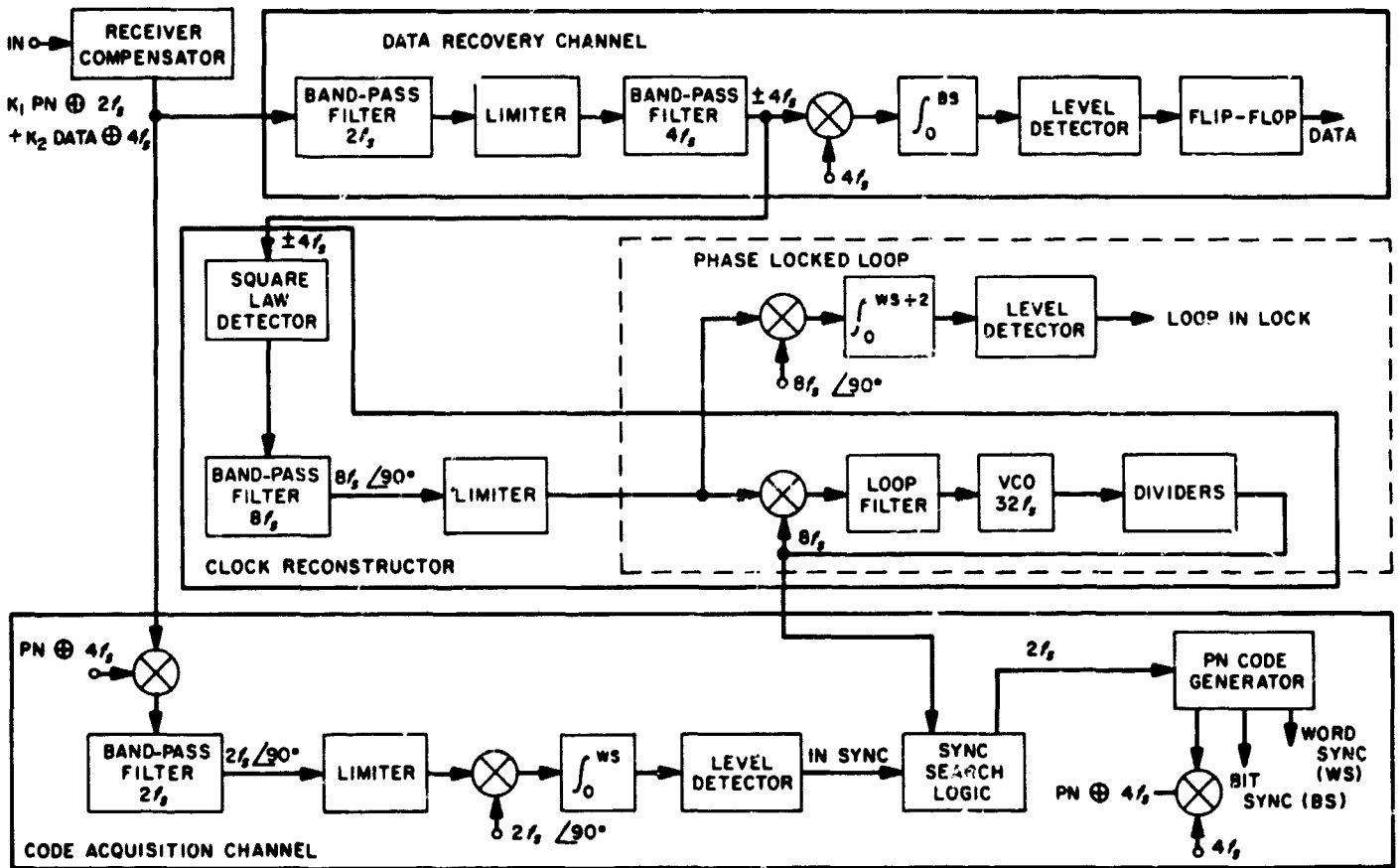
Fig. 7. PCM/PSK telemetry demodulator

use of an all-electrostatic image dissector, and (2) the use of a high-efficiency, series-resonant, intermediate, high voltage power supply.

The tracker generates an analog DC voltage which is proportional to the intensity of the star in the field of view. This signal drives the acquisition gate and is telemetered back to Earth for use in identifying the star which has been acquired. Large dynamic range of the telemetered intensity is obtained by utilizing the high voltage on the electron multiplier. This voltage is a function of star intensity since the star signal is servo-controlled to a constant output by adjusting the voltage on the electron multiplier. The faintest detectable star has been limited to 0.02 times Canopus by adjusting the maximum voltage capability of the high voltage power supply. The high voltage has been limited to minimize the stress on the components.

The ability of the Canopus tracker to reject the stellar background is limited by: (1) the uniformity of the over-all sensitivity within the scanned field of view, and (2)

the shot noise inherent in the photocurrent caused by the background. The degree to which a particular unit is limited by shot noise or uniformity can be determined by inspection of a graph of apparent intensity versus background brightness. If the apparent intensity increases as the square root of the background, shot noise is controlling the response of the tracker. If the apparent intensity increases linearly with the background, non-uniformity of sensitivity is controlling the response of the tracker. Fig. 9 compares the response of two of the flight trackers with an estimate of the response of the tracker to a flat background, assuming the sensitivity is perfectly uniform and that the response is caused by shot noise. The reason that the flight trackers appear to be less sensitive to flat backgrounds than to the calculated theoretical limit is because of uncertainties in the assumption upon which the estimate was made. The largest uncertainty is response of the intensity channel to noise. It is significant that S/N 003 is free from nonuniformities in sensitivity since the apparent intensity goes as the square root of the background brightness. This demonstrates that the optical system is free from vignetting within the scanned field of view.

Fig. 8. Canopus tracker flight unit with and without cover

Fig. 9. Response of two flight trackers compared with estimated response to shot noise

Superimposed on the flat background calibration (Fig. 9) is the brightness of the background of several areas of the sky. Also shown on the plot are the minimum pull-in and drop-out intensities of the flight trackers. Since the absolute brightness of the sky plotted on Fig. 9 is uncertain by a factor of two, the margin between the low gate and the background makes the probability of automatic Canopus acquisition substantially less than one.

Tests have been made on a model of the Milky Way which simulates the brightness and brightness gradients

of the Milky Way near Canopus. The data used have a resolution of 2.5 × 2.5 deg and include all stars of 7.0 visual magnitude and dimmer. Fig. 10 is a photograph of the brightness model which was constructed using paints with calibrated reflectance. Since the triangular patterns cannot be resolved by the tracker, they appear as a smooth gradient of brightness.

The results of scans through the model Milky Way have shown that the largest roll error signal is less than 4 v, so there is little chance of acquiring the Milky Way and going into a broader than normal limit cycle. However, it is possible to have a faint star plus a Milky Way background and still be within the gate and give the proper error signal for acquisition. If this occurs, a roll override radio command may be sent from the Earth to continue search. Models are currently under construction which will simulate both the Milky Way gradients and the discrete stars which are found on that background. Through these models, it will hopefully be learned how the tracker will respond during the roll search.

Image dissector. Qualification of the image dissector has been the biggest problem encountered in the development of the Canopus tracker. A rugged tube program was finally evolved which attacked the fundamental engineering problems—the high stress on the wires at the stem and the weldability of the assembly. Fig. 11 shows the two primary changes which were made in the design—the snubbers that constrain the multiplier in the glass envelope, and the necked stem lead to make it more weldable while retaining the required flexibility

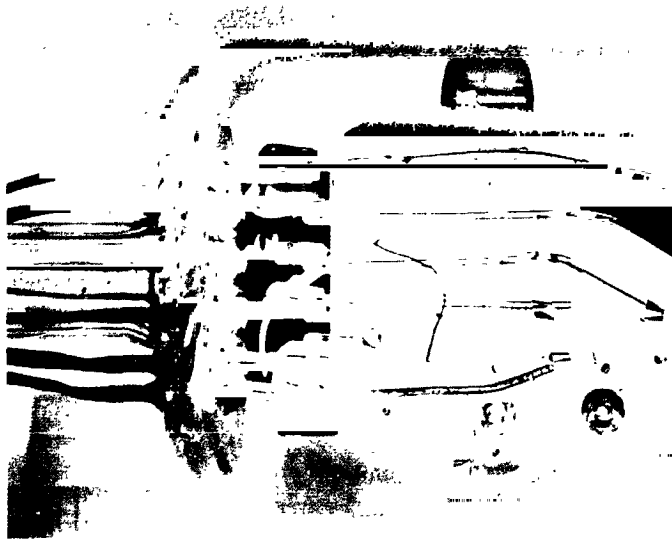Fig. 10. Brightness model of the Milky Way near Canopus

Fig. 11. Structure of rugged image dissector tube

Fig. 12. Baffle and assembled optics of
Canopus tracker

in the external leads. This tube has passed a full-level component type-approval test.

Optics assembly. Because of tracker susceptibility to spacecraft stray light and bright objects (like the Earth) 10 to 25 deg outside the field of view, considerable effort has been expended to minimize the intensity of stray light reaching the image plane. The aluminizing patterns on the catadioptric lens were modified The edges of the lens were polished and painted with Cat-a-lac paint. The lenses were refabricated using the highest grades of synthetic quartz and light flint glass. The flight lenses are image-plane quality, have exceptional polish and are free of bubbles and other defects. The front element has been tested for radiation susceptibility, and no degradation is expected. Since the geometric speed is $f/0.6$, centering and mounting are critical; however, no problems have been encountered. An assembled set of optics and a baffle assembly are shown in Fig. 12.

Baffle assembly. The ability of the tracker to operate without being disturbed by stray light is strongly affected

by the effectiveness of the baffles to attenuate light coming from outside the field of view. The baffles are made of black-anodized aluminum and have sharp knife edges (approximately 0.0001 in. radius). The "as anodized" surface is quite specular and its diffuse reflectance is about 0.6%. The use of 3M Black Velvet paint on the baffles improved the sensitivity to stray light by a factor of 2

High-voltage magnetics. The original high-voltage magnetics designed for the tracker utilized random-wound toroidal cores to obtain a compact, low-field device. However, during testing failures occurred in a high-voltage transformer and a high-voltage inductor, and both parts were redesigned. The random-winding was replaced by a progressive bank-wind in which the highest voltage turn and the lowest voltage turn were separated by a physical barrier, and the winding was controlled to assure the minimum gradient between all adjacent turns. This type of winding has a less efficient packaging factor, requiring the selection of a higher permeability core material for identical performance and over-all size. Tracker tests confirmed that the new units have identical performance haracteristics, and special destructive tests indicated that the voltage breakdown level has been increased by a factor of 10.

THE DEEP SPACE NETWORK

IV. Introduction

The Deep Space Network (DSN) is a precision communication system which is designed to communicate with, and permit control of, spacecraft designed for deep space exploration. The DSN consists of the Deep Space Instrumentation Facility (DSIF), the Space Flight Operations Facility (SFOF), and the DSN Ground Communication System.

The DSIF utilizes large antennas, low-noise phase-lock receiving systems, and high-power transmitters located at stations positioned approximately 120 deg around the Earth to track, command, and receive data from deep space probes. Overseas stations are generally operated by personnel of the respective countries. The DSIF stations are:

Station	Location

Goldstone
  Pioneer site
  Echo site
  Venus site (R&D)
  Mars site (under construction)
	Goldstone, California

Woomera	Island Lagoon, Australia
Canberra (under construction)	Canberra, Australia
Johannesburg	Johannesburg, South Africa
Mobile Tracking Station	Johannesburg, South Africa
Madrid (under construction)	Madrid, Spain
Spacecraft Monitoring	Cape Kennedy, Florida

The SFOF is located in a three-story building at the Jet Propulsion Laboratory in Pasadena, California, and utilizes operations control consoles, status and operations displays, computers, data processing equipment for analysis of spacecraft performance and space science experiments, and communication facilities to control space flight operations. This control is accomplished by generating trajectories and orbits, and command and control data, from tracking and telemetry data received from the DSIF in near real-time. The SFOF also reduces the telemetry, tracking, command and station performance data recorded by the DSIF into engineering and scientific information for analysis and use by the scientific experimenters and spacecraft engineers.

The DSN Ground Communication System consists of: voice circuits, and normal and high data-rate teletype circuits provided by the NASA World-Wide Communications Network between each overseas station and the SFOF; teletype and voice circuits between the SFOF, Goldstone Stations, and Cape Kennedy, and a microwave link between the SFOF and Goldstone, provided by the DSN.

The DSN has facilities for simultaneously controlling a newly launched spacecraft and a second one already in flight. Within a few months, it will be able to control simultaneously either two newly launched spacecraft plus two in flight, or the operations of four spacecraft in flight

at the same time. The DSIF is equipped with 85-ft antennas having gains of 53 db at 2300 Mc and a system temperature of 55°K, making it possible to receive significant data rates at distances as far as the planet Mars. To improve the data rate and distance capability, a 210-ft antenna is under construction at the Goldstone Mars site, and two additional antennas of this size are scheduled for installation at overseas stations.

It is the policy of the DSN to continuously conduct research and development of new components and systems and to engineer them into the DSN to maintain a state-of-the-art capability.

The DSN is a NASA facility, managed by JPL through a contract between NASA and the California Institute of Technology. The Office of Tracking and Data Acquisition is the cognizant NASA office.

Section V that follows is a digest of the information that appears in SPS 37-29, Vol. III.

V. The Deep Space Instrumentation Facility

A. Tracking Stations Engineering and Operations

1. Ranger 7 Tracking

The *Ranger 7* spacecraft was launched with the *Atlas D/Agena B* booster system from Cape Kennedy on July 28, 1964. Liftoff occurred at 16:50:07.873[1] Greenwich Mean Time[2] (GMT in hours, minutes, and seconds), and injection into the lunar transfer orbit at 17:20:01.0.[1] DSIF Stations provided continuous angular and doppler tracking data from initial acquisition by the Mobile Tracking Station, Johannesburg at 17:20:50, July 28, until lunar impact at 13:25:50.029,[3] July 31. In general, the over-all quality of the tracking data was extremely good. Data

---

[1] Liftoff and injection times reported by Air Force Eastern Test Range.

[2] All times referred to will be GMT unless otherwise noted.

[3] Impact time recorded at Goldstone Echo site does not include signal propagation time correction.

---

types used in the Orbit Determination Program were angular data taken during the first pass over Woomera and Johannesburg, two-way doppler taken during the first pass over the Mobile Tracking Station, and two-way doppler taken during all passes over Goldstone Echo site, Woomera, and Johannesburg.

2. DSIF/Mariner C Tests

The RF portion of the DSIF/*Mariner* C tests was conducted at Goldstone to ascertain the signal levels when loss of carrier signal was reached. Values were determined for the down-link conditions with and without telemetry modulation applied to the spacecraft radio system. Similarly, up-link loss of carrier lock signals, and two-way loss of signal values with the presence of down-link telemetry modulation, were determined.

The DSIF receiver AGC voltage, which varies as a function of the input carrier signal level, was used to determine the received carrier level from the *Mariner* C

spacecraft. A typical plot was prepared for the various RF loop bandwidths. The accuracy of the received signal level obtained from this type of plot was determined by using parameters such as: (1) the accuracy of the known levels of inserted signal strength during subsystem calibration, (2) the stability of the receiver AGC loop and its net fixed-gain (amplifier and losses), (3) the random-phase characteristics of the actual received carrier signal, (4) resolution of the calibrated plot, and (5) the errors in interpolating from the calibration curve.

3. Mariner C 100-kw Transmitter Testing

Ground testing of the Mariner C Cassegrain cone 100-kw transmitter has been completed at the Goldstone Venus site. The 85-ft Az–El antenna was rigged with additional cabling and coolant lines to adapt it for handling the Mariner C transmitter. Fig. 1 illustrates the interior of the cone from the top; the feedhorn assembly connects to the top of the waveguide-switch port, shown covered and taped. Fig. 2 shows a Cassegrain cone in position for testing on the elevator in the high-voltage power supply building.

Fig. 2. Cone in position on test elevator
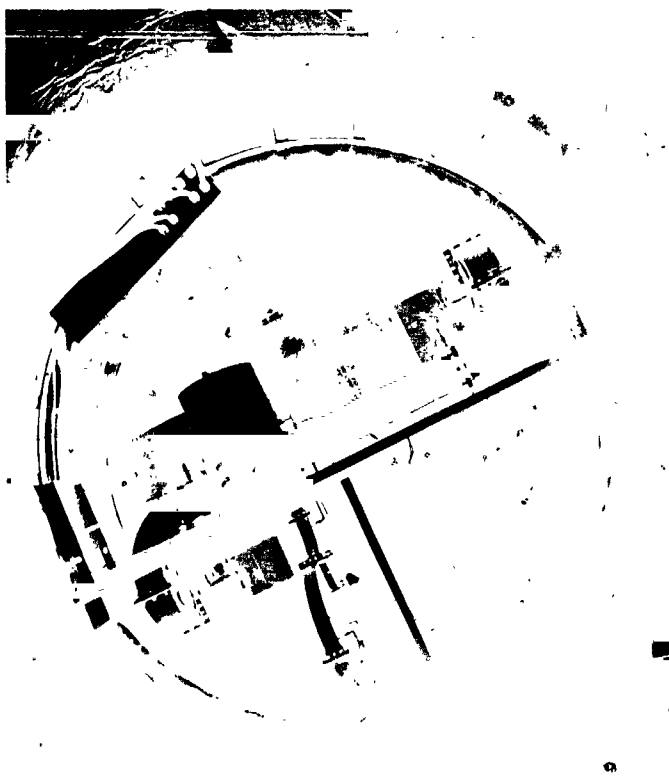
Fig. 1. Interior of Mariner C cone transmitter
(viewed from the top)

4. Ground Instrumentation for Mariner C Occultation Measurements

The Mariner C occultation experiment will attempt to measure the perturbations which are produced by the refraction of the Martian atmosphere on the radio signal received at DSIF Stations. The effects to be measured are perturbations of the received signal doppler frequency and perturbations on the received signal amplitude due to Fresnel diffraction phenomena. Since both these phenomena are time functions of short duration, it will not be possible to integrate in the manner normally used in tracking operations. If all the negative tolerances in the communications system obtain, operation will be very close to threshold. The precision of measurements made close to threshold is severely compromised by the presence of noise This takes the form of random power fluctuations in measurement of received signal strength and of intermittent loss of lock which causes gain or loss of cycles in doppler count. A simulator has been constructed to investigate the achievable performance of several different alternative receiver configurations. This simulator uses a synchronous motor to drive a cam which varies an attenuator as a function of time.

B. Communications Research and Development

1. Precision Servo Drive System for 30-ft Antenna

The primary objective of the new precision servo drive system on the 30-ft antenna at the Goldstone Venus site is to provide very precise steering over a wide speed range; this objective will provide versatile performance for test-aircraft-, satellite-, and astronomical-target tracking over a range of frequencies from S-band to 20 to 30 Gc.

The precision servo drive system was installed for the experimental measurements of the 20- to 24-Gc radiation from the planet Venus. The experiment, whose scientific purpose was to determine the water content of the Venus atmosphere, was successfully conducted on a daily basis from June 29 through July 20, 1964. Performance of the antenna and servo drive system during the entire experiment was good.

Repeated calibrated measurements of the error signal during the Venus experiment indicated that the 3-σ tracking error on either axis for wind velocities less than 22 mph is well within the required +0.006 deg in the design specification. By repeated RF boresighting on the radiation from Venus, it was established that the absolute steering of the beam to within a tenth of the 0.1-deg beamwidth was well within the system capability.

2. Structural Computing Programs for 85-ft Antenna Reflector

The structural data of one-half of the reflector structure of the 85-ft Az–El antenna were inputted in the STAIR Program. The STAIR was programmed to compute the gravity off–on load cases from the zenith and the horizon look positions. The deformation data from these two positions was then manipulated to compute the deformations of the joints relative to the elevation angle where the reflector panels were initially set to the true paraboloid shape.
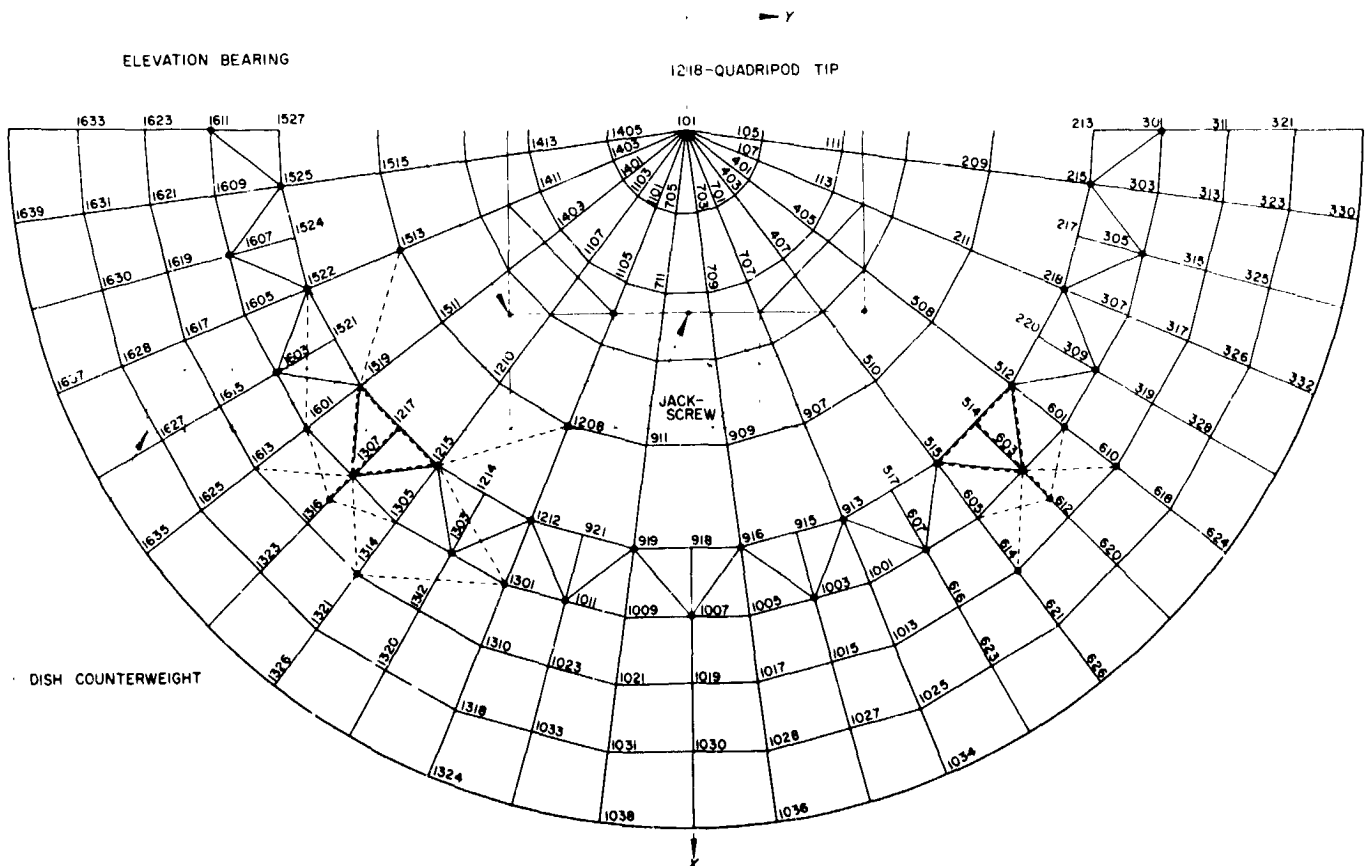

Fig. 3. 85-ft Az-El antenna surface panel joint numbers

Fig. 3 shows a 90-deg rotated view of the right half of the antenna as one looks into the face of the reflector; the joint numbers shown were those actually used in the STAIR computations. A total of 399 joints were inputted; this resulted in an equivalent solution by the computer of a 399 by 399 matrix.

The deformation data as outputted by the computing program were in the form of three orthogonal components of the displacement vector. The normal errors were reduced from the three-component format by the best-fitting RMS Computing Program. Results gave rms values for deformations in terms of ½ path length errors from the best-fitted paraboloid with the original focal length for the four cases computed. The rms values referred only to the structural joints or the panel supporting points.

3. Venus Voice-Bounce Experiment

The Venus voice-bounce experiment [conducted at the Venus site with the radar transmitter in either a single-sideband (SSB) or a frequency-modulated (FM) mode]

is considered a technical success in that the returned signals closely approximated the expected values. The quality of the recorded voice signals was very poor due to low signal-to-noise ratio; however, the signals were understandable to the majority of listeners. Valuable information on the implementation and operation of such a system was obtained and the effect of the rotation of Venus on both FM and SSB signals was recorded. In addition, a new record for long distance transmission of voice signals was established with round-trip distances of 58 million miles covered. The results indicate that if at the next conjunction more transmitter power or a larger antenna or both are available, good voice-bounce signals should be possible.

4. Components of Experimental X-Band Lunar/ Planetary Radar Program

The complete Dewar-mounted maser assembly is shown in Fig. 4 installed in a welded aluminum mounting frame. Fig. 5 shows the 10-liter Linde Dewar Model

Fig. 4. Packaged H-band maser amplifier
(shown with some panels removed)

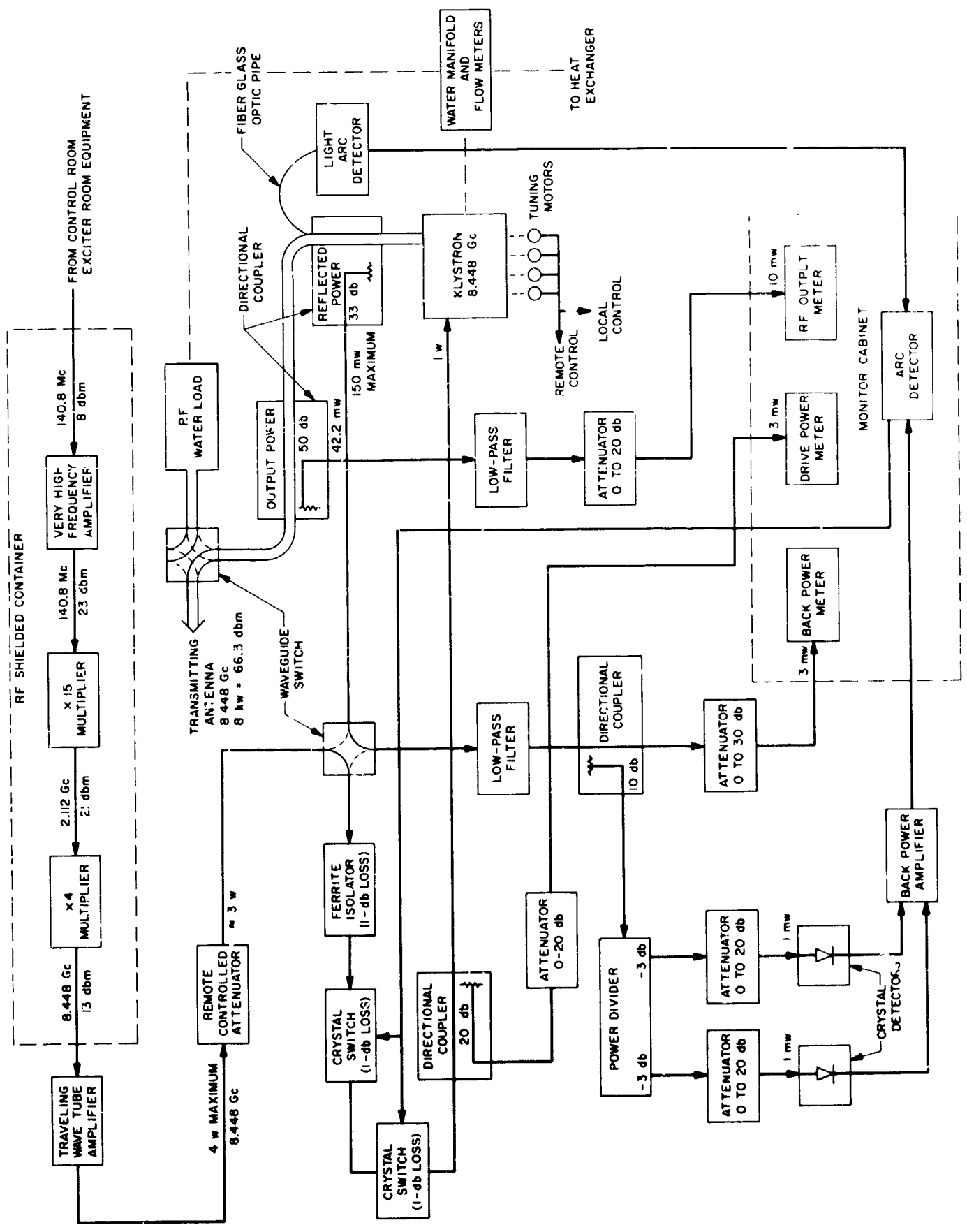Fig. 5. 10-liter Linde transfer Dewar
Model CD-206

Fig. 6. X-band transmitter: RF section block diagram

CD-206 which will be used to transfer liquid helium from the large 25-liter storage Dewars to the maser on the antenna. Remote readout at the maser amplifier is provided for reading liquid helium level. A crystal detector with calibrating attenuator is used to provide pump power monitor at the control panel. The monitor receiver has a balanced crystal mixer and a 30-Mc IF amplifier. Crystal current can be monitored through a removable plug on the receiver top. The single channel equivalent noise temperature is about 1000°K.

The X-band 8.448-Gc lunar radar transmitter (Fig. 6) is a hybrid system using new antenna-mounted equipment and the existing 10-kw S-band power supply. During transmitter shutdown, the system incorporates a con-

venient method of directing approximately 1 to 2 mw of exciter power out of the antenna feedhorn via the output waveguide. A waveguide switch is used in this klytron drive chain to direct approximately 4 w of exciter power into the 33-db reflected-power directional coupler. This exciter power may be used for making phase jitter measurements, antenna gain measurements, or other experiments requiring phase and frequency stable signals at low power.

New equipment for the S- to X-band conversion of the Mod IV receiver includes the X-band to 30-Mc converter and power supply (Fig. 7), and the solid-state frequency multipliers and modulators for the X-band exciter, receiver local oscillator, and signal generator.
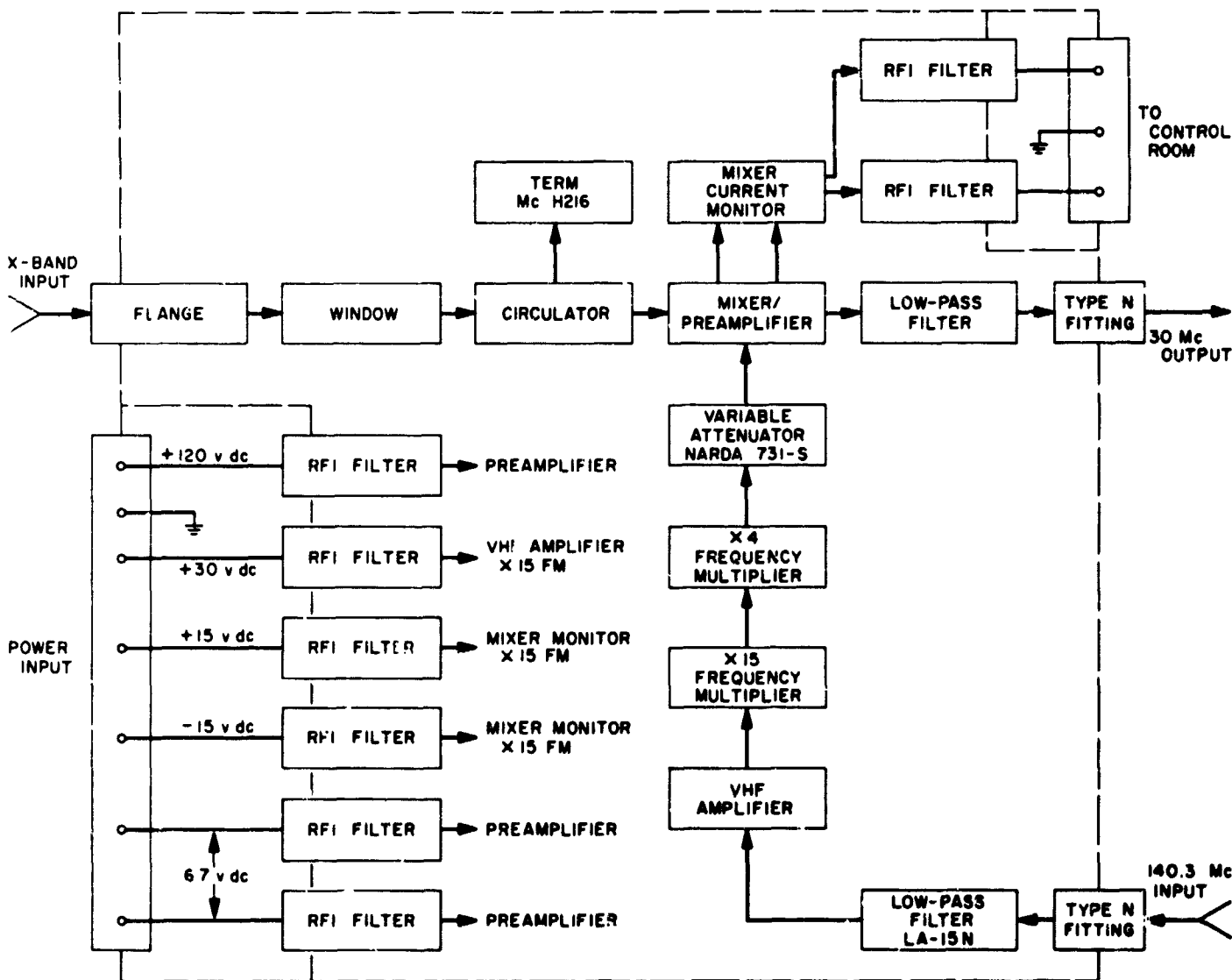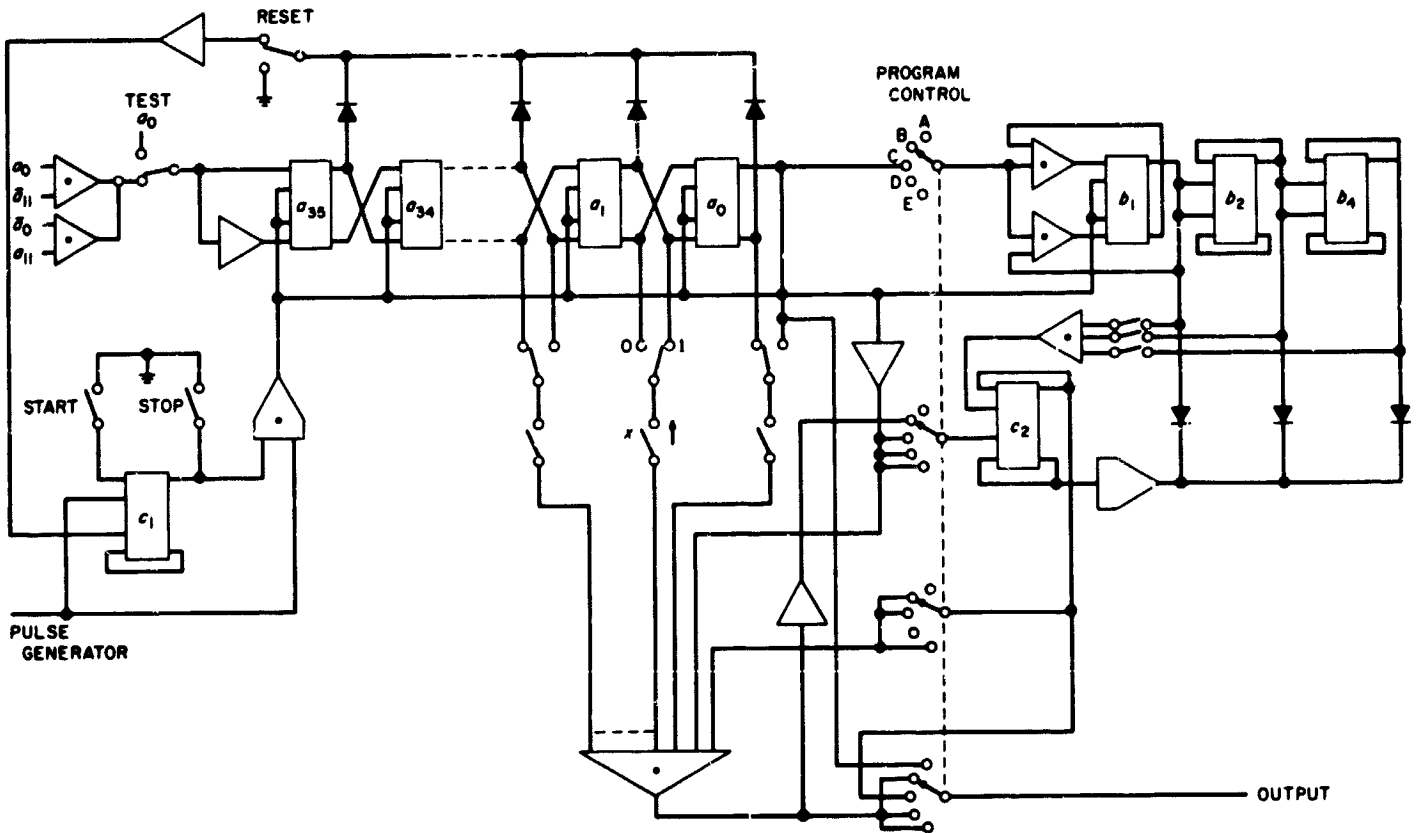

Fig. 7. X-band to 30-Mc converter

Fig. 8. Random pulse generator

5. Random Pulse Generator

A random pulse generator was designed (Fig. 8). This machine produces outputs, or pulses, depending on the last 7 bits from a length-36 maximal-length shift-register generator. This machine will be used to generate data for the quantile data compression system and noise for the punctured-cyclic coder–decoder. It was built using the new line of digital circuit modules being developed at JPL.

C. Advanced Antenna System

1. Azimuth Drive System

The function of the azimuth drive system for the Advanced Antenna System (Fig. 9) is to convert electrical and hydraulic servo signals to antenna rotation. The rotation of the antenna structure about the azimuth axis is accomplished by four azimuth gear reducers attached to and rotating with the alidade. Pinions on the output shaft of the reducers mesh with a fixed azimuth bull gear (Fig. 10). A single reducer is mounted at each of the two front alidade legs, and two reducers are mounted at the rear alidade leg.

2. One-Seventh-Scale Model Feed

The objective of the K_u-band scale model studies is to simulate Advanced Antenna System angle tracking feed performance with the Goldstone 30-ft reflector. The JPL precision-machined monopulse assembly, operating in the K_u-band (16,330 Mc), is intended to simulate the performance of an available S-band feed—the SCM (S-band Cassegrain Monopulse). As shown in Fig. 11, the JPL scale feed consists of a linearly polarized bridge assembly and a pyramidal horn. This feed utilized the TE_{10} mode for the sum channel radiation pattern, the resultant of the TE_{11} and TM_{11} modes for the E-plane error channel, and the TE_{20} mode for the H-plane error channel.

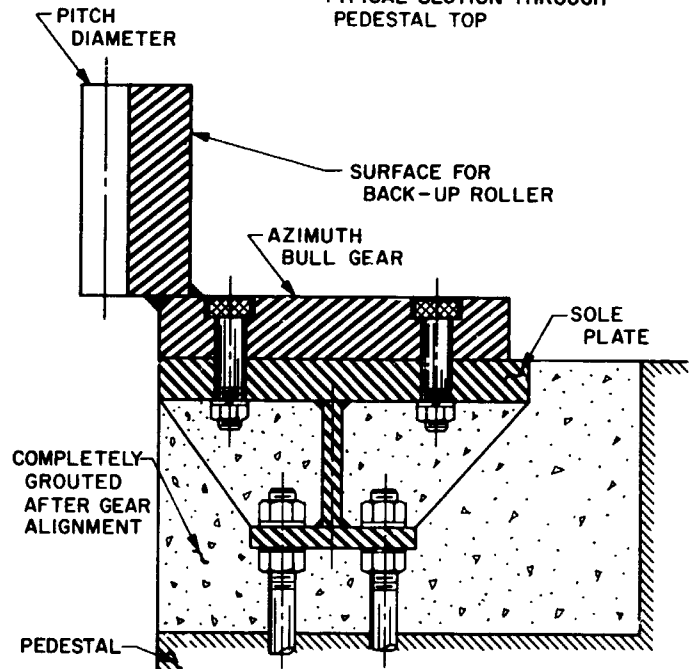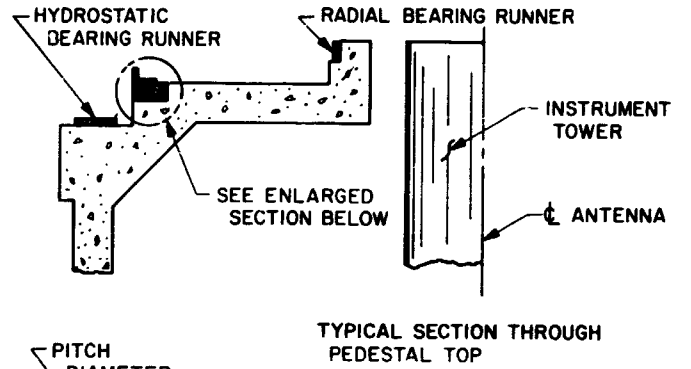The radiation S-band patterns for the ⅐-scale model feed (taken at the scaled frequency on the Mesa Antenna

TYPICAL SECTION THROUGH
PEDESTAL TOP

Fig. 9. Combined photograph and line drawing of the Advanced Antenna System

Range) have been evaluated, and the simulated performance is entirely acceptable. Boresight null depths (approximately 55 and 58 db for the E- and H-planes, respectively) indicate that a very high degree of mechanical symmetry was achieved during both construction of the individual parts and assembly of the waveguides.

Fig. 10. Advanced Antenna System azimuth bull gear

Phase-front patterns obtained for the feed alone also simulate the S-band performance of the SCM.

Fig. 11. 16,330-Mc monopulse feed

VI. Space Flight Operations Facility

A. Display Systems

1. Closed Circuit TV System

The closed circuit TV display system within the Space Flight Operations Facility has been designed to increase the effectiveness and efficiency of space flight operations. The 95 closed circuit TV cameras and the 212 closed circuit TV monitors provide three capabilities: (1) permit remote viewing of display boards and devices, (2) serve as a prime display of manually generated information required for simultaneous viewing in several separate areas, and (3) facilitate operational control by means of area surveillance.

In its present configuration the closed circuit TV system affords two general means of TV viewing: (1) by console monitors which are 14-in. TV tubes placed in the operational consoles, permitting a nominal viewing distance of from 2 to 3 ft (Fig. 1); and (2) by banks of
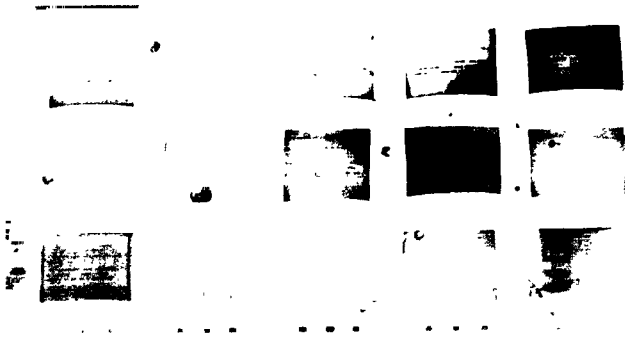

Fig. 1. Typical console TV Installation

Fig. 2. Typical wall-mounted TV installation

(a)

(b)

Fig. 3. Hard copy TV cameras and special frames

23-in. TV monitor tubes mounted as wall displays (Fig. 2).

Care has been taken to design original fixed displays with particular viewing positions in mind. Where changeable material is presented, as in the case of the hard copy TV cameras illustrated in Fig. 3(a), special frames have been designed which force the use of precisely the correct size of original copy [Fig. 3(b)]. Forms have been designed which are lightly printed with blocks visible to the naked eye but which are not "picked up" by the TV camera. These blocks indicate the correct size and spacing for characters.
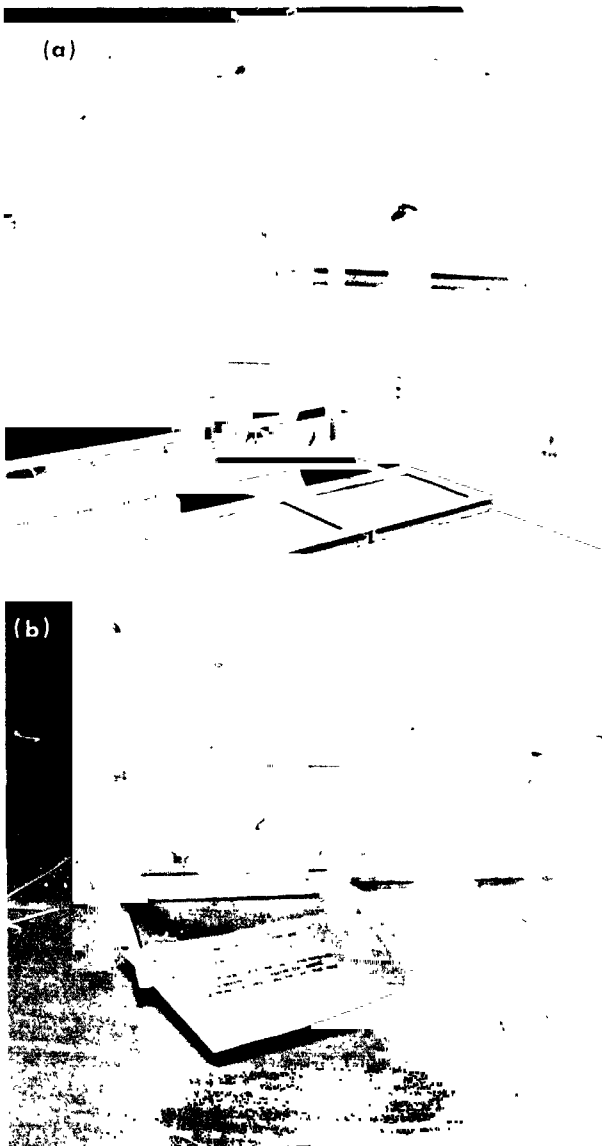
2. Spacecraft SFOF Functional Model System

The spacecraft model system (Fig. 4), located in the spacecraft performance analysis area of the Space Flight Operations Facility, provides a means of simulating the spacecraft and its motions in celestial environment, and assists cognizant personnel in evaluating performance and/or planning corrective maneuvers to be executed by the spacecraft. The system consists of four components: a 17½-ft hemispherical enclosure, an active spacecraft

Fig. 4. Spacecraft model system

model and gimbal assembly, a computer/control console, and a power supply rack.

The interior surface of the hemisphere is marked with azimuth and elevation lines which correspond to a spacecraft-centered coordinate system defined by the ecliptic plane and the direction of the vernal equinox. In this coordinate system the pertinent stellar bodies are located at fixed positions on the hemisphere while the positions of the solar bodies are a function of the particular trajectory and are available from the computer trajectory program. The northern and southern ecliptic hemispheres are represented in different colors, and thus the full environment of the spacecraft is illustrated.

The removable spacecraft model is mounted on a three-degrees-of-freedom gimbal assembly at the center of the hemisphere. The model contains small optical projectors which illuminate the interior surface of the hemisphere with scaled representations of the spacecraft sensors fields of view.

The automated gimbal assembly is driven from the control console. This console contains the equipment necessary to place the model in any required initial attitude, and then to duplicate the attitude motions of the spacecraft in space. As the spacecraft refers to no coordinate system other than its own, the console contains a small analog computer which provides the conversion from the input commands in body-centered coordinates to gimbal-referenced motion.

The system can be used to visually analyze a space-craft maneuver prior to the actual performance of the maneuver. The projected view fields provide the operator with a continuous illustration of what the spacecraft should sense with its various sensors during the course of its flight.

B. *Surveyor* On-Site Telemetry and Command Data Handling System

The Deep Space Network on-site data processing (OSDP) subsystem was integrated into the *Surveyor* telemetry and command data handling system. This enables the *Surveyor* equipment to function within the expanded data handling configuration and to output telemetry data directly onto the high-speed data line in the event the OSDP subsystem is unavailable.

The *Surveyor* on-site telemetry and command data handling system consists of (1) the Deep Space Network on-site data processing subsystem; (2) the command and data handling console (CDC); (3) the buffering equipment necessary to establish a compatible electrical interface between the CDC and the OSDP subsystem; (4) the communications signal converting equipment necessary to establish a compatible electrical interface between the CDC and the operational communications system; and (5) the control, switching, patching, and input–output equipment necessary to integrate the CDC and the OSDP subsystem into an operational entity.

BLANK PAGE

SPACE SCIENCES

VII. Space Instrument Development

A. Mariner C TV Subsystem Camera-Shutter Electronics

Experience with the *Mariner C* TV subsystem flight cameras has indicated that, with extended operation, the shutter action may become uncertain. This has been attributed to the increased friction caused by wear. It has been noted that, at times when "open-shutter" has been maintained, "close-shutter" has faltered. Among other steps that have been taken to alleviate this problem, the electronic mechanization has been more closely investigated in order to determine operating margins and possible improvements.

a. Description of electromechanism. The TV camera used a two-pulse electromechanical shutter where the exposure time is determined by the spacing between the pulses. The shutter drive is by rotary electrical solenoid. The axial thrust of the solenoid plunger is transferred to rotary motion by a self-contained mechanism, using the principle of a frictionless screw thread. The screw-thread action is provided by a suitably indented rotary plate that is driven by the plunger through ball bearings. The relationship of the drive to the magnetic circuit is illustrated in Fig. 1. With a nominal power input to the solenoid coil of 14 w, 0.5 amp at 28 v, a torque of 3.5 in.-oz is produced at the plate. The associated electronic circuitry provides two synchronized power pulses that have an absolute minimum drain on the spacecraft power supply. This is accomplished by using charged capacitors as the source of supply for the solenoid drive. The basic circuitry
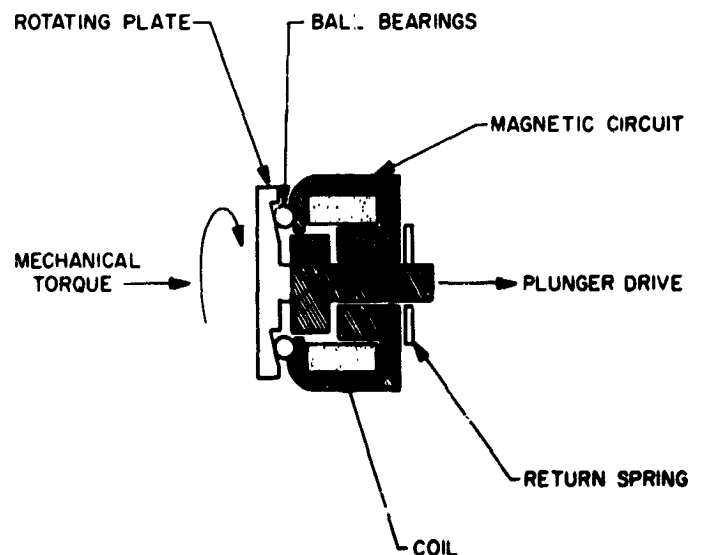

Fig. 1. Magnetic circuit operation of Mariner C TV subsystem shutter solenoid
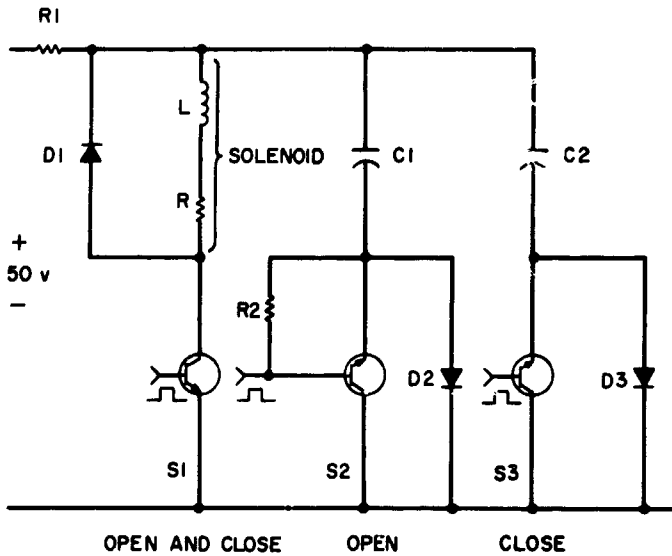
Fig. 2. Capacitor discharge drive to solenoid

is shown in Fig. 2. Drive pulses to the solenoid are controlled by power transistor gates. The power transistor switch S1 closes with alternate closure of S2 and S3, the open and close gates. At all other times, S1, S2, and S3 are open and capacitors C1 and C2 are charging through diodes D2 and D3, respectively. The charging time is the time between pictures: 48 sec. Unwanted energy stored in the solenoid inductance after application of the pulse is discharged through D1 after S1, S2, and S3 open.

b. Efficiency. The relationship between electrical power input and torque is of interest. To a close approximation the torque produced by the solenoid is a direct function of power input, i.e.,

$$F = k_1 W = k_2 I^2.$$

It should be noted that power dissipated in the resistive component of the coil performs no useful work. For this solenoid, close to 90% of the total power input is dissipated in resistive losses. Power applied following plunger operation is also wasted power, but possible losses here can be minimized by controlling the pulse length. A preliminary estimate of electromechanical conversion efficiency η may be made by expressing the peak power taken to drive the shutter in terms of the current and an effective electrical resistance R_e that will be higher than R, the coil dc resistance. Neglecting for the present incidental electromechanical losses that are difficult to assess,

$$\eta = \frac{R_e - R}{R_e}.$$

For the solenoid of interest,

$$\eta = \frac{100 - 85}{100} = 0.15.$$

A conversion factor of 1 w = 141.5 in.-oz/sec permits an estimate of the torque F for a given power pulse. Thus,

$$F = 141.5\,Wt\eta,$$

where W is the peak power, and t is the width of the applied current pulse. An optimum pulse width has been found to be 25 msec; hence, for an applied peak power of 14 w, $F = 141.5 \times 14 \times 0.025 \times 0.15 = 7.5$ in.-oz.

The manufacturer's specified torque verified in the laboratory for a 14-w input is 3.5 in.-oz, which reduces the efficiency estimated to above 0.07. This latter figure includes incidental electromechanical losses not allowed for in the preliminary estimate. The effective torque produced is thus 0.25 in.-oz/w. The required minimum power input to activate the solenoid only against the solenoid return spring was measured to be 6 w or 1.5 in.-oz torque. With the shutter mechanism attached to the solenoid, the minimum power input required was 12 w or 3 in.-oz torque. The electronic drive for *Mariner C* was designed for a minimum peak-power pulse for all expected conditions of 16 w or a torque of 4.0 in.-oz. This provides a 30% reserve for a normally operating shutter mechanism.

c. Available power. Power for the solenoid is derived from a charged capacitor. The input energy requirement W_i for a 16-w, 25-msec pulse is $16 \times 0.025 = 0.4$ w-sec. The capacitor discharge must be adequate to supply this solenoid energy over the 25-msec interval. The percentage of power utilized may be determined by integration in terms of the discharge time constant. Thus, the normalized power discharge

$$W_d = \int_0^t \exp\left(-\frac{2t}{T}\right) dt = \frac{1}{2}\left[\exp\left(-\frac{2t}{T}\right)\right]_0^t$$

When t is infinite, $W_d = 0.5$. For a discharge capacitance $C = 660\ \mu f$, a solenoid $R = 85$ ohms, $T = RC = 56$ msec. The normalized power removed from the capacitor during a 25-msec pulse is $W_d = 1 - 0.4/2 = 0.3$. Hence, 60% of the stored energy is available for use in the first 25 msec. The power discharge is illustrated in Fig. 3. The available stored energy in the capacitor

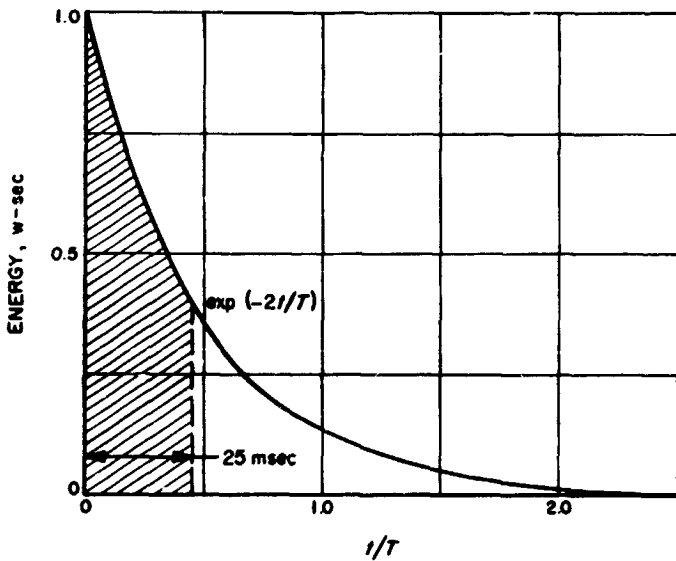$$W_s = \frac{1}{2} CE^2 = 0.83 \text{ w-sec}$$

Fig. 3. Normalized energy discharge of capacitor

for a charging potential of 50 v. Hence, the available power in a 25-msec interval $W_d = 0.83 \times 0.6 = 0.5$ w-sec. This indicates that the capacitor storage is adequate for a 16-w drive pulse of 25-msec duration.

d. Current pulse. Because of the presence of storage elements, deviations from an ideal square-wave current pulse are to be expected. The current pulse waveform may be determined from the impedance function LCR that represents the solenoid circuit shown in Fig. 4. The transform current

$$I(s) = \frac{E(s)}{sL + R + \frac{1}{sC}}.$$

For unit voltage drive,

$$i = \frac{\frac{1}{s} \cdot \frac{s}{L}}{s^2 + \frac{R}{L}s + \frac{1}{LC}} = \frac{\frac{1}{L}}{(s + a_1)(s + a_2)},$$

where a_1 and a_2 are the roots of the equations. Using the Laplace transformation, the solution is of the form

$$i = A_1 \exp(-a_1 t) + A_2 \exp(-a_2 t),$$

where

$$a_{1,2} = -\frac{R}{2L} \pm \left[\left(\frac{R}{2L}\right)^2 - \left(\frac{1}{LC}\right)\right]^{1/2}.$$
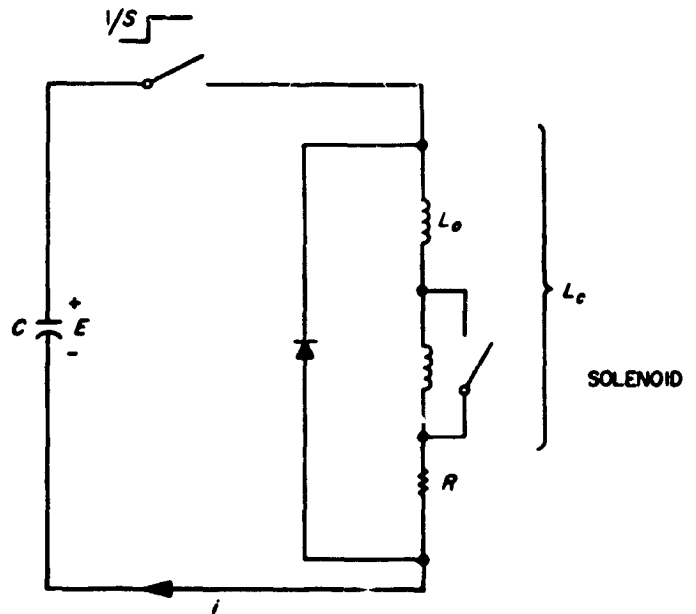

Fig. 4. Solenoid operation as a switched impedance function

In this particular case where $(R/2L)^2$ is substantially greater than $1/LC$, the roots of the equation may be expressed with sufficient accuracy and with more meaning in terms of the time constants RC and L/R, noting $(1 - \delta)^{1/2} \approx 1 - \delta/2$. Hence,

$$i = \frac{\frac{1}{L}}{\left(s + \frac{1}{RC}\right)\left(s + \frac{R}{L}\right)},$$

so that

$$i = A_1 \exp\left(-\frac{t}{RC}\right) + A_2 \exp\left(-\frac{Rt}{L}\right).$$

Evaluating the constants by partial fractions,

$$A_1 = \frac{1}{s + \frac{R}{L}}\bigg|_{s=-1/RC} \qquad A_2 = \frac{1}{s + \frac{1}{RC}}\bigg|_{s=-R/L}$$

$$\approx \frac{RCL}{R^2CL} \qquad\qquad \approx \frac{RCL}{-R^2CL} \quad \text{as } R^2C > 4L$$

$$= \frac{L}{R} \qquad\qquad\qquad = -\frac{L}{R}$$

For a voltage pulse of amplitude E,

$$i = \frac{E}{R}\left[\exp\left(-\frac{t}{RC}\right) - \exp\left(-\frac{Rt}{L}\right)\right].$$

The current is seen to be the difference of two exponentials associated with the time constants of L and C.

The value of L may be found by applying a step function current of appropriate magnitude to the solenoid, first with the relay held open and then with the relay held closed. In this particular application, 400-cps bridge measurements of L without dc current are quite erroneous. The value of L is estimated from the time-constant characteristic as observed on an oscilloscope trace. The measured value for the solenoid relay held open was $L_o = 0.22H$, and that for the solenoid held closed was $L_c = 0.5H$. Briefly, the flow of solenoid current with the application of a voltage pulse is as follows: At transistor switch closure, e_L is in direct oppostion to e_c so that the current at t_0 is zero. The current rapidly rises to a peak as e_L drops to zero. After reaching a peak, i steadily decreases as the capacitor discharges. However, as the plunger is fully inserted, L is suddenly increased. The inductive potential e_L is, at this time, in phase conjunction with e_c by virtue of

$$e_L = -L\frac{di}{dt}.$$

The resultant discontinuity produces a current boost to the solenoid. The switch now opens, and the inductive energy is discharged through diode D1. Using the equation developed above, a plot of current versus time was made, as shown in Fig. 5. After the initial current surge, $E^{-(R/L)t}$ becomes insignificant, and the current falls off at the rate of $E^{-(t/RC)}$. Following switch opening at $t = 25$ msec, the current decays at the rate of $E^{-(R/L)t}$. For comparison purposes, a photograph of the actual current waveform is shown in Fig. 6(a). The waveforms agree within the tolerances of the various circuit parameters, including the value of the applied potential.

e. Unequal pulses. Fig 6(a) indicates that the close-current pulse magnitude is somewhat less than that of the open pulse, representing a 20% drop in torque. Returning to Fig. 2, the open pulse is produced when C1 discharges through S1 and S2. A short time later (200 msec or less), S1 and S3 close to produce the close-current pulse. However, part of the charge on C2 boosts the charge on C1 via the diode D2, resulting in a loss of energy to the solenoid. This loss in charge may be prevented by removing the diode D2. This deletion is possible since the charge cycle can, in fact, proceed through the transistor switch S2 without the diode D2 being connected. This is because, during charge, the base-collector contact becomes reverse-biased and acts as a forward-biased diode. But, in this case, the base resistor R2 is sufficiently high to allow only
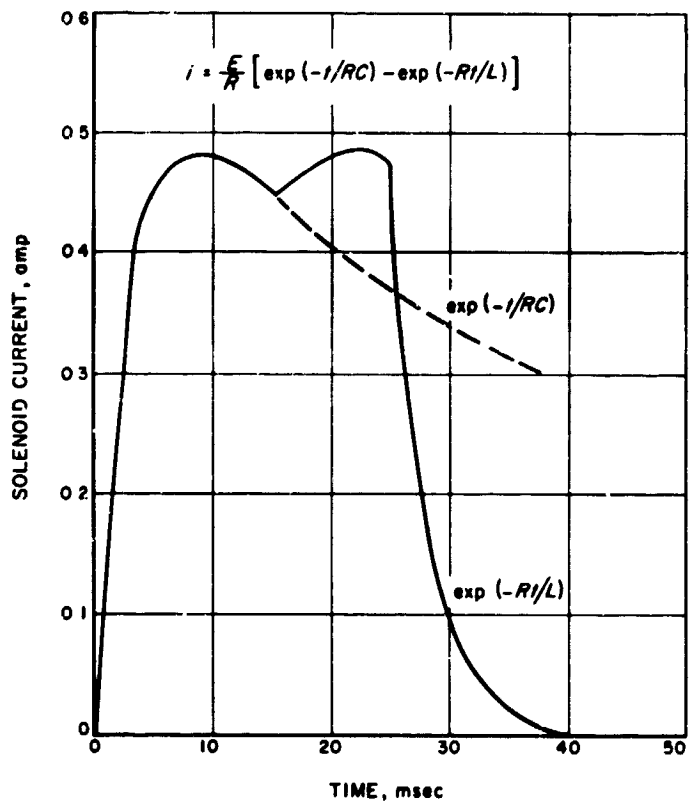

$$i = \frac{E}{R}\left[\exp(-t/RC) - \exp(-Rt/L)\right]$$

exp $(-t/RC)$

exp $(-Rt/L)$

Fig. 5. Calculated solenoid-current waveform

(a) WITH DIODE D2 CONNECTED

20 msec

150 ma

CURRENT

TIME

(b) WITH DIODE D2 DISCONNECTED

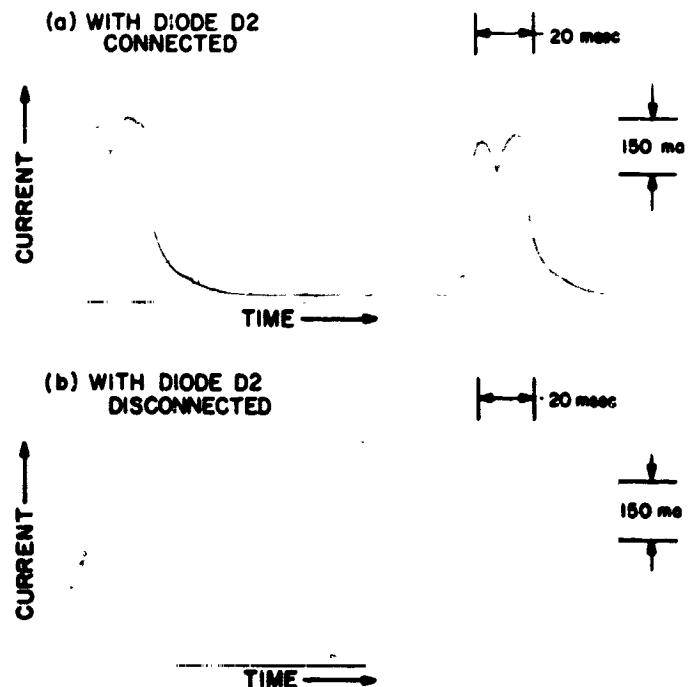20 msec

150 ma

CURRENT

TIME

Fig. 6. Measured solenoid-current waveform

a small fraction of the charge on C2 to be transferred and yet is inconsequential in the charging of C1. Without the diode, the current pulses are almost identical, as shown in Fig. 6(b).

Replacement of the transistor switches by hard-circuit elements, i.e., mechanical relays, has indicated that any losses introduced by the transistor switching are negligible.

f. Conclusion. The design of the shutter drive illustrates a typical difficulty encountered with an integrated electro-mechanical subassembly. Whereas for the mechanical designer a 50% increase in torque requirement probably presents no real hardship, for the electronic designer a change in power, say from 20 to 30 w, may represent a complete redesign with the replacement of many of the key components.

In the design of the *Mariner* TV subsystem shutter mechanization, an inadequate allowance was made for any increased torque requirements produced by wear. However, the margin of power reserve built into the electronics appears to be sufficient to accommodate a 50% increase in the torque demand resulting from wear. Equalizing the pulse drive on open- and close-shutter operation increases the operating margin. Extensive tests give no indication of any new problems arising when D2 is disconnected.